Modeling of Pulsed Jet Impingement on Brittle Materials

Detailed Design Report

ME 492 006 — Prof. Labus, Dr. Prantil

Team: Pulsed Water Jet

Paul Gessler
Marshall Schaeffer
Alex Zelhofer

Mechanical Engineering Department
Milwaukee School of Engineering

Version 1.05
May 29, 2012

1 Executive Summary

The goal of this project was the modeling of a water jet penetrating road-grade concrete, causing a mushroom-shaped material failure, as shown in Fig. 1. The purpose of this model is to predict the

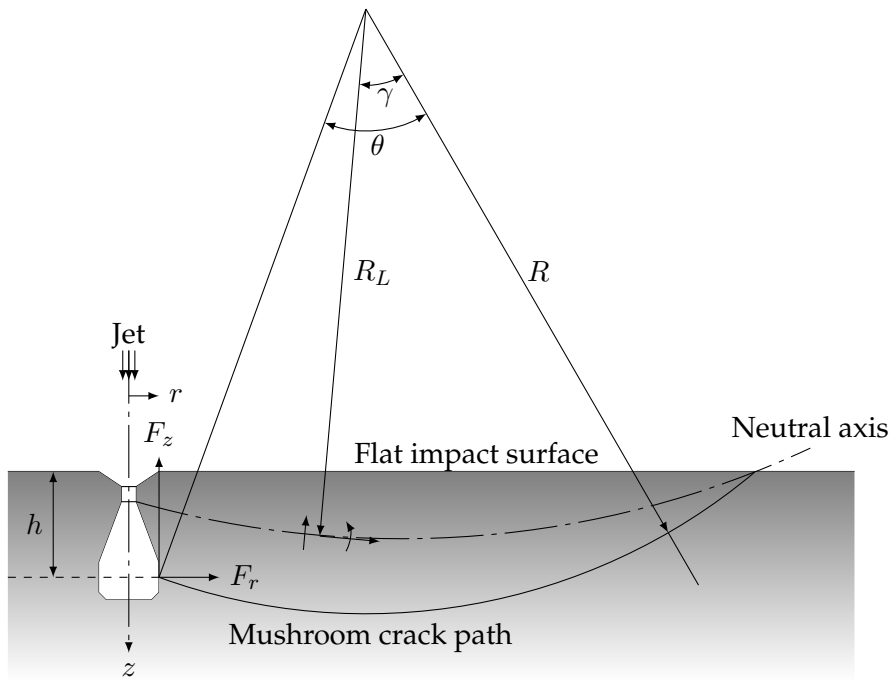

Figure 1: Schematic of Water Jet, Cavity Shape, and Loading Configuration (Adapted from [1])

size and shape of the failure surface for a given water jet system design, allowing optimization of the design for maximum material removal per unit energy expenditure. The mushroom-shaped failure is caused by forces on the walls of a bottle-shaped cavity. The cavity is created through erosion by the water jet. The device used to create the water jet is called a differential area intensifier (DAI) and can generate high velocities and pressures on the order of 2,000 ft/s and 75,000 psia, respectively. The DAI does not provide a continuous stream of water, but creates a pulse generated by moving a piston through the expansion of a driving gas. The DAI is shown schematically in Fig. 2, with labeled components.

Significant research was conducted investigating these four areas: brittle material fracture, hydrocodes and numerical modeling, DAI, and compressed water properties. Ryhming [2] used an analogous mechanical system to cause mushroom-shaped brittle material failure. Ryhming offered data showing forces and traction force angles required to generate the mushroom failure in a brittle material based on the fracture energy and elastic modulus of the material. The modeling effort includes hydrodynamics analysis codes (hydrocodes), which are used to simulate high-velocity impacts. An introduction to hydrocodes was provided by Zukas [3], who also discussed common mistakes made in hydrocodes. In addition, Schwer [4] covered large deformation problems related to solution time and accuracy of hydrocodes. Information regarding the DAI came from two previous MSOE senior design projects by Garity [5] and Bergesen [6]. Garity created a numerical model of the DAI, including compressibility and friction, where Bergesen offers dimensions of essential DAI parts. In the area of compressed water properties, Bridgman [7] offers the specific volume of water as a function of pressure from 1-8 kbar.

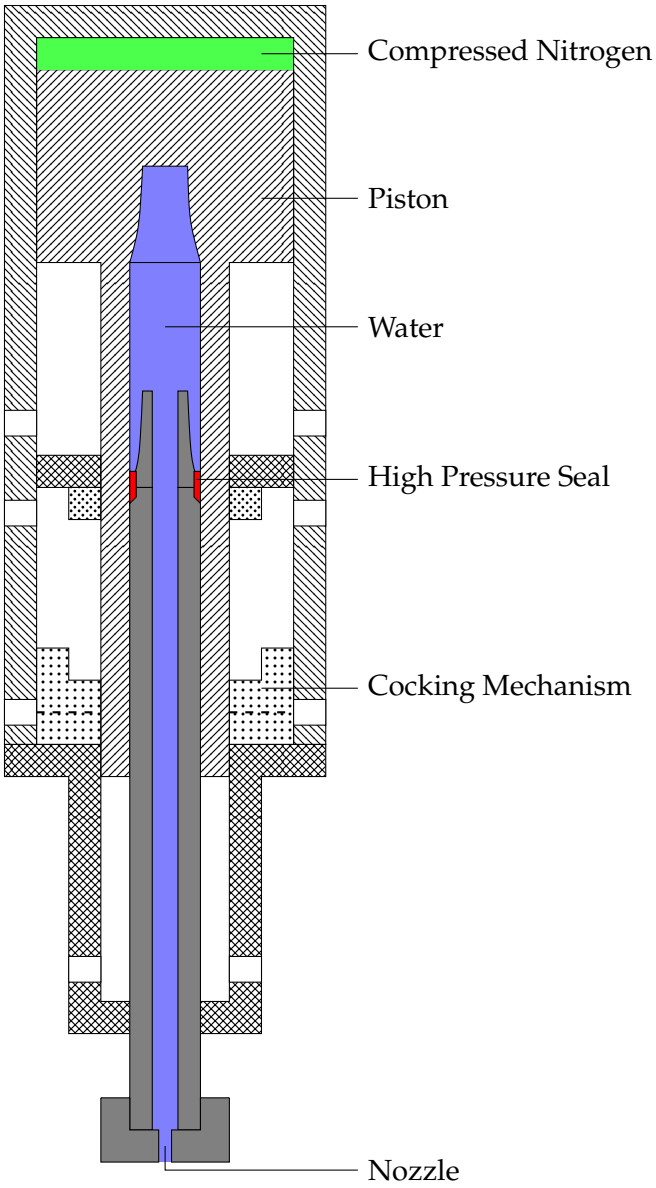

Figure 2: Differential Area Intensifier Schematic

The overall required specifications of the project are numerical models which relate the macro-scale fracture of concrete to parameters of key DAI parts such as nozzle diameter and piston mass. The model will be used in the optimization of the DAI design to minimize the amount of energy expended per unit mass of concrete removed.

The model of the water jet impingement is comprised of three components: a MATLAB/Simulink-based DAI model, a fixed-boundary transient fluid flow analysis in STAR-CCM+ (performed during Fall Quarter), and a hydrocode simulation in a software package called CTH (performed during Spring Quarter). The specifications of each model are:

DAI Model: Relate the DAI parameters to jet velocity and mass flow rate as functions of time in tabular form for input to the CTH Hydrocode model.

STAR-CCM+: Use the DAI model jet characteristic outputs to predict:

- Steady-state flow condition,
- Bottle boundary pressure and shear forces, and
- Resultant force vector angle on the bottle boundaries.

CTH Hydrocode: Use DAI model output to fully simulate the water jet impingement on concrete, predicting:

- Velocity fields,
- Pressure fields,
- Material failure,
- Stress fields, and
- Forces on the walls of the cavity.

Several DAI models were developed and implemented in MATLAB/Simulink during Fall Quarter, which included compressibility effects but assumed no friction losses or seal leakage in the device. During Winter Quarter, the model was refined to include seal friction and the dynamics of the cushioning apparatus which stops the piston at the end of the stroke. Velocity and mass flow over time are the outputs of the DAI models for input to STAR-CCM+ or CTH.

STAR-CCM+ simulations modeled the transient fluid flow of water, air, and the cavitation of water in a fixed geometry bottle shape until a steady-state flow condition was reached. These steady-state solutions of the transient simulations were meant to represent an instant in time where the concrete has failed on a micro-scale to create a specified bottle shape. The wall boundary force vectors generated by the fluid flowing in the bottle geometry were compared to Ryhming's data to determine if the specified bottle geometry and DAI parameters used are likely to cause macro-scale fracturing of the concrete. These simulations during Fall Quarter showed boundary forces an order of magnitude lower than required for failure (according to Ryhming). Further investigation with a more dynamic representation of the bottle cavity erosion was required.

CTH Hydrocode simulations were then used to model the jet impingement on a flat concrete surface. The simulations used outputs from the DAI model to predict the eroded cavity shape and ultimately the forces on the material causing macro-scale failure.

A baseline problem was run in CTH to verify the operation of the code. Simulations of the water jet impingement on concrete were conducted to predict the extent of material failure. The results of the CTH simulations were not yet compared to Ryhming's fracture data, but a qualitative comparison of the pressure field output from CTH with isochromatic fringe patterns by Daniel [8] confirmed that the physics of the problem are well captured by CTH, and corellate well enough to warrant further investigation.

Table of Contents

1 Executive Summary **i**

2 Project Background **1**
2.1 Project Statement . . . 1
2.2 Design Specifications . . . 5
2.3 Background Research . . . 6
2.3.1 Rock Fracture Research . . . 6
2.3.2 Hydrocode and Numerical Research . . . 7
2.3.3 Differential Area Intensifier Research . . . 10
2.3.4 Compressed Water Properties Research . . . 10
2.4 Conceptual Designs . . . 10
2.5 Feasibility Study . . . 10
2.5.1 DAI Model Feasibility . . . 11
2.5.2 CTH Hydrocode Model Feasibility . . . 11
2.5.3 Concrete Fracture Feasibility . . . 11

3 Detailed Model Design - Overview **12**

4 Detailed Model Design - DAI Model **12**
4.1 Model Assumptions . . . 13
4.2 Variable Compressibility Model with Cushion Dynamics and Friction . . . 13
4.3 Friction Model . . . 14
4.4 Cushion Model . . . 17
4.5 Dimensional Analysis . . . 19
4.6 Validation . . . 21
4.7 Future Work . . . 21

5 Detailed Model Design - STAR-CCM+ Model **22**

6 Detailed Model Design - CTH Hydrocode **24**
6.1 CTH Overview . . . 24
6.2 Background . . . 24
6.2.1 Eulerian vs. Lagrangian Mesh . . . 24
6.3 Material Types . . . 25
6.3.1 BFK Concrete Model . . . 25
6.3.2 Water Model . . . 26
6.3.3 Void Material . . . 26
6.4 Material Dynamics . . . 26
6.5 Loads/Constraints/Boundary Conditions . . . 27
6.5.1 Symmetric Boundary (type 0 - symmetric) . . . 27
6.5.2 Extrapolated Pressure Boundary (type 3 - inflow) . . . 27
6.5.3 Sound Speed-Based Absorbing Boundary (type 1 - semi-infinite medium) . . . 27
6.5.4 Extrapolated Pressure Boundary Condition (type 2 - outlet) . . . 27
6.6 Mesh . . . 28
6.6.1 Initial Mesh . . . 28
6.6.2 Adaptive Mesh Refinement . . . 28
6.7 Time Step Control . . . 28

6.8 Model Verification 29

7 Budget **30**

8 Environmental Impact **32**
8.1 Materials Contained in Design 32
8.2 Special Handling Instructions 32
8.3 Special Storage Instructions 32
8.4 Disposal Instructions 32

9 Project Schedule **33**

10 Results - DAI Model **35**

11 Results - CTH Hydrocode **48**
11.1 Axisymmetric Simulation 48
11.2 Three-Dimensional Simulation 52

12 Conclusion and Recommendations **53**

References **55**

Appendices **56**

Appendix A Team Member Résumés **56**

Appendix B DAI Model and Scripts **59**

Appendix C Embedded MATLAB Functions **66**

Appendix D Compressibility Model MATLAB Functions **68**

Appendix E Sample CTH Input Files **69**

Appendix F POLYOX MSDS **78**

Appendix G Hydraulic Fluid MSDS **93**

List of Figures

1 Schematic of Water Jet, Cavity Shape, and Loading Configuration . . . i
2 Differential Area Intensifier Schematic . . . ii
3 Schematic of Water Jet, Cavity Shape, and Loading Configuration . . . 1
4 Differential Area Intensifier Schematic . . . 2
5 DAI Operation - Full Cycle . . . 4
6 DAI Specification Metrics [1] . . . 5
7 Mechanical System Experiment Configuration . . . 6
8 Experimental Mechanically-Generated Failure Surface . . . 7
9 Hydrocode Operation Flowchart . . . 9
10 Overall Project Workflow . . . 12
11 Free Body Diagram of DAI Piston . . . 13
12 Beryllium-Copper High Pressure Seal . . . 14
13 Effects of Friction Chattering . . . 15
14 Chatter Reduction Logic . . . 16
15 Chatter Reduction Logic Flowchart . . . 16
16 Piccolo Cushion Operation and Dimensions . . . 17
17 Cushion Gap Hypotenuse Calculation . . . 19
18 Hydrodynamic Forces on Bottle Geometry . . . 22
19 CFD Simulation Boundary Conditions . . . 22
20 Water Flow Progress . . . 23
21 Arbitrary Langrangian-Eulerian Time Step . . . 24
22 Computational Domain Representations . . . 25
23 Material Model Inputs and Outputs . . . 25
24 Example Initial Mesh for CTH Hydrocode Simulation . . . 28
25 Extreme Mesh Distortion in Plate Perforation Calculation [3] . . . 29
26 Rezoning Near Areas of Extreme Mesh Distortion [3] . . . 29
27 Eroded Cavity Shapes for Various Jet Stand-Off Distances [9] . . . 30
28 Project Schedule . . . 34
29 Jet Mass Flow Rate and Velocity Profile . . . 37
30 Dimensionless Jet Mass Flow Rate and Velocity . . . 38
31 Dimensionless Jet Velocity and Mass Flow Rate - Detail . . . 39
32 Dimensionless Water Pressure in the High Pressure Chamber . . . 40
33 Dimensionless Piston Velocity and Acceleration . . . 41
34 Dimensionless Piston Velocity and Acceleration - Detail . . . 42
35 Dimensionless Piston Motion . . . 43
36 Dimensionless Piston Motion - Detail . . . 43
37 Dimensionless Forces Acting on the Piston . . . 44
38 Dimensionless Forces Acting on the Piston after Cushion Engagement . . . 45
39 Dimensionless Stopping Pressure . . . 46
40 Dimensionless Driving Air Pressure . . . 47
41 Dimensionless Driving Air Pressure - Detail . . . 47
42 Cavity Depth vs. Time - Axisymmetric Geometry, Homogeneous Concrete . . . 48
43 Eroded Cavity Shape - Axisymmetric Geometry, Homogeneous Concrete Model . . . 49
44 Comparison of CTH Jet/Impact Surface Interface Shape (top) with Pritchett Simulations (bottom) upon Impact ($t = 1.1$) [10] . . . 50
45 Pressure Field Verification . . . 51

46 Three-Dimensional Simulation with Random Aggregate Distribution 52
47 DAI Model - MATLAB/Simulink Block Diagram Top Level 59
48 DAI Model - MATLAB/Simulink Block Diagram Subsystem 60

List of Tables

1 DAI Concrete Fracture Specifications 5
2 Properties Used for Non-Dimensionalization 20
3 Finalized Project Budget 31
4 DAI Model Parameters 35
5 Properties Used for Non-Dimensionalization 36
6 Definitions of Dimensionless Variables 36

Nomenclature

A_D	Driving Piston Area
A_n	Nozzle Area
A_p	High-Pressure Cylinder Area
A_{os}	Area of the Cushion Orifices
β	Water Bulk Modulus
C_o	Orifice Coefficient
C_{og}	Orifice Coefficient of the Cushion Gap
C_{os}	Orifice Coefficient of the Cushion Orifices
E	Young's (Elastic) Modulus
γ	Nitrogen Specific Heat Ratio
g	Gravity
$\dot{m}_{\text{out}}$	Water Jet Mass Flow Rate
μ	Coefficient of Friction
M_P	Piston Mass
M	Number of Orifices in a Ring
N	Number of Rings of Orifices in a Cushion
P, P_a, P_g	Water Pressure; subscript denotes absolute or gage pressure
p_{cont}	Seal Contact Pressure
P_{D0}	Initial Driving Pressure
P_{Da}, P_{Dg}	Driving Pressure; second subscript denotes absolute or gage pressure
Q_{orifice}	Volume Flow through Orifice
r_{bi}, r_{bo}	Inner and Outer High Pressure Cylinder Radii
r_{si}, r_{so}	Inner and Outer Seal Radii
ρ	Water Density
r_{clear}	Radial Clearance Before Pressurization
t	Time
t_s	Seal Thickness
ν	Poisson's Ratio
V	Water Volume
V_0	Initial Water Volume

V_{D0}	Initial Driving Gas Volume
x	Driving Piston Displacement from Fully Cocked
CFD	Computational Fluid Dynamics
CTH	CHARTD^3, Hydrocode Software by Sandia National Laboratories
DAI	Differential Area Intensifier

2 Project Background

2.1 Project Statement

The project will provide a first-principles model of concrete demolition by a pulsed water jet. The impinging jet erodes a bottle-shaped cavity and puts the concrete on the walls of the cavity in tension, resulting in macro-scale fracture of the material. The purpose of this model is to predict the size and shape of the failure surface for a given water jet system design, allowing optimization of the design for maximum material removal per unit energy expenditure. Figure 3 shows the general configuration of the scenario under investigation.

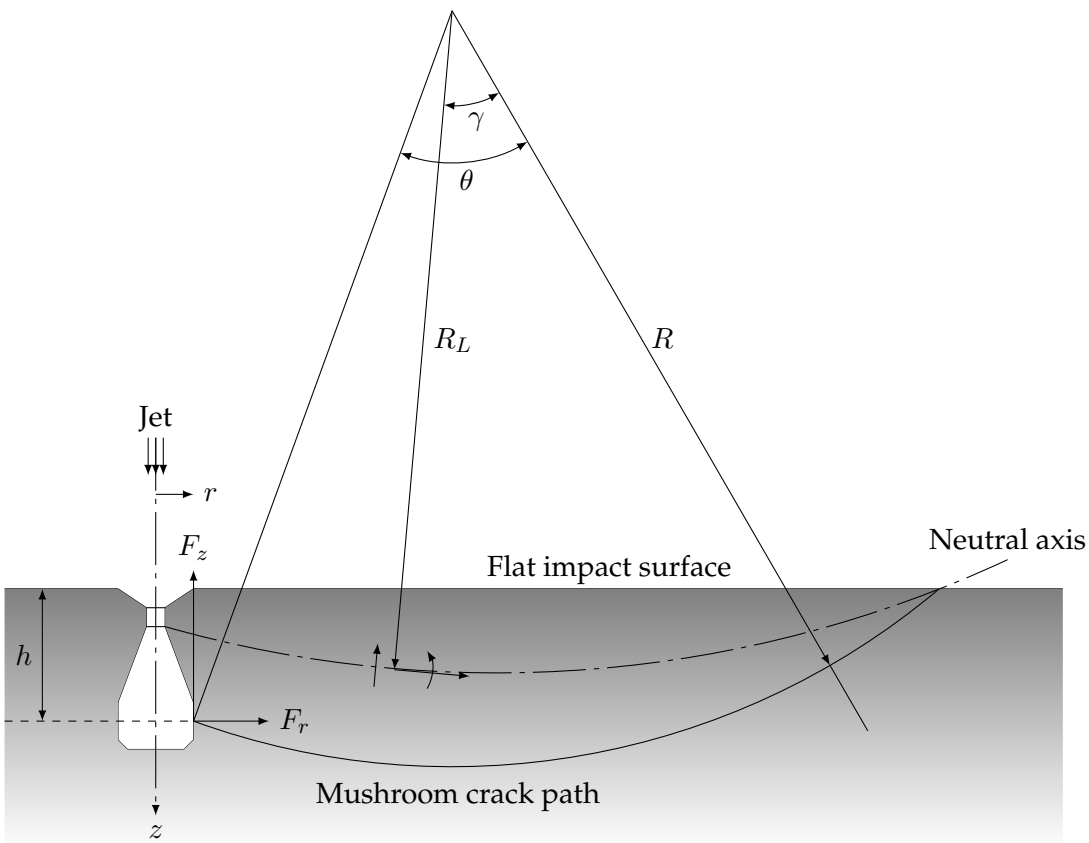

Figure 3: Schematic of Water Jet, Cavity Shape, and Loading Configuration (Adapted from [1])

The water jet forms the bottle-shaped cavity though micro-scale failure, such as erosion, and ultimately causes a macro-scale failure along the mushroom crack path of Fig. 3. The mushroom crack path is caused by tensile forces in the material, generated by the hydrodynamic forces on the hole walls. The device used to create the water jet pulses is called a differential area intensifier (DAI), presented schematically in Fig. 4 with labeled components. The DAI uses a large difference in areas to put water under very high pressure (on the order of 75,000 psi). This produces a high velocity jet ($\sim$2,000 ft/s) emitted through the nozzle.

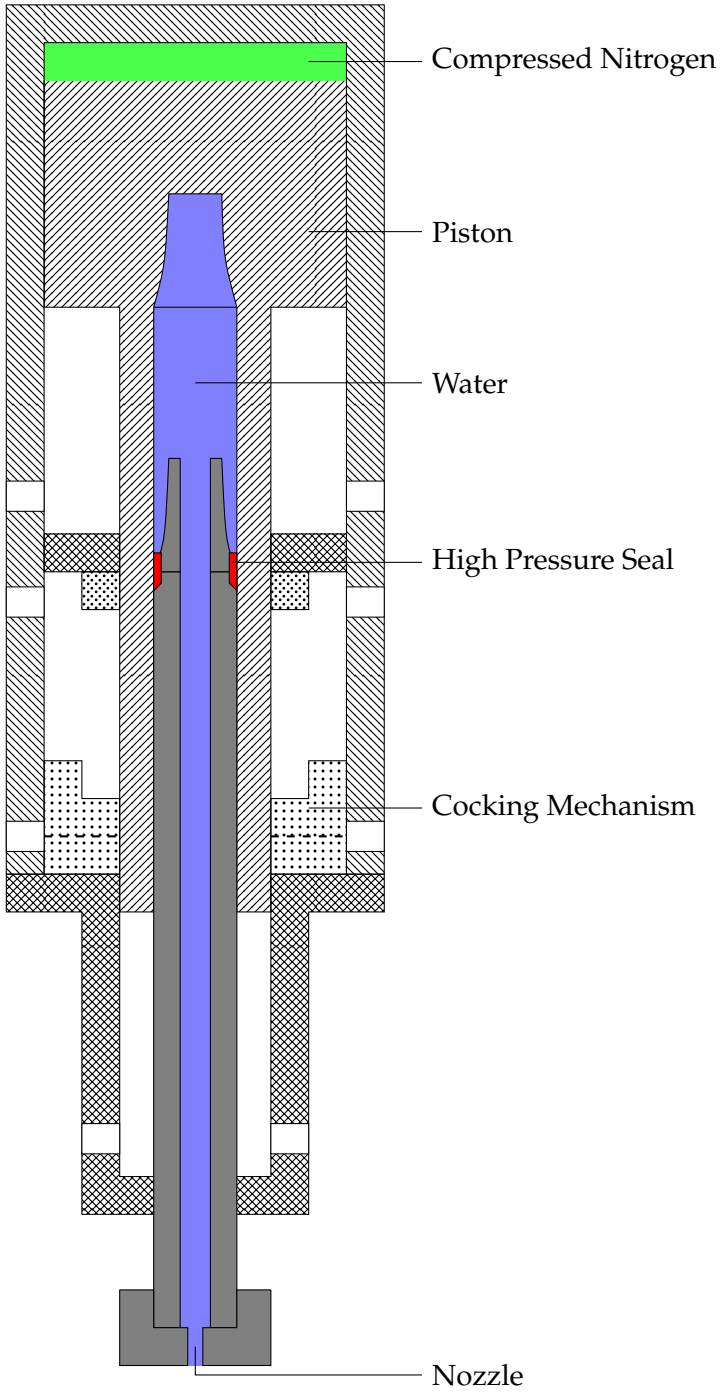

Figure 4: Differential Area Intensifier Schematic

Figure 5 shows how the DAI operates. At the end of the stroke, the driving piston has just been stopped by the cushion, which forces water out of a cavity to provide an impulse to the driving piston without a large dynamic force. To cock the mechanism, hydraulic oil pushes the cocking mechanism up and the nitrogen (the driving gas) is compressed. Once the cocking mechanism has been retracted, the DAI is ready to fire. In the power stroke, the nitrogen applies a driving force to the piston. This causes the high pressure water piston to force water out of the nozzle at a high velocity until the cushion stops the piston motion. The cycle may then repeat for any desired number of pulses.

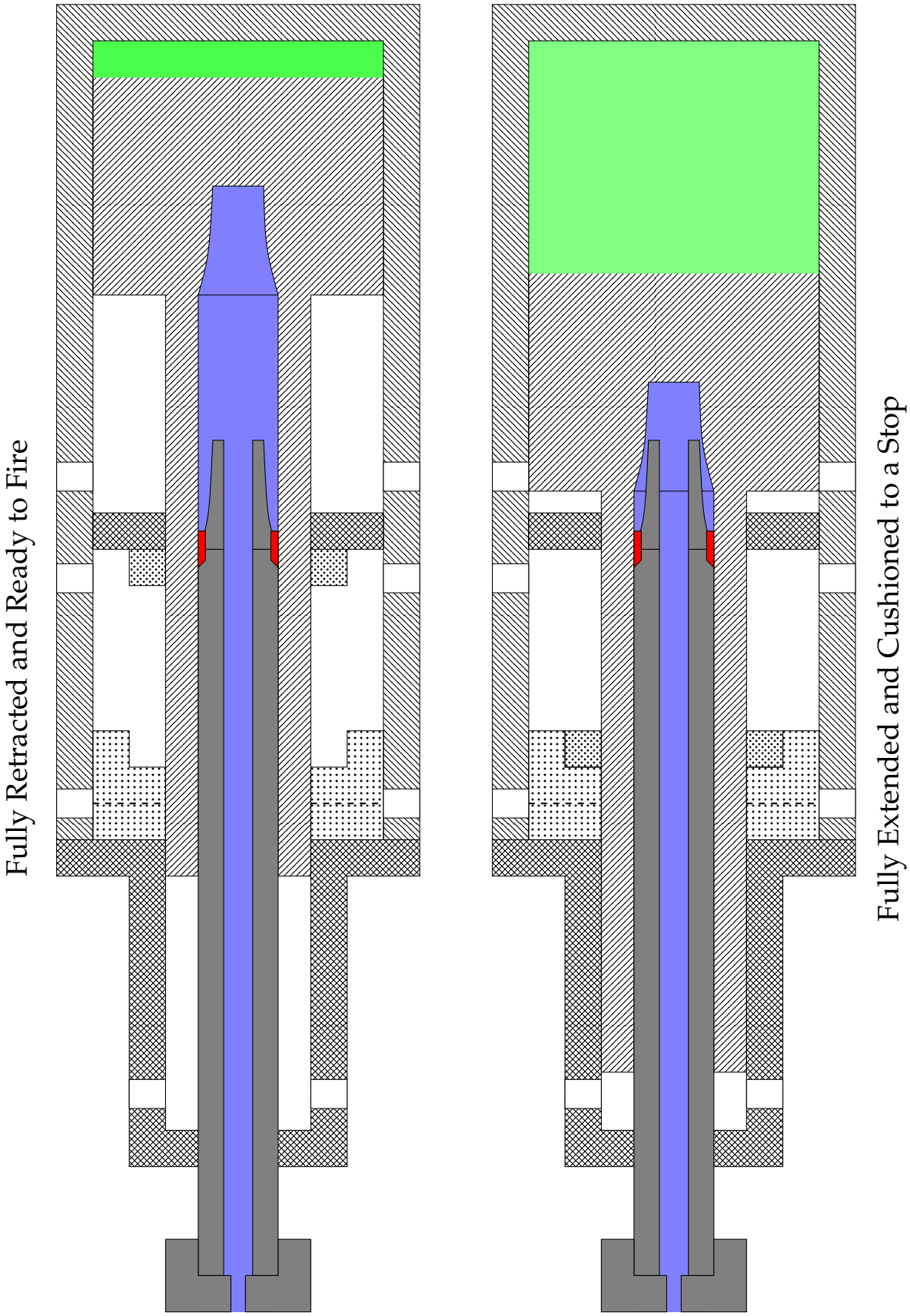

Figure 5: DAI Operation - Full Cycle

A mathematical model of the DAI has been created to predict exiting jet velocity and mass flow. These jet characteristics become the input to hydrodynamic models in one of two software packages:

STAR-CCM+: Static Boundary, Unsteady Flow Computational Fluid Dynamics (CFD)

CTH: Full Hydrocode Simulation; Coupling Water Jet, Erosion, and Material Failure

These two models will relate jet characteristics to predictions of material failure by comparison to referenced experimental data. Further explanation of the models is presented in Sections 3 to 6.

2.2 Design Specifications

The specifications shown in Table 1 were chosen to represent minimum performance parameters of the DAI. The specifications were taken from Figures 9 and 10 from [1], reproduced here as Fig. 6.

Table 1: DAI Concrete Fracture Specifications

Specification Type	Value
Specific energy for volume material fractured	$< 100\,\mathrm{Nm/cm^3}$
Energy stored in compressed Nitrogen	$> 50\,\mathrm{Nm}$
Flow rate	$> 180\,\mathrm{L/min}$

The ultimate goal is to achieve a lower specific energy of volume material fractured. Specifications associated with achieving a lower specific energy are ensuring a minimum potential energy stored in the compressed nitrogen gas and a minimum water jet flow rate. Figure 6 shows that the specific energy required to fracture material decreases with increasing pulse energy and pulse flow rate.

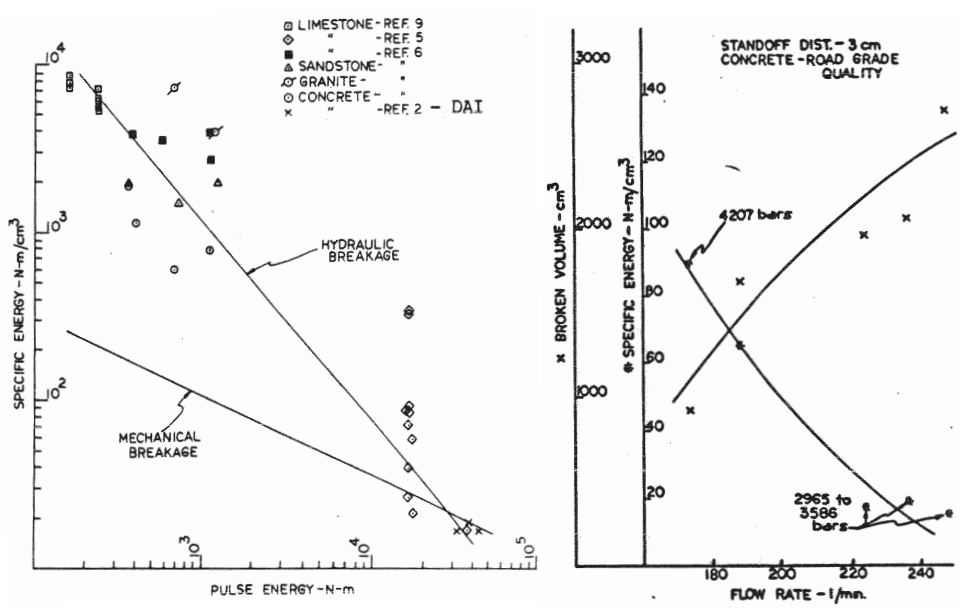

(a) (b)

Figure 6: DAI Specification Metrics [1]

2.3 Background Research

An extensive literature review was conducted on past and present studies of water jets interacting with brittle materials such as concrete. The research effort is summarized here, and is divided into four areas:

Rock Fracture Research: Previous work studying the failure of rock and concrete fracture, particularly the desired mushroom crack as shown in Fig. 3, whether generated by a water jet or by other means.

Hydrocode and Numerical Research: General information on hydrocodes and other numerical methods applicable to the project.

Differential Area Intensifier Research: Review of previous water jet designs, primarily used for creating the DAI model.

Compressed Water Properties Research: Survey of existing data on the compressibility of water, required for the DAI model.

2.3.1 Rock Fracture Research

An overview of the state of research in using pulsed water jets as rock breakers is presented by Labus [1]. This paper contains a compilation of several data sources that have shown the crater-type failure experimentally. One of the experiments, conducted by Ryhming [2], used a mechanical system with an expanding hydraulic wedge which gripped and pulled on a bored hole to cause material failure, as shown in Fig. 7.

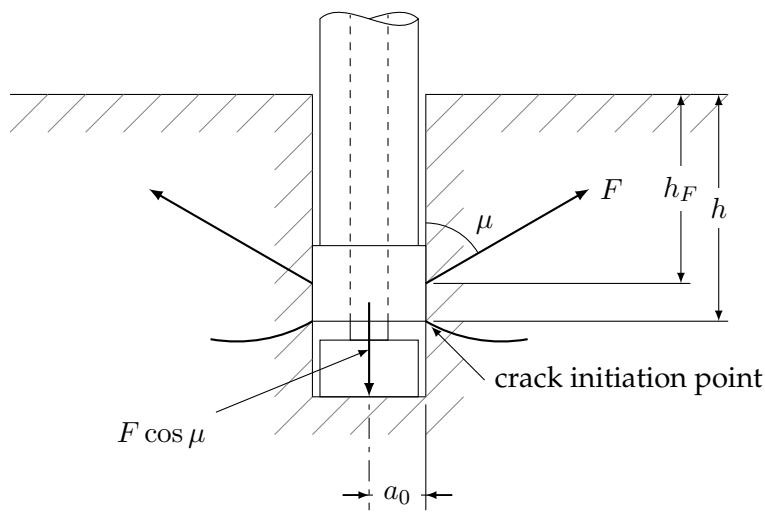

Figure 7: Mechanical System Experiment Configuration (Adapted from [2])

With this arrangement, Ryhming was able to generate the same type of conical failure surface produced in rock masses impinged by high velocity water jets, as shown in Fig. 8. This type of failure has a low specific energy which is desirable.

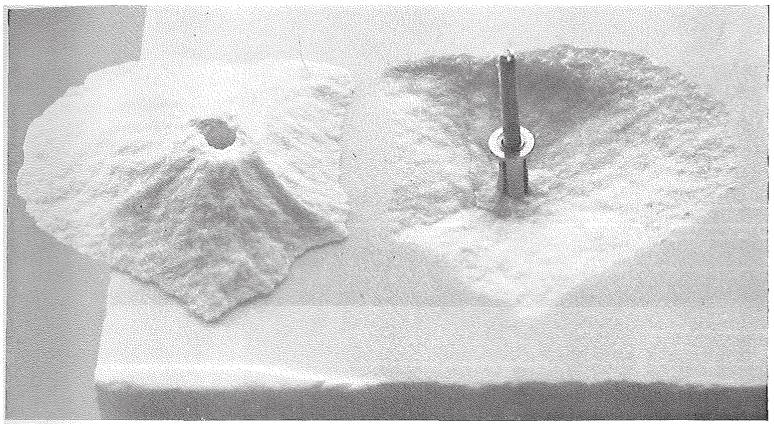

Figure 8: Experimental Mechanically-Generated Failure Surface [2]

Ryhming recorded the axial and radial components of force generated by the wedge at failure. The force results from the STAR-CCM+ and CTH models can be validated against these data. In addition, the experimental failure surface shape can be compared to predictions by the CTH model for further validation. Model validation plans are discussed further in Section 6.8.

2.3.2 Hydrocode and Numerical Research

Several sources were consulted to learn more about the numerical methods used within hydrocodes. Of primary benefit was a work by Zukas [3], which not only introduced the equations solved by hydrocodes, but highlighted the process followed within the code, as shown in Fig. 9. A typical hydrocode pre-processor assembles the global relationships through user-input boundary conditions, geometry, and material properties. These initial steps are completed and then saved so the job can be resumed, as shown in Fig. 9.

The computational sequence of Fig. 9 is executed in looped fashion. For each time step, the hydrocode begins with the velocities from the previous time step (or the initial conditions if it is the first time step), and integrates them over the time step to determine displacements. The contact algorithm is then executed, which checks for material interference with the new displacements and applies adjustments to the displacements, if necessary.

The strains and strain rates are calculated from the adjusted displacements, and a stress-strain relationship allows the stresses to be computed. Finally, the element sizes are used to obtain concentrated forces and the lumped nodal masses are used to calculate accelerations. The accelerations are integrated, resulting in the next set of velocities.

The simulation time is incremented by a time step, and the loop continues. The solution is advanced in time using this method until user-specified stopping criteria are met, such as physical time or maximum velocity.

In addition to Zukas, the documentation for a commercial hydrocode by Hallquist [11], LS-DYNA, was consulted to become more familiar with the technical workings of a hydrocode and the available element library.

To gain knowledge about complications of large-deformation simulations, such as mesh re-zoning

and wave propagation effects, two sources were considered: Zukas [12] and Schwer [4]. These sources explained the inherent problems encountered when large deformations generate high element skewness, mainly the effects on solution time and accuracy. For example, when a code has a Lagrangian formulation (mesh deforms with the material), a high skewness, or ratio of the element side lengths, can cause the time step to approach zero. This requires re-meshing locally to eliminate the highly skewed elements, or the simulation will continue to run with virtually no progress in time.

Since CTH uses an Eulerian formulation (fixed mesh; material flows through the mesh), the problems of skewness are eliminated as long as the initial mesh is of acceptable quality. However, other issues arise with Eulerian formulations, mainly particle tracking. According to Schwer [4], at least 3 elements across the width of a particle are required to accurately track it through the mesh. This means that an extremely fine mesh is required anywhere a material interface is predicted. Fortunately, CTH has a dynamic re-meshing module which aims to alleviate this issue automatically.

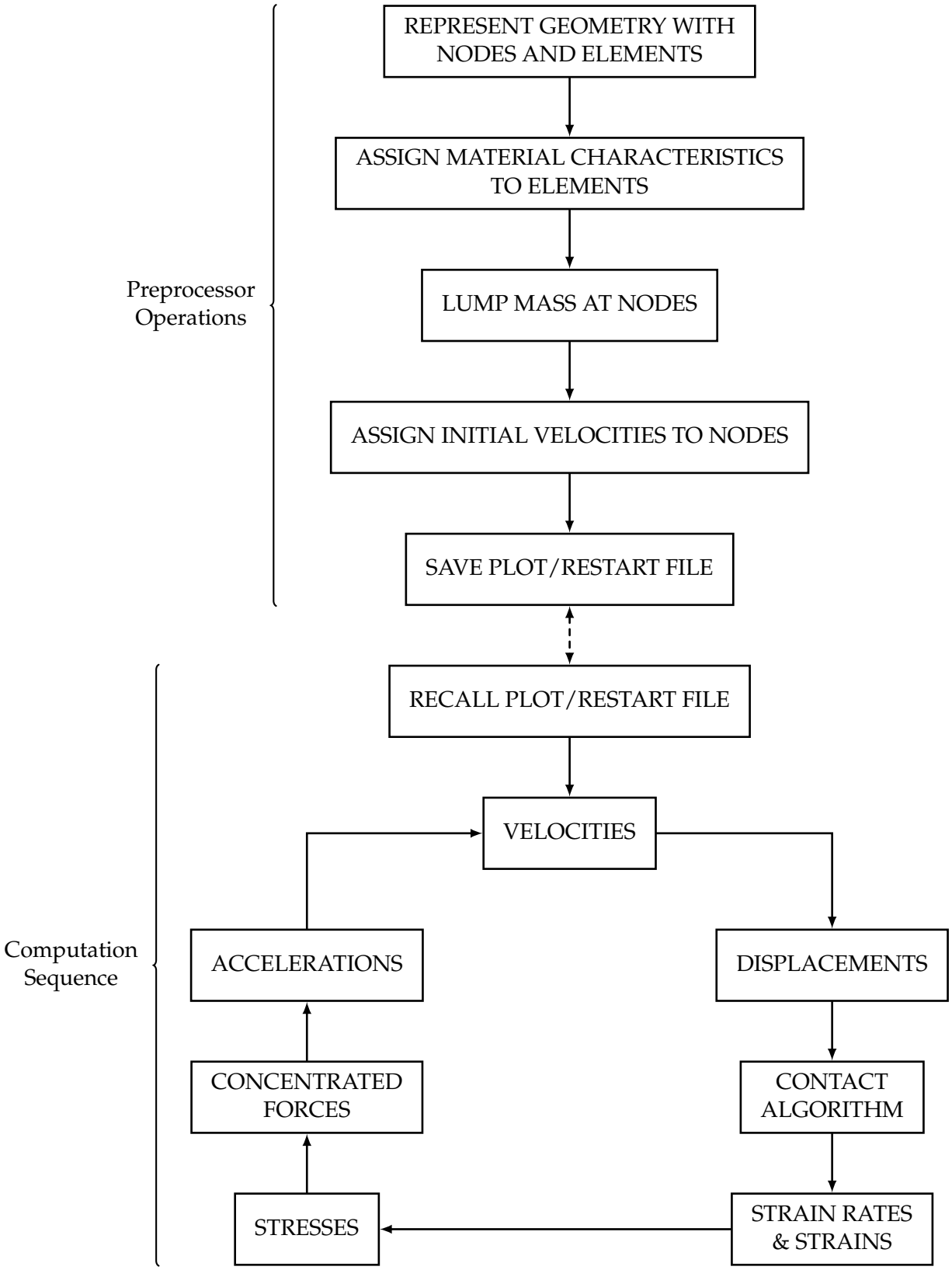

Figure 9: Hydrocode Operation Flowchart (Adapted from [3])

2.3.3 Differential Area Intensifier Research

To begin the DAI modeling process, two previous MSOE senior design projects were referenced: Garity [5] and Bergesen [6].

Garity constructed a numerical model of a DAI in 1995, and his work has been used as a starting point for the current model. It can also be used as a qualitative, and possibly quantitative, benchmark. The constants used in the current model that describe the characteristics of the DAI were taken from this source.

Bergesen, et. al. (2007) shows the feasibility of building a DAI for industrial use, although a physical prototype will not be constructed in this project. The part dimensions, weights, etc. from this design can be used as another set of constants for future simulations.

2.3.4 Compressed Water Properties Research

The DAI model requires information about the properties of water at high pressures to account for compressibility effects. This information was obtained from P. W. Bridgman [7] and developed in the ME 490 Proposal Report [13].

2.4 Conceptual Designs

The models created in STAR-CCM+ were used to evaluate the feasibility of water flows producing the normal and shear forces necessary to fracture the concrete according to Ryhming [2]. Details of the simulations and boundary conditions can be found in Section 5. Unfortunately, despite the variety of bottle geometry dimensions varied, the STAR-CCM+ models failed to produce the forces necessary to cause failure of the concrete. However, the STAR-CCM+ simulations were deemed inadequate for two reasons. The first reason was because of the smooth velocity flow fields through the bottle. In reality, the bottle shapes would be created by the water eroding the concrete and the walls would be irregular therefore causing boundary forces in arbitrary directions. Secondly, the equations of state for the water, air, and water vapor were chosen to be constant density to allow a manageable computational time per simulation of six days on a dedicated desktop computer. Variable densities would have required an even finer mesh to ensure the simulation would be computationally stable and accurate which would have taken substantially longer to compute. Therefore, realistic cavitation and flow dynamics were not achieved. STAR-CCM+ proved that only a hydrodynamics code such as CTH could handle the coupled dynamics of the problem.

2.5 Feasibility Study

Justifications for model implementation decisions are presented in this section. The work presented here is also outlined in the project schedule, Fig. 28.

2.5.1 DAI Model Feasibility

For the DAI model, MATLAB/Simulink was the software chosen for building and running the DAI model. It allows simultaneous solving of differential equations (linear or nonlinear) using block diagrams. Since Simulink is easily interfaced with MATLAB, there is substantial versatility in simulation methodology. For example, a simulation can be run from within Simulink for troubleshooting but can also be run from MATLAB for a turn-key simulation with a built-in pre- and post-processor. This would prove useful in any situation where repeated simulations are required, such as a parametric study of several DAI design parameters. In large functions, where MATLAB code is a better choice, an embedded MATLAB function block is used within the block diagram.

Also, Prof. Labus and Dr. Prantil are valuable resources as advisors. Prof. Labus, by his knowledge and experience in water jet technology, will be able to help hone the DAI model in on a realistic, accurate, and manufacturable solution. Dr. Prantil's strong background in numerical methods will help the DAI model through computational issues that may arise and as well as critical decision making with regards to modeling techniques.

The DAI model does not require any special computing equipment as it has not even come close to the limits of the standard MSOE laptops. All the simulations run with reasonable time steps have taken less than 5 minutes. The tools and the expert support available render this DAI model effort entirely feasible.

2.5.2 CTH Hydrocode Model Feasibility

The model required to simulate a water jet impact on the surface of a brittle material requires the basics of the conservation of mass, momentum, and energy. In addition, the model in development also requires the ability to handle strong field gradients caused by fluid-solid material interactions and also requires a complex material failure model to accurately predict the micro- and macro-scale failure of the brittle material. Dr. Prantil offered his expertise in simulations by suggesting the pursuit of two possible pieces of software: LS-DYNA and CTH.

LS-DYNA is used widely in areas such as automotive crashworthiness, metal forming, and aerospace industries. LS-DYNA is also well equipped to handle nonlinear modeling including failure analysis of concrete and soils interacting with the water jet being very applicable to the desired model [11]. However, LS-DYNA comes at a considerable monetary cost and therefore could not be obtained for the desired simulation.

The second code Dr. Prantil suggested was CTH, which has the ability to model nonlinear systems in addition to containing failure models for brittle materials. CTH was pursued since free academic licensing is available to institutions under strict export control. Further information regarding CTH is not available to the general public and will be disclosed to the team once the appropriate documentation has been submitted to Sandia National Laboratories.

2.5.3 Concrete Fracture Feasibility

A simple adiabatic compression calculation was performed to ensure the energy stored in the compressed Nitrogen is at least the desired amount of energy to be used in fracturing the concrete. The calculated storage energy in the Nitrogen compression was compared to Fig. 6(a) and the

average energy created from the realistic DAI designs was approximately the same as similar experimental devices at $5 \times 10^4 Nm$. The calculations also showed that the compression pressure required is within realistic limits in comparison with properties of available material of the DAI. Also, the volume of the chamber that would need to be compressed is within limits of a realistic DAI design.

After the initial compression calculations were performed, a simple model of the DAI was created using MATLAB/Simulink. With a variety of nozzle diameters and piston weights specified by Prof. Labus, the model achieved flow rates between 87.6 L/min and 350 L/min, which are reasonable according to Fig. 6.

3 Detailed Model Design - Overview

The scope of the project includes several elements, as shown in Fig. 10: a model of the water jet delivery device (DAI Model), a static-boundary time-dependent CFD simulation to predict boundary forces on the bottle walls caused by the impinging jet (STAR-CCM+ Simulation), and a full scale simulation of the water jet causing material failure (CTH Hydrocode).

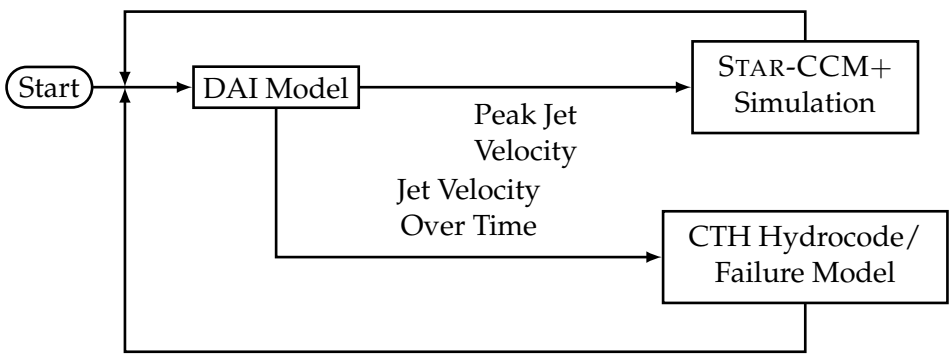

Figure 10: Overall Project Workflow

The DAI model outputs water jet velocity and mass flow to each model. The STAR-CCM+ is run as a transient simulation in order to establish the flow through the entire bottle. However, the desired forces are recorded once the simulation reaches a quasi-steady state. The CTH Hydrocode model will be a full transient Eulerian analysis starting without a pre-defined bottle shape. Each model/simulation is explained in further detail in Sections 4 to 6.

4 Detailed Model Design - DAI Model

The purpose of the DAI (differential area intensifier) model is to provide a realistic jet velocity as a function of time as an input to the CFD and hydrocode models. The DAI model would allow the design of a machine that could provide a water jet pulse required for maximum material removal with minimum energy input.

A stiff solver (`ode23s`) was used because the DAI models a rapidly changing water pressure and the default Runge-Kutta type solver (`ode45`) diverged in most cases.

4.1 Model Assumptions

Three models were developed, each assuming different constraints on water compressibility: constant compressibility, variable compressibility, and incompressible. The following assumptions were made for all three models:

- The driving gas is ideal,
- The expansion of the driving gas is isentropic (adiabatic and reversible),
- The driving gas instantaneously acts on the driving piston,
- The nozzle can be modeled as an orifice,
- There are no flow losses within the DAI (except within the cushioning mechanism (Section 4.4)), and
- None of the seals leak.

During Winter Quarter, the final variable compressibility model from Fall Quarter was updated and used for all simulations from then through Spring Quarter.

4.2 Variable Compressibility Model with Cushion Dynamics and Friction

To obtain the basis for the model, differential equations were derived from mass and force balances. Equation (1) was derived from continuity, accounting for water compression.

$$\dot{m}_{\text{out}} = \underbrace{-\frac{\rho V}{\beta}\frac{\mathrm{d}P}{\mathrm{d}t}}_{\text{compressible term}} + \underbrace{\rho A_p \frac{\mathrm{d}x}{\mathrm{d}t}}_{\text{control volume expansion}} \tag{1}$$

Using a free body diagram on the driving piston (Figure 11) and Newton's laws of motion, it can be shown that

$$M_P \frac{\mathrm{d}^2 x}{\mathrm{d}t^2} = P_{Dg} A_D + M_P g - A_P P_g - P_s A_s - F_f. \tag{2}$$

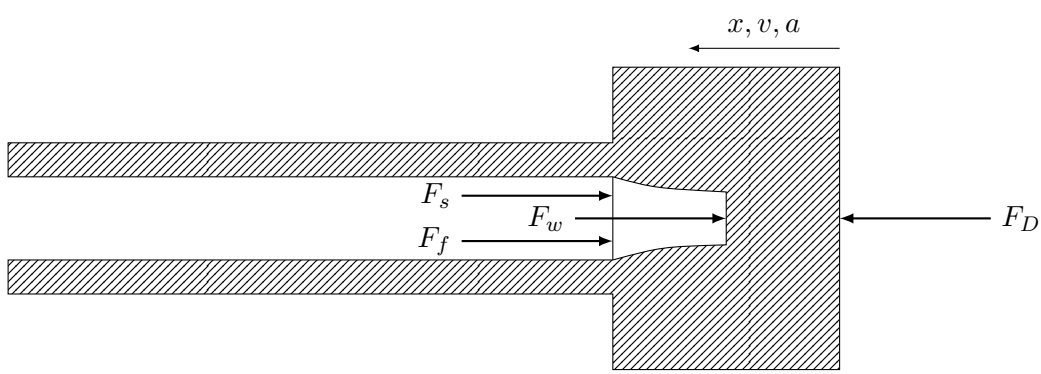

Figure 11: Free Body Diagram of DAI Piston

The driving pressure in an isentropic expansion is given by

$$P_{Da} = P_{D0}\left(\frac{V_{D0}}{V_{D0} - A_D x}\right)^{\gamma}. \tag{3}$$

Equation (4), used to model the nozzle, describes the flow through an orifice. The density used in Eq. (4) was the density of the water at the nozzle exit (atmospheric pressure).

$$\dot{m}_{\text{out}} = \rho Q_{\text{orifice}} = \rho C_o A_n \sqrt{\frac{2P_g}{\rho}} \tag{4}$$

Equations (5) and (6) are permutations of Eqs. (1) and (2), respectively, with geometrical relationships and Eq. (4) substituted.

$$\frac{\mathrm{d}P}{\mathrm{d}t} = \beta \frac{A_p \dfrac{\mathrm{d}x}{\mathrm{d}t} - C_o A_n \sqrt{\dfrac{2P_g}{\rho}}}{V_0 - A_P x} \tag{5}$$

$$\frac{\mathrm{d}^2 x}{\mathrm{d}t^2} = P_{Dg}\frac{A_D}{M_P} - P_g \frac{A_P}{M_P} + g \tag{6}$$

Equations (3) to (6) were solved simultaneously in MATLAB/Simulink.

The bulk modulus was defined by the methods discussed in Section 2.3.4. The Simulink block diagram for the variable compressibility DAI model and the MATLAB code are in Appendix B.

4.3 Friction Model

A Coulomb friction model is included in the DAI model. This friction force comes from a high pressure seal used to keep the water from leaving the high pressure cylinder (Figure 12). The seal is a beryllium-copper ring that is elastically expanded against the high pressure cylinder walls when the water is pressurized. According to the work done by Garity [5], this friction force is large enough to consider all others negligible. Therefore, no other friction forces were included in the model. The equations for the friction model (Equations (7) and (8)) were obtained from Garity [5]. Equation (7) treats the high pressure cylinder and the high pressure seal as thick-walled pressure vessels. Equation (8) calculates the friction force based on the pressure of the seal against the high pressure cylinder.

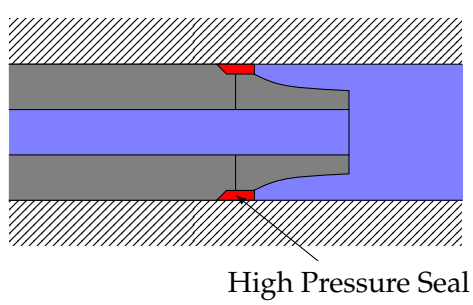

Figure 12: Beryllium-Copper High Pressure Seal

$$P_{\text{cont}} = \frac{\dfrac{2 r_{so} {r_{si}}^2 P}{E_s \left({r_{so}}^2 - {r_{si}}^2\right)} - r_{\text{clear}}}{\dfrac{\left(1-\nu_{\text{seal}}\right) {r_{so}}^3 + \left(1+\nu_{\text{seal}}\right) r_{so} {r_{si}}^2}{E_s \left({r_{so}}^2 - {r_{si}}^2\right)} + \dfrac{r_{si}\left(\left(1-\nu_{\text{barrel}}\right) {r_{bi}}^2 + \left(1+\nu_{\text{barrel}}\right) {r_{so}}^2\right)}{E_b \left({r_{bo}}^2 - {r_{bi}}^2\right)}} \tag{7}$$

$$F_f = 2\pi \mu r_{so} t_s P_{\text{cont}} \tag{8}$$

The Coulomb friction model required some unique modeling techniques. In most DAI simulations, the piston oscillates because the water acts as a spring under the high pressures calculated. This means the velocity is changing directions and therefore, so must the friction force (as it must always oppose the direction of motion). This becomes an issue if ever the piston is at a low velocity without largely imbalanced pressure forces on it. In these situations, the calculated frictional force can be much larger than any other force acting on the piston. If the friction force is balanced by dynamic forces in slowing the piston down it is entirely reasonable that friction can be the greatest force. However, if the piston's velocity is low enough, the velocity can change direction in one time step by means of the friction force alone. The change in velocity causes the friction force to change direction and accelerate the piston in the other direction, once again changing the direction of motion. The chattering described is pictured in Fig. 13. This chattering continues until another force can overcome the frictional force (which usually means that enough water has left the high pressure cylinder to decrease the water pressure). This chattering is completely non-physical because friction cannot induce motion, it can only impede motion. Even with decreasing time steps the issue does not subside. The numerical chattering simply happens on a finer scale. The chattering affected the output results (mass flow and jet velocity vs. time) less than 0.01%, but it made simulations take significantly longer because they were forced to run at the minimum time step for a portion of the simulation. It also produced unrealistic force, velocity, and acceleration plots such as those in Fig. 13.

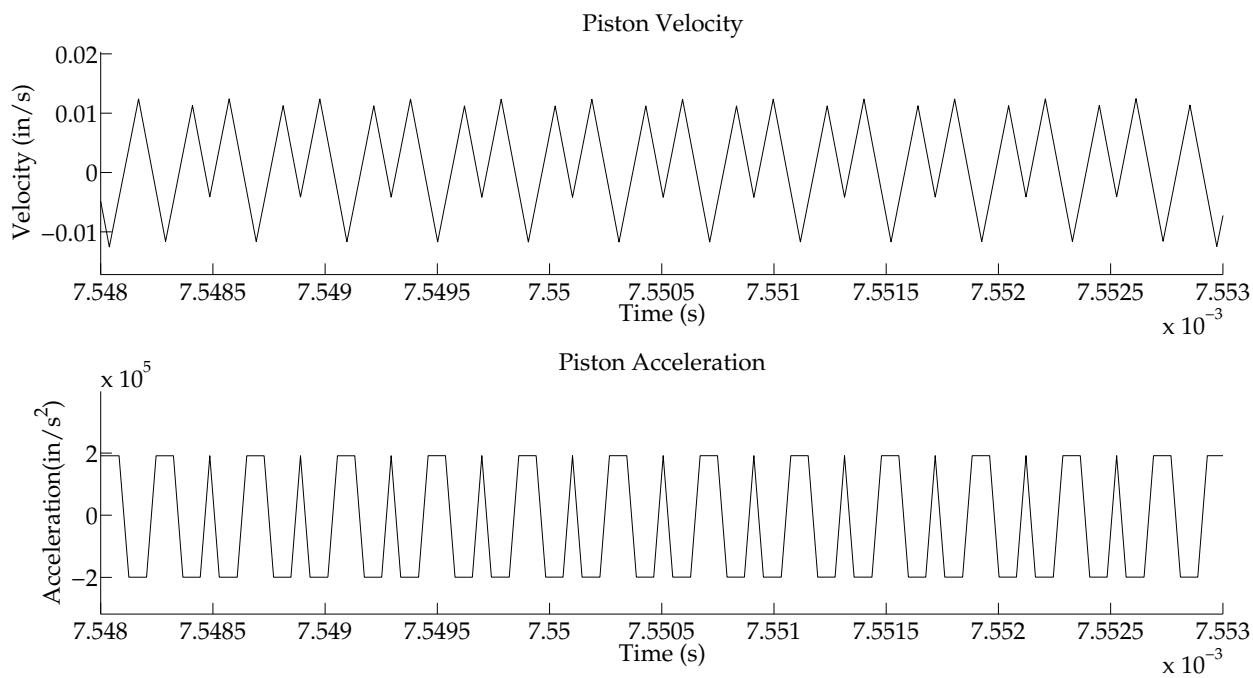

Figure 13: Effects of Friction Chattering

Since Coulomb friction can physically hold the piston in a complete stop, especially if static friction is considered, the model includes provisions to allow for this. A piston speed was chosen that was small enough to consider the piston stopped, defined by the acceptable error in jet mass flow, as shown in Eq. (9).

$$\varepsilon_{\text{acceptable}} = \frac{\Delta \dot{m}_{\text{out}}}{\dot{m}_I} = \frac{\Delta \dot{x}}{\dot{x}_{\max}} = \frac{v_{\text{small}}}{\dot{x}_{\max}} \Rightarrow \frac{\Delta \dot{m}_{\text{out}}^{\text{acceptable}}}{\rho A_P} = v_{\text{small}} \tag{9}$$

To prevent chattering, the friction force was limited at speeds below the low speed limit. Once the absolute value of the velocity of the piston is within the low speed range (Point 2 in Fig. 14) the frictional force is assigned a value equal to the sum of all the other forces acting on the piston as long as the maximum possible friction force exceeds the sum of the other forces. The flowchart in Fig. 15 shows the logic followed in the model. Even with the low speed condition, the minimum step size must still be small enough to keep the calculated piston velocity from 'jumping' the low speed range.

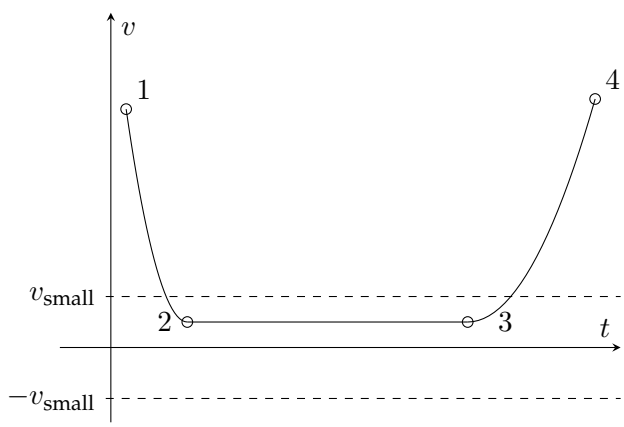

1. All forces acting on the piston normally
2. Equate friction to the sum of all other forces
3. Sum of other forces exceeds maximum friction force
4. All forces acting normally again

Figure 14: Chatter Reduction Logic

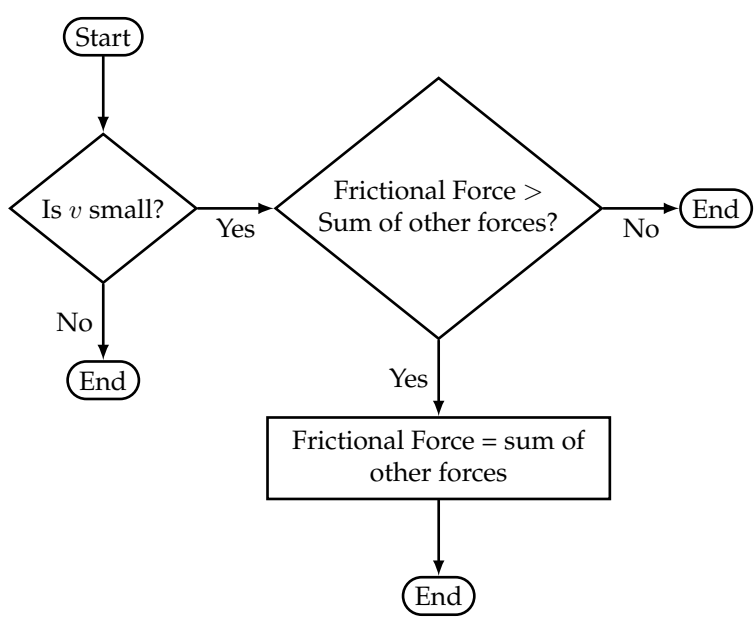

Figure 15: Chatter Reduction Logic Flowchart

4.4 Cushion Model

The DAI design contains a cushion at the end of its stroke, which decelerates the piston before it impacts hard boundaries. This cushion works by trapping water and forcing it through gaps and orifices so that there is an increase in pressure to oppose the piston's motion. The current cushion model is that of a piccolo cushion, which contains a series of orifices that are covered up as the piston reaches the limit of its motion. Figure 16 shows how a piccolo cushion works.

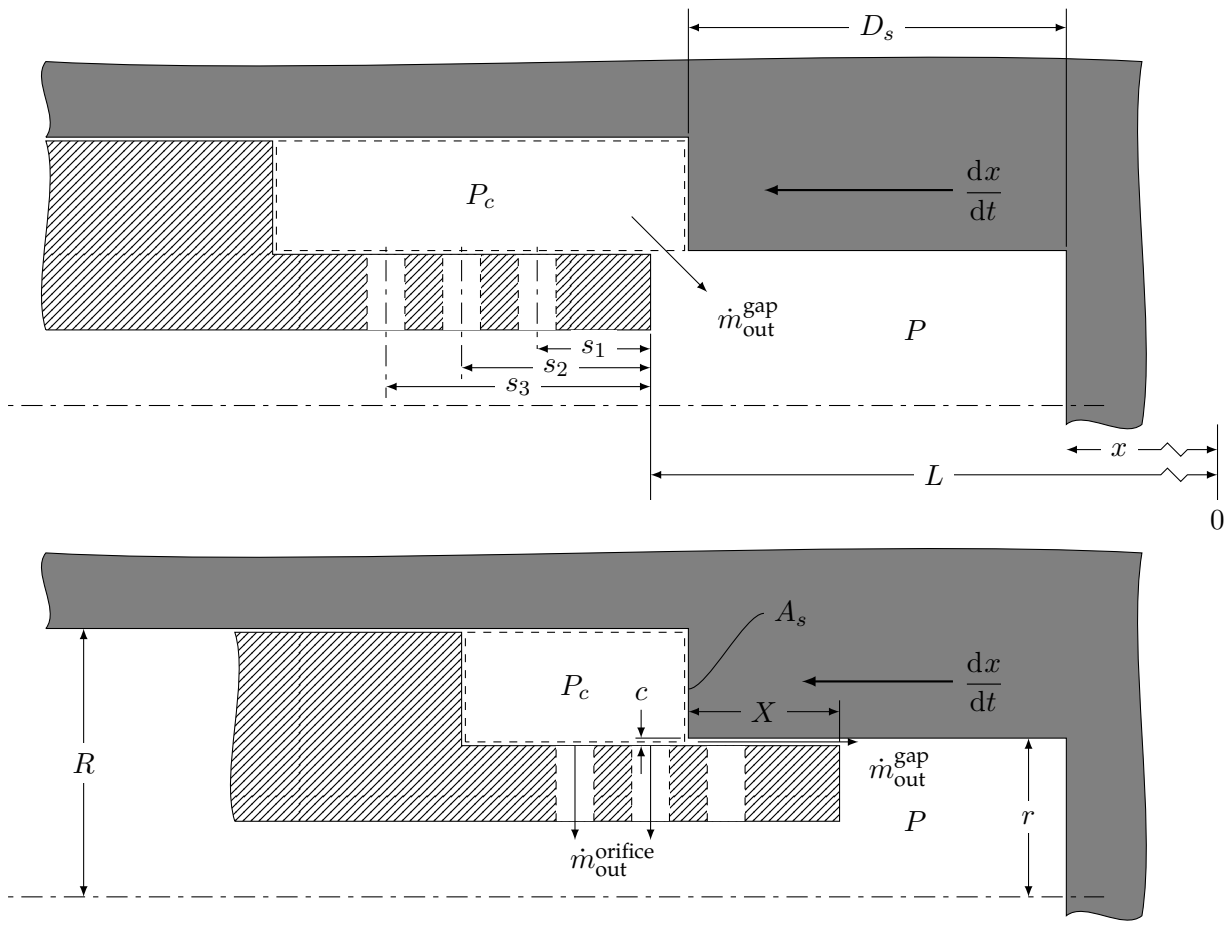

Figure 16: Piccolo Cushion Operation and Dimensions

The physics of the cushion are similar to that of the high pressure cylinder. Therefore, the derivation of the governing equations can start with Eq. (1), where the mass flow out of the cushion control volume is equal to the sum of the mass flow through the gap and the mass flow through the orifices. Flow through the gap can be treated as turbulent orifice flow per Merritt [14], and is defined by Eq. (10). The flow through the orifices is defined by Eq. (11) and depends on the number of orifices that are open. The number of orifices open is defined by Eq. (13).

$$\dot{m}_{\text{gap}} = \rho 2\pi r c C_{og} \sqrt{\frac{2\left(P_c - P\right)}{\rho}} \tag{10}$$

$$\dot{m}_{\text{orifices}} = \left(\rho A_{os} C_{os} \sqrt{\frac{2\left(P_c - P\right)}{\rho}}\right) n_o(x) \tag{11}$$

$$\dot{m}_{\text{out}} = \dot{m}_{\text{gap}} + \dot{m}_{\text{orifices}} \tag{12}$$

$$n_o(x) = \underbrace{NM}_{\text{total orifices}} - \underbrace{\sum_{i=1}^{N} \overbrace{u\left(X - s_i\right)}^{\text{unit step}} M}_{\text{closed orifices}} = M\left(N - \sum_{i=1}^{N} u\left(X - s_i\right)\right) \tag{13}$$

Combination of Eqs. (1) and (10) to (13) yields Eq. (14), describing the time derivative of the cushion pressure, P_c. This equation is similar to Eq. (5), and shows the change in control volume and the flow out. Equation (14) was redefined in terms of the stopping force P_s, which is defined as the difference between the water pressure in the high pressure cylinder and the water pressure in the cushion as shown in Eqs. (15) and (16). Equations (15) and (16) substituted into Eq. (14) produce Eq. (17).

$$\frac{\mathrm{d}P_c}{\mathrm{d}t} = \frac{\beta(P)}{V_{s0} - A_s X}\left(A_s \frac{\mathrm{d}x}{\mathrm{d}t} - 2\pi r c C_{og}\sqrt{\frac{2\left(P_c - P\right)}{\rho}} - n_o(x) A_{os} C_{os}\sqrt{\frac{2\left(P_c - P\right)}{\rho}}\right) \tag{14}$$

$$P_s = P_c - P \tag{15}$$

$$\frac{\mathrm{d}P_s}{\mathrm{d}t} = \frac{\mathrm{d}P_c}{\mathrm{d}t} - \frac{\mathrm{d}P}{\mathrm{d}t} \tag{16}$$

$$\frac{\mathrm{d}P_s}{\mathrm{d}t} = \frac{\beta(P)}{V_{s0} - A_s X}\left(A_s \frac{\mathrm{d}x}{\mathrm{d}t} - 2\pi r c C_{og}\sqrt{\frac{2P_s}{\rho}} - n_o(x) A_{os} C_{os}\sqrt{\frac{2P_s}{\rho}}\right) - \frac{\mathrm{d}P}{\mathrm{d}t} \tag{17}$$

A condition was included in the model that allowed for P_s to be negative. This means that water is flowing into the cushion instead of out of the cushion, which can occur if the piston is still oscillating when the cushion engages. In such a case Eq. (17) becomes Eq. (18).

$$\frac{\mathrm{d}P_s}{\mathrm{d}t} = \frac{\beta(P)}{V_{s0} - A_s X}\left(A_s \frac{\mathrm{d}x}{\mathrm{d}t} + 2\pi r c C_{og}\sqrt{\frac{2\left|P_s\right|}{\rho}} + n_o(x) A_{os} C_{os}\sqrt{\frac{2|P_s|}{\rho}}\right) - \frac{\mathrm{d}P}{\mathrm{d}t} \tag{18}$$

Another feature added to the model is what was termed the 'cushion approach'. This accounts for the fact that as the piston approaches the point in its stroke where the cushion engages, there is a gap closing that is much larger than the cushion gap but is still capable of restricting flow enough to raise the cushion pressure. Without the cushion approach, this part of the model becomes extremely stiff and can lead to simulation failures if time steps are not extremely small. For this reason, Eq. (17) is evaluated before the cushion engages. However, the gap width c is replaced by the large gap shown and defined in Fig. 17. The point at which Eq. (17) is first evaluated is the cushion approach factor times the gap width. Even with the 'cushion approach', the model is still stiff, because when Eq. (17) is evaluated for the first time, the stopping pressure is zero. Therefore, the stopping pressure was assigned an initial value that would not affect the rest of the simulation (1×10^{-6} times the intensified pressure) to smooth out this change.

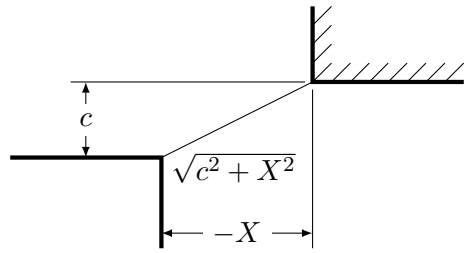

Figure 17: Cushion Gap Hypotenuse Calculation

4.5 Dimensional Analysis

Since each CTH simulation takes several days to complete, care must be taken in selecting jet velocity profiles to test. Dimensional analysis allows the jet velocity profiles and parameters to be analyzed at in a way that prevents repeats of tests that are effectively the same. Rebuilding the DAI simulation using dimensionless parameters would also make the DAI simulation less computationally intensive. The governing equations of the DAI were non-dimensionalized and quantities for non-dimensionalization were defined so that the CTH simulations can be planned more tactfully. Non-dimensionalization was performed by comparing states within the DAI model to properties under the intensified condition. This is the condition when the initial driving pressure is acting on the driving piston and the water is incompressible.

The constants used for non-dimensionalization are listed in Table 2. The intensified pressure is the pressure that would be measured in the high pressure cylinder if the nozzle was blocked off and the initial driving pressure was acting on the driving piston. The intensified mass flow is the flow rate of water through the nozzle when the intensified pressure is present in the water chamber. The intensified velocity is the jet velocity present under intensified flow conditions. Intensified piston velocity is the velocity that the piston must move at to sustain intensified flow assuming the density of water remains constant. Finally, the initial acceleration is the ideal acceleration experienced by the piston due to the driving pressure at the instant the driving pressure begins to act on the piston. Equations (19) to (23) present the non-dimensionalized forms of the governing equations.

$$\frac{\ddot{x}}{a_0} = \frac{P_D}{P_{D0}} + \frac{g}{a_0} - \frac{P}{P_I} - \frac{P_s A_s}{P_{D0} A_D} - \frac{F_f(P)}{P_{D0} A_D} \tag{19}$$

$$\frac{P_D}{P_{D0}} = \left(\frac{V_{D0}}{V_{D0} + A_D x}\right)^{\gamma} \tag{20}$$

$$\frac{\dot{m}_{\text{out}}}{\dot{m}_{\text{in}}} = \frac{\sqrt{P}}{\sqrt{P_I}} \tag{21}$$

$$\frac{\frac{\mathrm{d}P}{\mathrm{d}t}}{\left.\frac{\mathrm{d}P}{\mathrm{d}t}\right|_I} = \frac{\beta(P)}{\beta_{\text{atm}}} C_o \frac{\frac{\dot{x}}{\dot{x}_I} - \sqrt{\frac{P}{P_I}}}{\frac{V_0}{A_P L} - \frac{x}{L}} \tag{22}$$

$$\frac{\frac{\mathrm{d}P_s}{\mathrm{d}t}}{\left.\frac{\mathrm{d}P_s}{\mathrm{d}t}\right|_I} = \frac{\beta(P)}{\beta_{\text{atm}}} \frac{A_s L}{V_{s0} - A_s X} \left(\frac{\frac{\mathrm{d}x}{\mathrm{d}t}}{\dot{x}_I} - \frac{1}{C_o} \frac{A_P}{A_n} \sqrt{\frac{P_s}{P_I}} \left(C_{og} \frac{2\pi r c}{A_s} + n_o(x) C_{os} \frac{A_{os}}{A_s} \right) \right) - \frac{\frac{\mathrm{d}P}{\mathrm{d}t}}{\left.\frac{\mathrm{d}P_s}{\mathrm{d}t}\right|_I} \tag{23}$$

Table 2: Properties Used for Non-Dimensionalization

Property Name	Definition
Bulk Modulus at Atmospheric Pressure	β_{atm}
Intensified Pressure	$P_I = \frac{P_{D0} A_D}{A_P}$
Initial Driving Pressure	P_{D0}
Intensified Pressure Rate	$\left.\frac{\mathrm{d}P}{\mathrm{d}t}\right\|_I = \frac{\dot{x}_I \beta_{atm}}{L}$
Intensified Jet Mass Flow Rate	$\dot{m}_I = \rho C_o A_n \sqrt{\frac{2P_I}{\rho}}$
Intensified Jet Velocity	$V_I = C_o \sqrt{\frac{2P_I}{\rho}}$
Stroke	L
Intensified Piston Velocity	$\dot{x}_I = C_o \frac{A_n}{A_P} \sqrt{\frac{2P_I}{\rho}}$
Initial Acceleration	$a_0 = \frac{P_{D0} A_D}{M_P}$
Intensified Force	$F_I = P_{D0} A_D$
Intensified Time	$t_I = \frac{L}{\dot{x}_I}$

4.6 Validation

An incompressible model was created for the purpose of verifying the compressible models. Equations (4), (3), and (6) were used to validate the end behavior of the compressibility model. Equation (5) was replaced by Eq. (24) to express incompressibility. This was done by letting the compressible term in Eq. (1) equal zero.

$$P = \left(\frac{A_P}{C_o A_n}\right)^2 \frac{\rho}{2} \left(\frac{\mathrm{d}x}{\mathrm{d}t}\right)^2 \tag{24}$$

The DAI models were compared against experimental data and other models. The pressure profiles (water pressure vs. time) of the DAI models were on the same order of magnitude as pressure profiles shown in the experimental data by Burns [9]. The pressure profile for the incompressible DAI model also qualitatively matched the work by Garity [5]. A direct comparison was not performed because the models were not identical in nature.

4.7 Future Work

In order to make the numerical model of the DAI more realistic, a number of changes can be made:

- Polytropic ($PV^n =$ constant) of Van der Waals expansion of driving gas
- Seal leakage
- Smoother piston start to mimic actual DAI operation

Since the driving gas expansion is currently modeled as an isentropic ideal gas, the model could be improved by finding a suitable polytropic relationship. Also, since the driving gas is at a low temperature and a high pressure, a different gas model (such as a van der Waals gas) may be applicable. Leakage of the high pressure seal was modeled by Garity, so this aspect of the DAI may be beneficial to investigate. It may also be necessary to check if leakage anywhere else can be expected.

5 Detailed Model Design - STAR-CCM+ Model

STAR-CCM+ is a CFD package capable of multi-fluid flows. The main capabilities of STAR-CCM+ in relation to this project are the ability to simulate the transient flows of water and air, including cavitation of water at static pressures below 0.256 psia at 60 °F.

The goal of using STAR-CCM+ was to better predict the desired bottle geometry and jet characteristics required to cause macro failure of the concrete. Although STAR-CCM+ cannot directly predict material failure because of static boundary walls, the normal and shear forces on the bottom of the bottle and sides at quasi-steady state water flow are used to help predict material failure. Figure 18 shows that all faces are subject to shear and pressure forces contributing to macro material failure of an axisymmetric model.

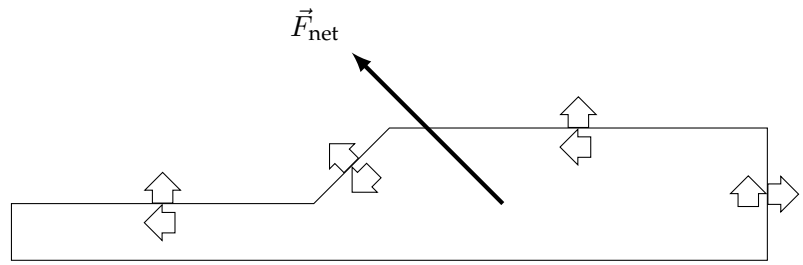

Figure 18: Hydrodynamic Forces on Bottle Geometry

The forces generated in the STAR-CCM+ model are compared to results from an experiment conducted by Ryhming [2] in which an analogous mechanical system was used to cause material failure. Figure 7 presents Ryhming's analogous design. Ryhming uses a hydraulic wedge to push off the bottom of the hole and create axial and radial force summing to the force vector $\vec{F}_{\text{net}}$.

The comparison of the STAR-CCM+ model results are made with both the magnitude of the force and the angle of the force relative to the incoming jet. If the angle of the force predicted by the STAR-CCM+ model is less than the angle predicted by Ryhming, the material should exhibit macro-scale failure.

For a better understanding of the STAR-CCM+ simulation, the boundary conditions are shown in Fig. 19.

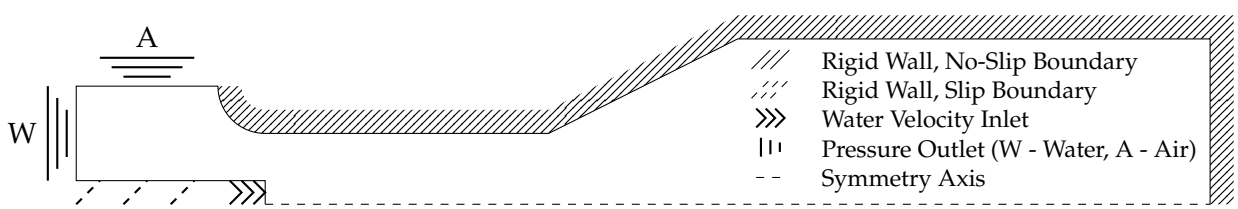

Figure 19: CFD Simulation Boundary Conditions

The simulation consists of transient two phase (air and water) flow through the bottle geometry. The bottle is initially filled with air with a constant velocity inlet of water and separate exit pressure boundaries allowing air and water to leave the computational domain. The shear and pressure forces are recorded on the desired walls at each consecutive time step. Figure 20 depicts a simulation at various time steps, showing the progress of water though the geometry.

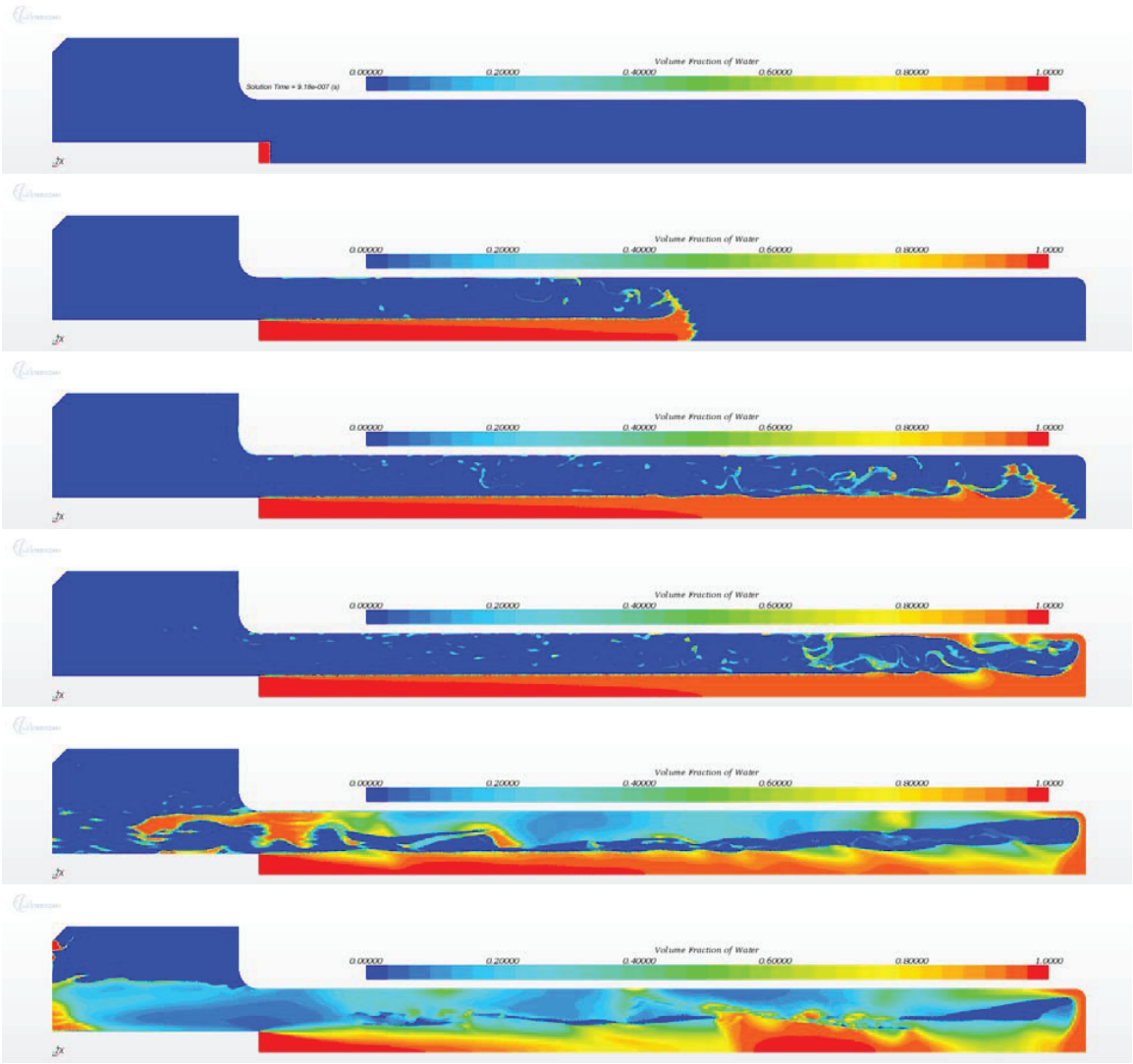

Figure 20: Water Flow Progress

The simulation shown in Fig. 20 had $\theta = 90°$ and $R_2 = R_1$. The results of this simulation yielded forces an order of magnitude lower than required for failure according to Ryhming. As discussed in Section 2.4, several key dynamics of the problem are not captured in the STAR-CCM+ models, so the remainder of simulations must be conducted with the CTH hydrocode, discussed in Section 6.

6 Detailed Model Design - CTH Hydrocode

6.1 CTH Overview

CTH is designed to simulate shock wave propagation and solid or liquid material flow in one, two, or three dimensions. Momentum and energy conservations are used in a two-step Lagrangian-Eulerian method. In the first step, the mesh deforms under the conservation laws of energy and mass. The second step remaps the distorted mesh back to a Lagrangian mesh via Eulerian methods. A general flowchart is shown in Fig. 21.

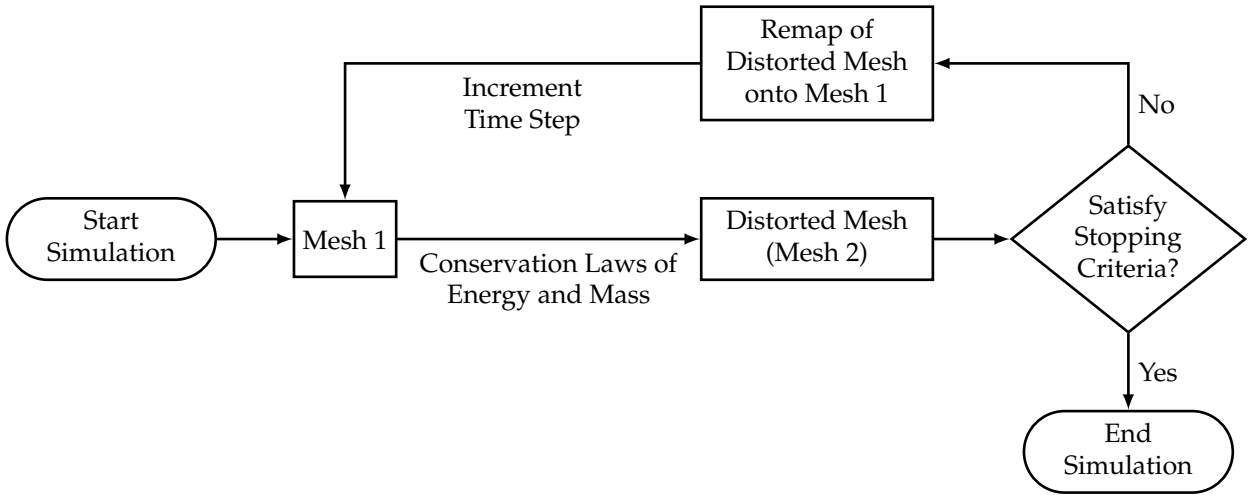

Figure 21: Arbitrary Langrangian-Eulerian Time Step

Materials in the simulation are represented though equations of state in either a tabular or analytical form.

6.2 Background

6.2.1 Eulerian vs. Lagrangian Mesh

With almost any computational model the domain of the problem must be discretized, or in other words meshed. The mesh allows for conservation laws to be applied to the elements of the mesh to accurately simulate the response of materials to various situations. CTH utilizes a hybrid mesh method–holding to the conservation laws of mass and energy while accurately predicting large deformations. Figure 22 shows the difference between a Lagrangian and Eulerian mesh shown as (a) and (b), respectively. The primary mesh in CTH is Lagrangian, where only the objects of concern are meshed and the cells become skewed with the deformation of the object. However, the motion of the material is computed through an Eulerian method whose mesh represents the parts and general area of interest so that material can flow through the mesh.

The advantage of using a Lagrangian mesh is that it more accurately tracks the interface of materials or objects, where the Eulerian mesh allows several materials to exist in one element and averages the associated properties. The advantage of an Eulerian mesh is that it keeps the cell size

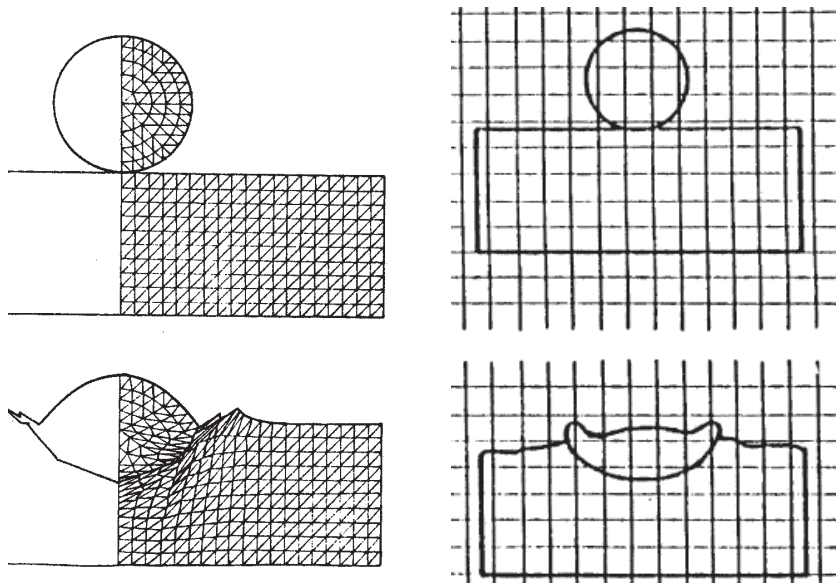

(a) (b)

Figure 22: Computational Domain Representations: (a) Lagrangian, (b) Eulerian [3]

and skew constant and therefore is less prone to numerical instability compared to a skewed element in the Lagrangian mesh. Since CTH uses an Eulerian method to map back to a Lagrangian mesh, interface tracking algorithms may be utilized to prevent interface distortion.

6.3 Material Types

Four material models are used in the water jet simulation using CTH. Each material type takes into account specific methods of energy transfer and element dynamics. The basic input and output structure of the model is shown in Fig. 23, with temperature T and density ρ as inputs, and pressure p and internal energy u as outputs.

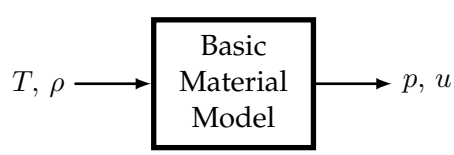

Figure 23: Material Model Inputs and Outputs

More complicated models, such as the BFK model mentioned in Section 6.3.1, require additional inputs such as the degradation of the material which influences properties such as compressive strength.

6.3.1 BFK Concrete Model

The concrete model used in the simulation is the BFK (brittle fracture kinetics) Model for Concrete [15]. The model contains equations of state for a 'SAC5' concrete, similar to road grade concrete,

formed from experimental data. The BFK model takes into account the damage associated with a given material cell and how the damage impacts the properties of the material. For instance, as a cell increases in damage the compressive strength of the cell increases linearly due to a percent of the material being considered a void material, which is discussed in Section 6.3.3. In addition, if a cell face fails in tension the model will track the broken interface and not allow normal tensile or shear forces to be exerted on that cell face.

6.3.2 Water Model

The water and steam model is taken from SESAME CTH library of tabulated material data for a range of temperatures and densities.

Cavitation Model Unfortunately, CTH does not have a model for the cavitation of water. Further literature study will be required to determine the dependence of cavitation on parameters such as temperature, density, and fluid velocity generally seen in the simulations. Once a model of cavitation is developed, a multiphase equation of state will be created using the PANDA code included with the CTH software.

6.3.3 Void Material

The cells of the simulation can be filled with a material specified as void. This void material has no mass, is thermally insulating, and has a user specified constant pressure. The advantage of using void material is to decrease the number of cells evaluated in a time step. In the case of the BFK model the void material is used in the Eulerian method remeshing where a crack develops in a material.

After each simulation, the maximum and minimum values each model experiences will be compared to the range of experimental data to ensure material properties were not extrapolated at a maximum or minimum. Ideally, the material models will be valid for all temperatures and densities seen in the model.

6.4 Material Dynamics

The most important material dynamics to capture in the simulation is the erosion of the concrete. One primary method of erosion is shear force developed between the flowing water and the concrete surface. Another primary interaction is the erosion of the concrete due to spalling, which is a shedding of fine particles under a rapid loading. The spalling of the concrete is a result of the large force changes due to cavitation forming and disappearing. According to A. W. Momber in [16], cavitation can cause damage to a material through one or more of the methods listed, with the original research cited.

- Generation of shock waves due to symmetric bubble implosion [17]
- Formation of micro-jets due to non-symmetric bubble implosion [17]
- Formation of micro-jets due to shock-induced bubble collapse [18]

- Collapse of bubble clusters [19]

6.5 Loads/Constraints/Boundary Conditions

CTH has several standard boundary conditions and an associated type number. The boundary conditions applicable to the water jet impact simulation are discussed in Sections 6.5.1 to 6.5.4.

6.5.1 Symmetric Boundary (type 0 - symmetric)

The type 0 has a boundary normal velocity of zero. The water jet simulations will be setup as axisymmetric due to the axial symmetry of the water jet, concrete material, and material failure.

6.5.2 Extrapolated Pressure Boundary (type 3 - inflow)

The type 3 boundary condition is one where mass is allowed to flow into the mesh and the pressure in the boundary cell is extrapolated from the two adjacent cells. The inflow of mass will allow the boundary cells to have a specified velocity as a function of time. The velocity is specified from the DAI model as a magnitude associated with a time step. Also note that the velocity magnitude is constant in the radial direction at any given time step. The radius of the jet will be constant as specified from the radius input to the DAI model.

6.5.3 Sound Speed-Based Absorbing Boundary (type 1 - semi-infinite medium)

The type 1 boundary condition allows mass to flow in and out of the mesh as a transmitting boundary condition. This is desirable because modeling the response of the concrete can be unnecessarily time consuming. The mesh required to model a complete concrete slab would be extensive. The whole slab could be meshed, but the amount of cells involved would considerably increase the computation time of the simulation. Instead, one can narrow the area of studied concrete to a fraction of the real slab and place at the edges sound speed-based absorbing boundary conditions. The type 1 boundary condition can be thought of as a semi-infinite medium boundary condition allowing shock waves to travel through the material at the speed of sound and released from the mesh as if they kept traveling into the medium. Without this release, a normal fixed boundary condition would unrealistically reflect those waves back into the mesh.

6.5.4 Extrapolated Pressure Boundary Condition (type 2 - outlet)

The type 2 boundary condition allows mass to leave the mesh but not enter it. Eroded concrete and water are allowed to exit the mesh regardless of the volume fraction. Unlike the STAR-CCM+ formulation where separate boundaries were required for each material, in CTH, multiple materials can exit the computational domain through the same boundary.

6.6 Mesh

In a two-dimensional mesh, a shape or coordinates of points are specified. The mesh is first generated by initial mesh conditions, but is later influenced by adaptive mesh refinement and coarsening.

6.6.1 Initial Mesh

The initial mesh for the simulation is shown in Fig. 24, with boundary conditions as listed in Section 6.5. Note that the cell density grows toward the center axis of the geometry, with extra refinement in the areas where the cavity is expected to erode. Adaptive mesh refinement, detailed in Section 6.6.2, will be used to dynamically remesh as needed, ensuring computational effectiveness in areas of extreme stress or pressure gradients.

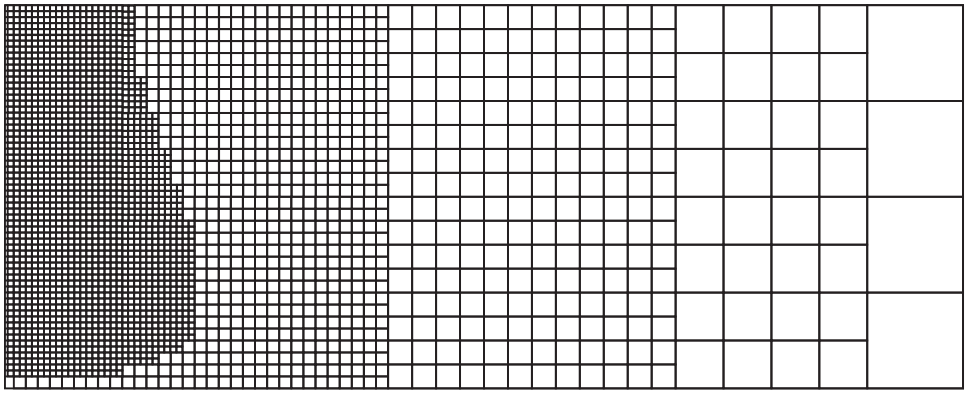

Figure 24: Example Initial Mesh for CTH Hydrocode Simulation

6.6.2 Adaptive Mesh Refinement

For greater computational efficiency and accuracy, CTH allows for both mesh refinement and mesh coarsening. Mesh refinement is defined as increasing the mesh density in an area of interest. For example, Fig. 25 shows a mesh with a significant amount of distortion that would have benefited from gradual mesh refinement to reduce cell skewness as the projectile impacted the target.

Mesh refinement allows greater accuracy in regions of high gradients, which can reduce computational instability, while coarsening helps to decrease overall computation time. If adaptive mesh refinement (AMR) is enabled, CTH will create mesh refinements every three time steps and coarsen every six time steps if necessary. Figure 26 shows: (a) an original mesh, and (b) a mesh that benefited from mesh rezoning to reduce skewness in the mesh of the target.

6.7 Time Step Control

The time step is calculated so that a shock wave traveling at the speed of sound through the smallest element of a material will take at least one time step to travel across the element. In

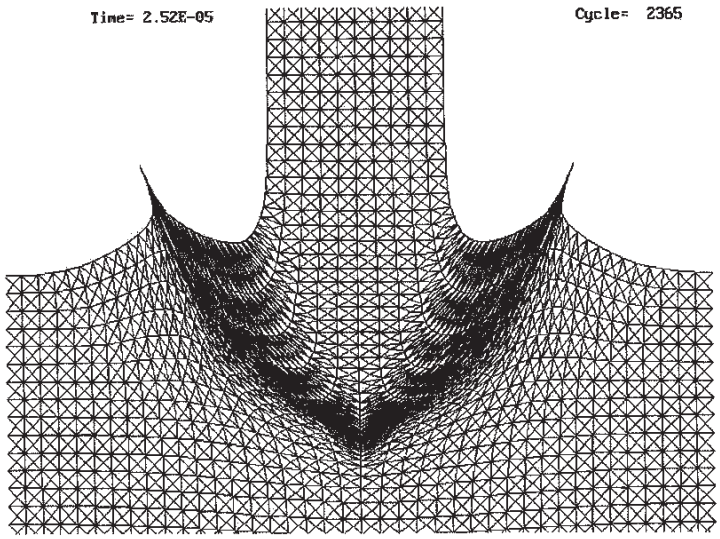

Figure 25: Extreme Mesh Distortion in Plate Perforation Calculation [3]

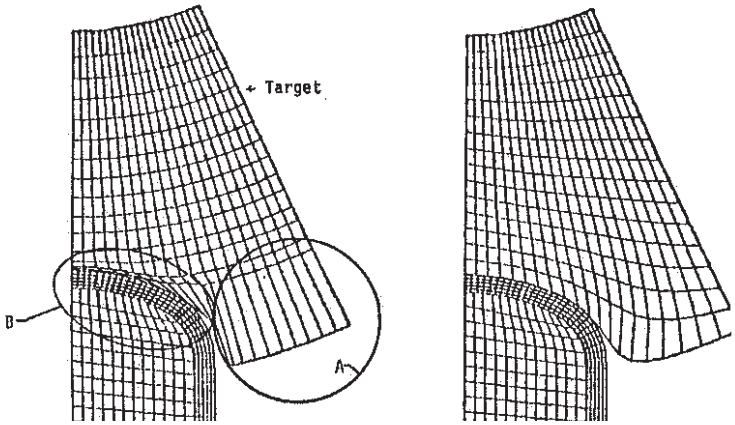

Figure 26: Rezoning Near Areas of Extreme Mesh Distortion [3]

addition, the velocity of the water jet will have to be taken into consideration so that the distance the water jet travels in one time step is less than the smallest element.

6.8 Model Verification

To verify the CTH model, the results will be compared to the experimental data presented by Ryhming [2]. If CTH predicts crack propagation from the base of the eroded cavity, the forces generated on the walls of the eroded surface should agree with the data which Ryhming obtained. If they do not, the CTH model should be checked for invalid assumptions or other modeling decisions which alter the physical nature of the problem.

In addition, Burns [9] took rubber casts of eroded cavities in concrete. These cavities are reproduced in Fig. 27, and show the different shapes produced for a water jet at different stand-off distances from the concrete surfaces. These images will be useful in comparing the erosion modeling of CTH to the physical phenomena.

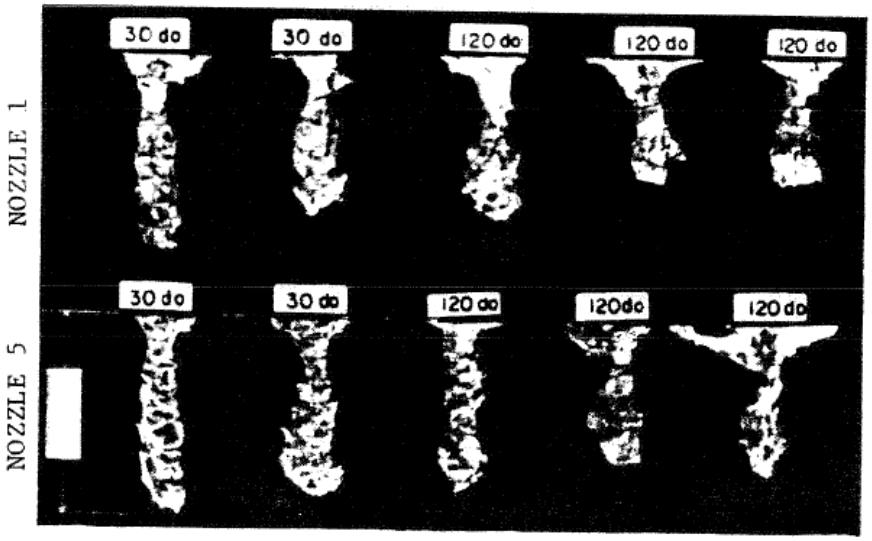

Figure 27: Eroded Cavity Shapes for Various Jet Stand-Off Distances [9]

To truly validate the model predictions, however, a physical DAI unit must be constructed and used in experiments. By studying the breakage in an actual experiment and comparing the model predictions, the validity and accuracy of the model can be determined.

7 Budget

The largest project cost has been the acquisition of a computer workstation capable of running the CTH Hydrocode. Two of the software packages used, STAR-CCM+ and MATLAB/Simulink, are already licensed for non-commercial use through MSOE Academic Licenses. Sandia National Laboratories has provided the CTH Hydrocode free of charge on an Academic Research license.

The literature review had no direct costs through the all quarters. All papers have been found in online databases or sourced through Inter-Library Loan. The Walter Schroeder Library (WSL) has been gracious enough to cover the cost of obtaining requested literature throughout the duration of the project.

The projected labor costs for the engineering effort are based on a standard rate of $25 per hour. The expected time required per quarter is:

- Fall Quarter: 100 hrs per student
- Winter Quarter: 100 hrs per student
- Spring Quarter: 150 hrs per student

For three students actively working on the project, this yields an estimated fictitious labor cost of $26,250.

Given the approximate costs listed above, a final budget for the project is $43,000. The final budget data are summarized in Table 3.

Table 3: Finalized Project Budget

Item	**Funding Source**	**Amount**
Workstation	ME Department	$17,000
CTH Hydrocode	Sandia National Labs	$0
Other Software	MSOE Academic Licenses	$0
Literature	Walter Schroeder Library	$0
Labor	ME Department	$26,000
Total		**$43,000**

8 Environmental Impact

The environmental impact and safety concerns of any potential DAI design are presented in Sections 8.1 to 8.4.

8.1 Materials Contained in Design

The differential area intensifier is made almost exclusively of metal so it is very recyclable. The steel, stainless steel, and beryllium copper are all recyclable. Nitrogen gas and biodegradable hydraulic fluid are also used in the operation of the DAI. The nitrogen gas can be safely expelled into the atmosphere or reused and the hydraulic fluid can be recycled. Finally, there are small concentrations of POLYOX, a long carbon chain polymer, mixed with the jet water to prevent fraying of the jet once it leaves the nozzle. This polymer is safe in the environment, especially in such low concentrations. The material safety data sheets (MSDS) for POLYOX and a generic hydraulic fluid are listed in Appendices F and G, respectively.

8.2 Special Handling Instructions

The DAI weighs approximately 500 lbf and should not be moved by hand. The DAI should only be moved with appropriate equipment such as a backhoe or a fork lift. Also the DAI is capable of firing in any orientation. Be aware of the orientation of the DAI and stay out of the line of fire.

The DAI is a powerful industrial machine and should be used with the same care as other heavy machinery. Firstly, the DAI is capable of pressures over 75,000 psi. These pressures are many times greater than those found in most machinery. Seal leakage could result in a dangerous high velocity jet of oil, water, or air and component failure could result in high velocity projectiles. Therefore, routine maintenance is vital to ensure the DAI can operate safely under these pressures. This includes regular inspection of bolt torques, ultrasonic inspection for cracks, and inspection for leaks. The high jet velocity also has the potential to propel concrete fragments into the air. All guards on the DAI should be in place to ensure material removed by the DAI does not harm the operator and others. Also, eye protection should be worn at all times, even when the guards are in place.

8.3 Special Storage Instructions

The DAI should not be stored in the cocked position. All energy forms must be brought to their lowest state before storage. Fill the DAI with oil to preserve all working parts for long term storage. In both cases the DAI should be stored over a container that will catch and contain any leaking fluids.

8.4 Disposal Instructions

The hydraulic fluid can be disposed of at a local government operated oil collection site. Most cities have such collection sites. Alternatively, some companies provide services to dispose of used oil properly. The metals can be recycled at a scrap yard.

9 Project Schedule

The project schedule, with all completed tasks, is presented in a Gantt chart, Fig. 28. The original Microsoft Project file containing this schedule is available from the authors. The schedule was delayed significantly due to CTH licensing issues and export control regulations. During Spring Quarter, the team worked to finish most of what was originally scheduled on time. The schedule has been updated to reflect all work completed at the end of Spring Quarter 2012.

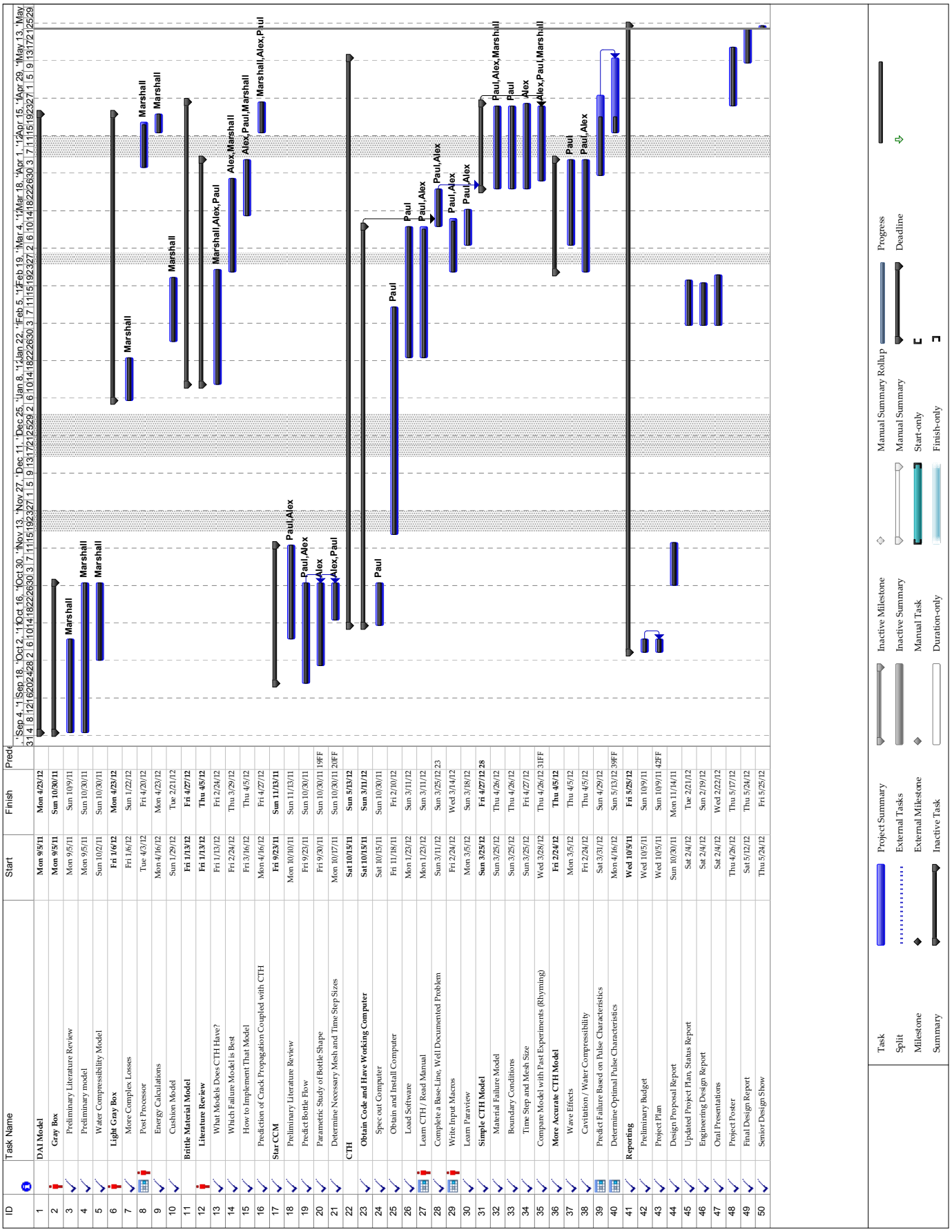

ID	Task Name	Start	Finish	Predecessors
1	**DAI Model**	**Mon 9/5/11**	**Mon 4/23/12**	
2	**Gray Box**	**Mon 9/5/11**	**Sun 10/30/11**	
3	Preliminary Literature Review	Mon 9/5/11	Sun 10/9/11	
4	Preliminary model	Mon 9/5/11	Sun 10/30/11	
5	Water Compressibility Model	Sun 10/2/11	Sun 10/30/11	
6	**Light Gray Box**	**Fri 1/6/12**	**Mon 4/23/12**	
7	More Complex Losses	Fri 1/6/12	Sun 1/22/12	
8	Post Processor	Tue 4/3/12	Fri 4/20/12	
9	Energy Calculations	Mon 4/16/12	Mon 4/23/12	
10	Cushion Model	Sun 1/29/12	Tue 2/21/12	
11	**Brittle Material Model**	**Fri 1/13/12**	**Fri 4/27/12**	
12	**Literature Review**	**Fri 1/13/12**	**Thu 4/5/12**	
13	What Models Does CTH Have?	Fri 1/13/12	Fri 2/24/12	
14	Which Failure Model is Best	Fri 2/24/12	Thu 3/29/12	
15	How to Implement That Model	Fri 3/16/12	Thu 4/5/12	
16	Prediction of Crack Propagation Coupled with CTH	Mon 4/16/12	Fri 4/27/12	
17	**Star CCM**	**Fri 9/23/11**	**Sun 11/13/11**	
18	Preliminary Literature Review	Mon 10/10/11	Sun 11/13/11	
19	Predict Bottle Flow	Fri 9/23/11	Sun 10/30/11	
20	Parametric Study of Bottle Shape	Fri 9/30/11	Sun 10/30/11	19FF
21	Determine Necessary Mesh and Time Step Sizes	Mon 10/17/11	Sun 10/30/11	20FF
22	**CTH**	**Sat 10/15/11**	**Sun 5/13/12**	
23	**Obtain Code and Have Working Computer**	**Sat 10/15/11**	**Sun 3/11/12**	
24	Spec out Computer	Sat 10/15/11	Sun 10/30/11	
25	Obtain and Install Computer	Fri 11/18/11	Fri 2/10/12	
26	Load Software	Mon 1/23/12	Sun 3/11/12	
27	Learn CTH / Read Manual	Mon 1/23/12	Sun 3/11/12	
28	Complete a Base-Line, Well Documented Problem	Sun 3/11/12	Sun 3/25/12	23
29	Write Input Macros	Fri 2/24/12	Wed 3/14/12	
30	Learn Paraview	Mon 3/5/12	Sun 3/18/12	
31	**Simple CTH Model**	**Sun 3/25/12**	**Fri 4/27/12**	**28**
32	Material Failure Model	Sun 3/25/12	Thu 4/26/12	
33	Boundary Conditions	Sun 3/25/12	Thu 4/26/12	
34	Time Step and Mesh Size	Sun 3/25/12	Fri 4/27/12	
35	Compare Model with Past Experiments (Rhyming)	Wed 3/28/12	Thu 4/26/12	31FF
36	**More Accurate CTH Model**	**Fri 2/24/12**	**Thu 4/5/12**	
37	Wave Effects	Mon 3/5/12	Thu 4/5/12	
38	Cavitation / Water Compressibility	Fri 2/24/12	Thu 4/5/12	
39	Predict Failure Based on Pulse Characteristics	Sat 3/31/12	Sun 4/29/12	
40	Determine Optimal Pulse Characteristics	Mon 4/16/12	Sun 5/13/12	39FF
41	**Reporting**	**Wed 10/5/11**	**Fri 5/25/12**	
42	Preliminary Budget	Wed 10/5/11	Sun 10/9/11	
43	Project Plan	Wed 10/5/11	Sun 10/9/11	42FF
44	Design Proposal Report	Sun 10/30/11	Mon 11/14/11	
45	Updated Project Plan, Status Report	Sat 2/4/12	Tue 2/21/12	
46	Engineering Design Report	Sat 2/4/12	Sun 2/19/12	
47	Oral Presentations	Sat 2/4/12	Wed 2/22/12	
48	Project Poster	Thu 4/26/12	Thu 5/17/12	
49	Final Design Report	Sat 5/12/12	Thu 5/24/12	
50	Senior Design Show	Thu 5/24/12	Fri 5/25/12	

Figure 28: Project Schedule

10 Results - DAI Model

The DAI model outputs are listed below. All outputs are functions of time.

- water pressure
- water pressure change with respect to time (referred to as pressure rate in this writing)
- piston displacement
- piston velocity
- water jet mass flow rate
- water mass expelled
- water jet velocity
- driving pressure
- stopping pressure
- stopping pressure rate
- water density
- total jet energy expelled

Figures 29 to 41 show outputs of the DAI model that was used as an input for the CTH simulation results discussed in Section 11. The DAI parameters used in this model are listed in Table 4. The results in Figs. 29 to 41 have been non-dimensionalized using the non-dimensional properties in Table 5. Table 6 shows how these properties are applied to the variables in non-dimensionalizing.

Table 4: DAI Model Parameters

Parameter	Value	Units
Initial Gas Pressure	2000	psi
Gas Compressed Volume	316	in^3
Driving Piston Diameter	9.4	in
Water Piston Diameter	2	in
Nozzle Diameter	2	mm
Stroke Length	5	in
Piston Mass	55	lbm

Table 5: Properties Used for Non-Dimensionalization

Non-Dimensionalization Property	Symbol	Value	Units
Intensified Pressure	P_I	44,180	psia
Initial Driving Pressure	P_{D0}	2,000	psig
Intensified Pressure Rate	$\left.\frac{\mathrm{d}P}{\mathrm{d}t}\right\|_I$	1,844,305	psi/s
Intensified Jet Mass Flow Rate	$\dot{m}_I$	0.104084	slugs/s
Intensified Jet Velocity	v_I	1589.04	ft/s
Stroke	L	5	in
Intensified Piston Velocity	$\dot{x}_I$	2.46314	ft/s
Initial Acceleration	a_0	81,192.8	ft/s^2
Intensified Force	F_I	138,795	lbf
Intensified Time	t_I	0.169169	s

Table 6: Definitions of Dimensionless Variables

Dimensionless Variable	Definition
Pressure	$\frac{P}{P_I}$
Pressure Rate	$\frac{\mathrm{d}P}{\mathrm{d}t}\left(\left.\frac{\mathrm{d}P}{\mathrm{d}t}\right\|_I\right)^{-1}$
Mass Flow Rate	$\frac{\dot{m}}{\dot{m}_I}$
Jet Velocity	$\frac{v}{v_I}$
Displacement	$\frac{x}{L}$
Piston Velocity	$\frac{\dot{x}}{\dot{x}_I}$
Acceleration	$\frac{a}{a_0}$
Force	$\frac{F}{F_I}$
Time	$\frac{t}{t_I}$

Of all the outputs of the DAI model, the jet profile (jet velocity vs. time) is of primary interest because it is used in CTH simulations. Figure 29 shows the properties of the jet generated by the DAI model that was used as an input for the CTH simulation results discussed in Section 11.

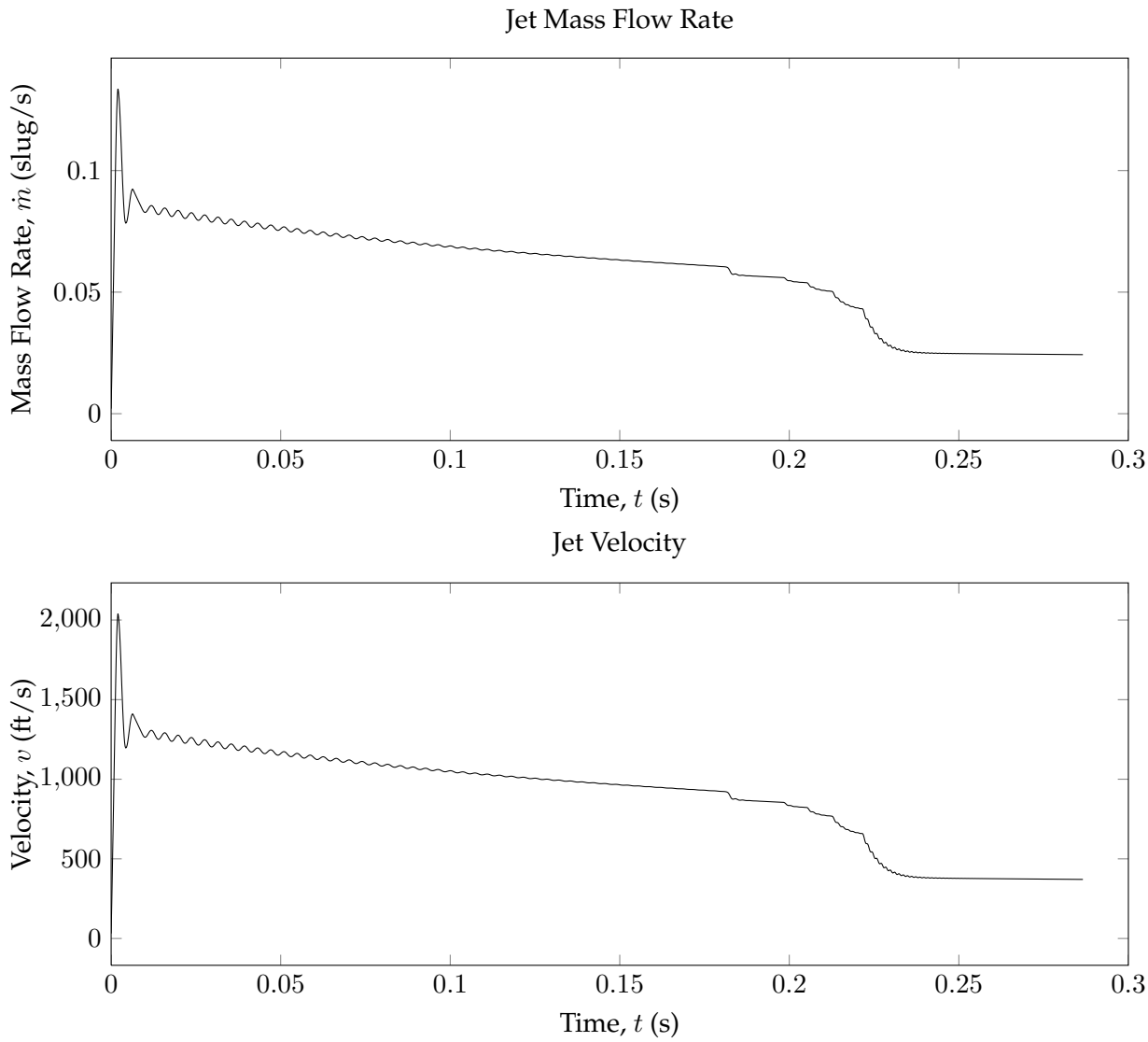

Figure 29: Jet Mass Flow Rate and Velocity Profile

The jet velocity and mass flow rate are related by a constant and both are a function of the water pressure in the high pressure chamber. The initial spike in the jet velocity is caused by the dynamic forces of the piston on the water. Since this spike is caused by dynamic forces, it is greater than the intensified jet velocity which is based only on the driving pressure (Figs. 30 and 31). The sudden drop in jet velocity at the end of the jet pulse is caused by the cushion.

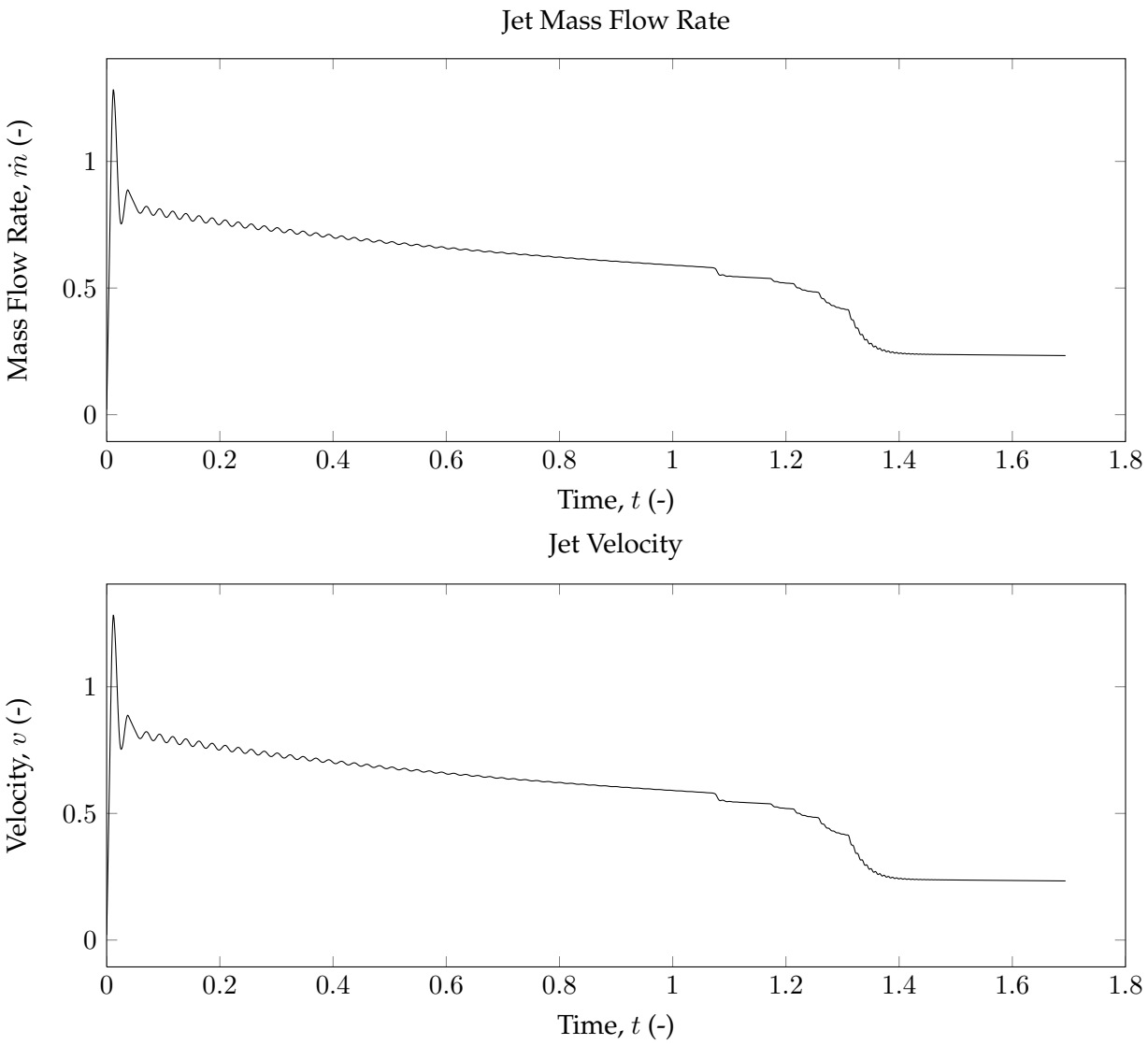

Figure 30: Dimensionless Jet Mass Flow Rate and Velocity

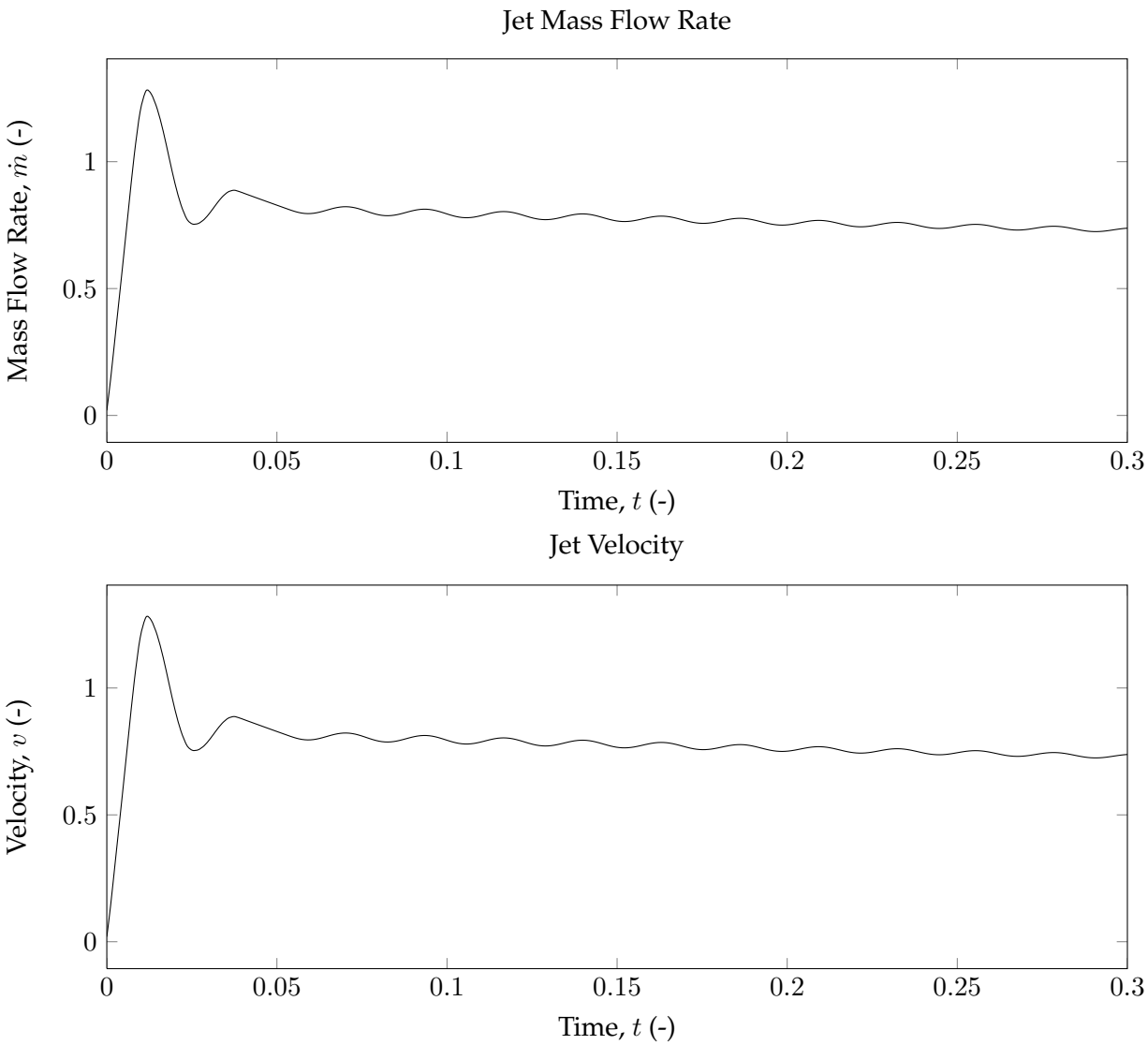

Figure 31: Dimensionless Jet Velocity and Mass Flow Rate - Detail

The water pressure as a function of time is plotted in Fig. 32. The steep increase in pressure, which causes the spike in the jet velocity, shows the effect of the piston compressing water as it moves forward. (Fig. 35 shows the piston displacement as a function of time.) Water is being expelled from the DAI but the piston is reducing the volume of the high pressure cylinder more quickly than the water can exit the small nozzle. This causes the water to act as a spring and the piston rebounds. The piston then oscillates between the forces of the driving pressure and the water pressure (Fig. 37), damped by the friction of the high pressure seal and by the expulsion of energy in the form of the water jet.

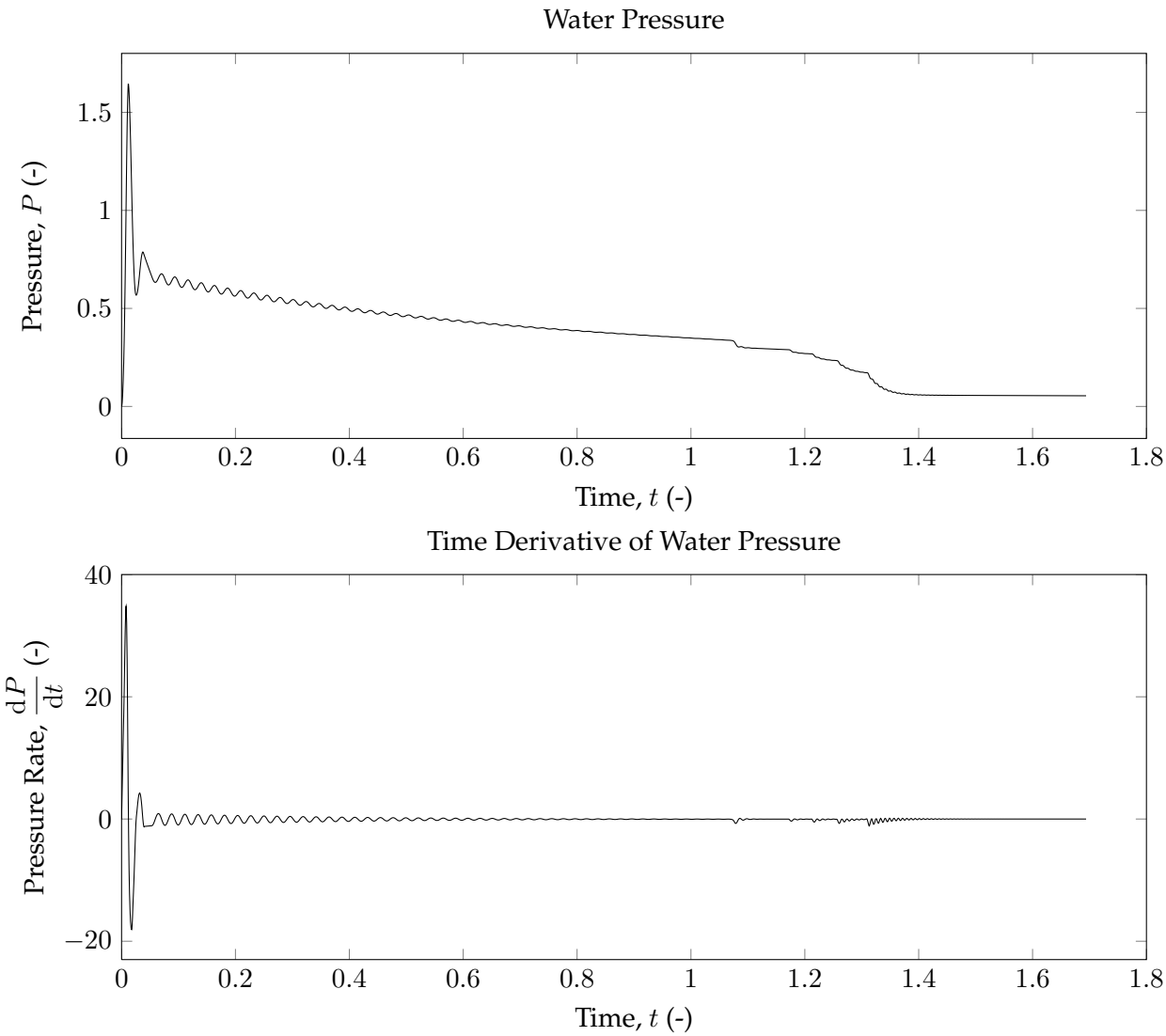

Figure 32: Dimensionless Water Pressure in the High Pressure Chamber

The piston velocity and acceleration are plotted in Fig. 33, and a detail view of the beginning of the simulation is plotted in Fig. 34. The sharp changes in the acceleration are the effect of the Coulomb friction exhibited by the high pressure seal. In general, the magnitude of the friction is a function of the water pressure only, but the direction must always be opposite that of the piston's velocity. Hence, the force of friction changes direction while maintaining its magnitude every time the piston velocity changes sign. These discontinuities in the friction force cause discontinuities in the piston acceleration and are the cause of the sharp corners in the velocity plots (Figs. 33 and 34) when the piston velocity crosses zero.

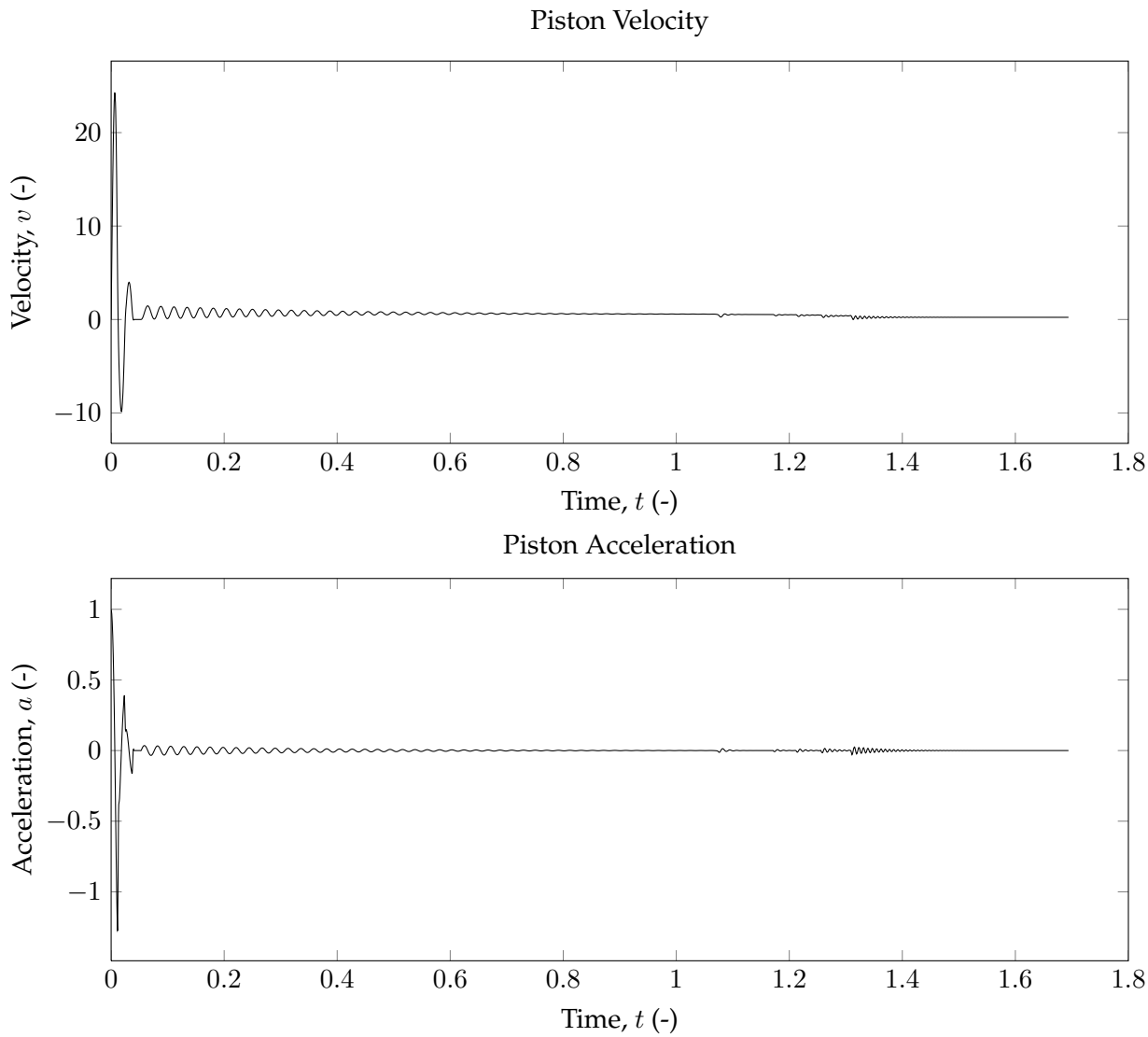

Figure 33: Dimensionless Piston Velocity and Acceleration

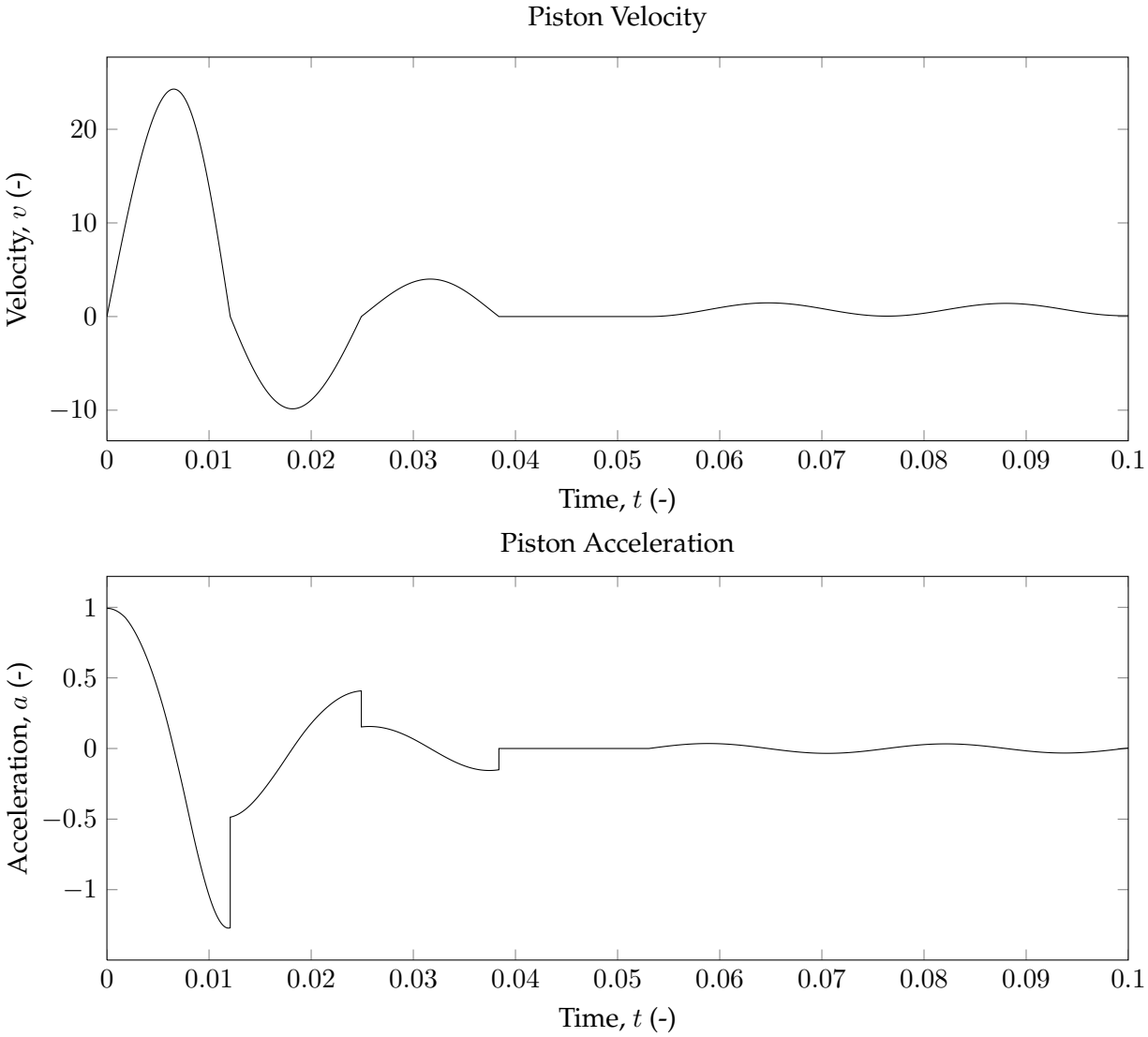

Figure 34: Dimensionless Piston Velocity and Acceleration - Detail

As discussed in Section 4.3, the piston can stop for a moment under the right conditions. This stop is evident in the results displayed in Figs. 35 and 36 at a dimensionless time $t \approx 0.04$.

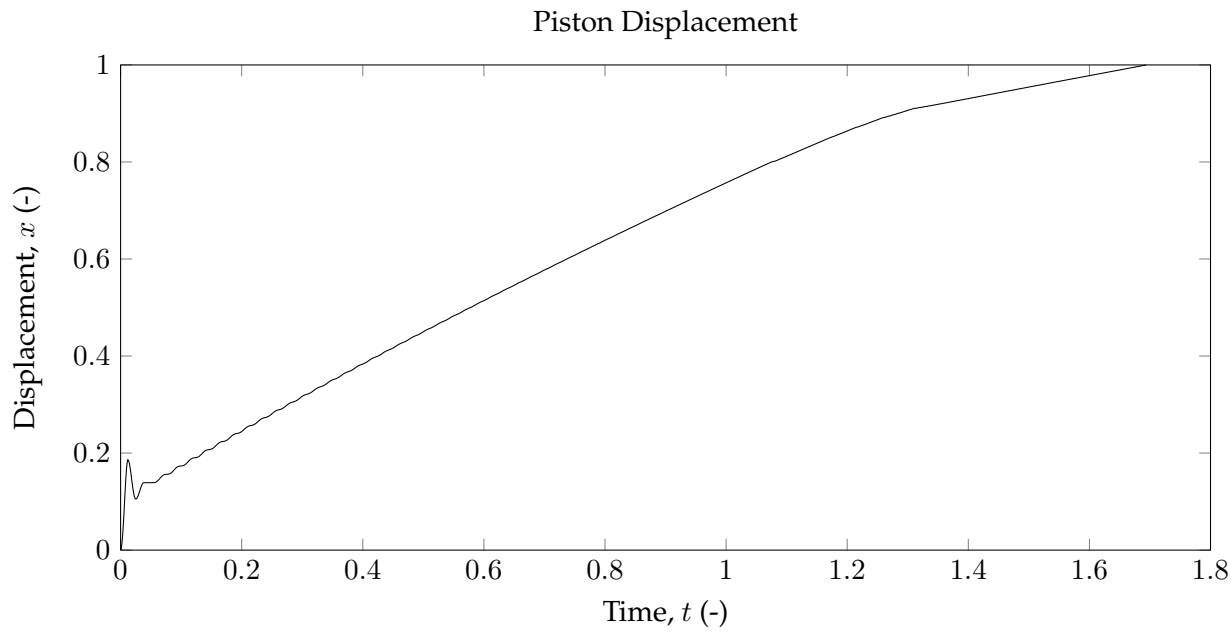

Figure 35: Dimensionless Piston Motion

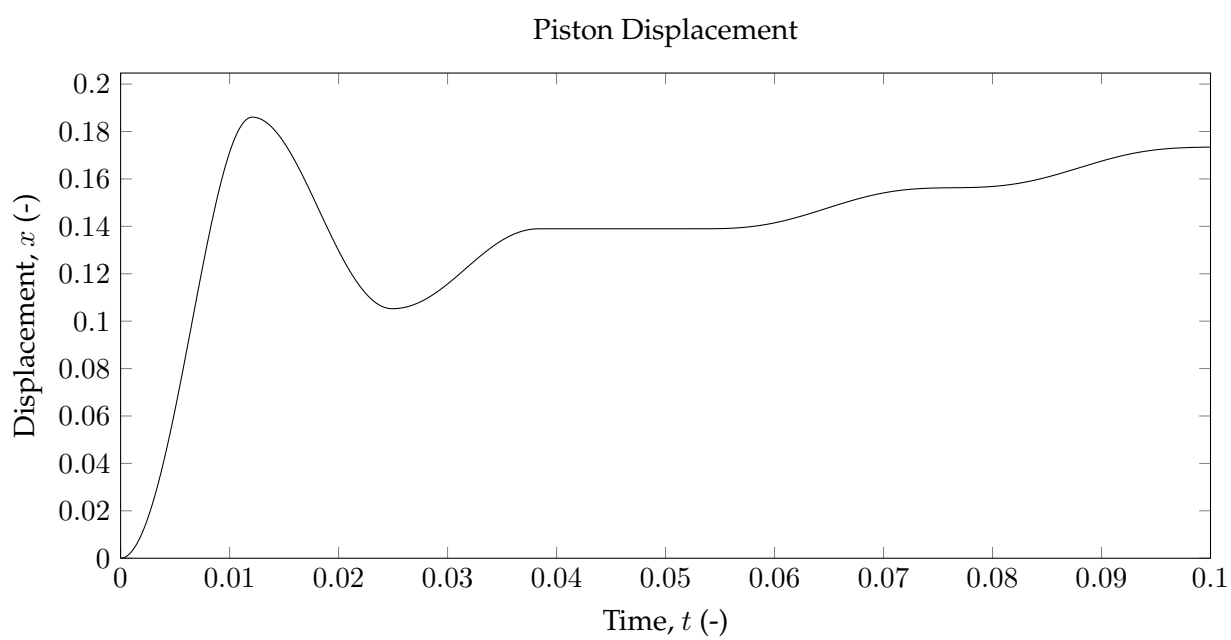

Figure 36: Dimensionless Piston Motion - Detail

While the piston is stopped, the driving pressure is constant but the water pressure decreases as the water is allowed to expand. (Figure 37 shows how the forces on the piston vary with time immediately after the piston is released.) The expansion of the water maintains the jet flow while the piston is stopped. Once the difference between the water pressure force and the driving pressure force exceed the maximum friction force, the piston breaks free. As shown in Fig. 37, the piston breaks free at $t \approx 0.055$.

The discontinuities in the friction force F_f discussed in Section 4.3 occur at $t \approx 0.012$ and $t \approx 0.026$. In comparing to Fig. 34, it is evident that these discontinuities occur when the velocity changes direction, as expected. After the piston stops at $t = 0.04$, the friction force is maintained at the value that causes a net force of zero until the maximum friction force is reached. From this time till the piston breaks free, the change in the friction force matches that of the water pressure force.

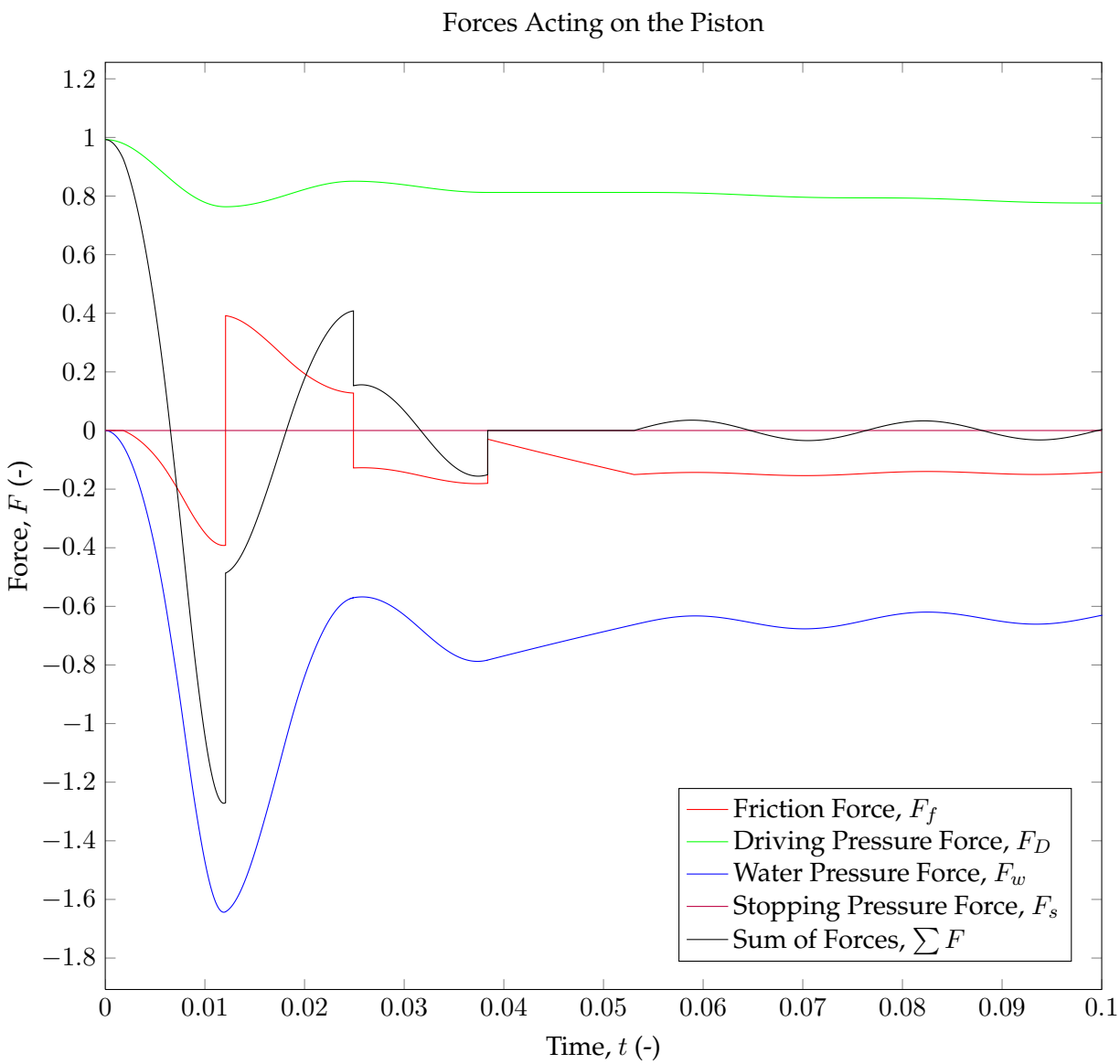

Figure 37: Dimensionless Forces Acting on the Piston

From the final time in Fig. 37 to the starting time in Fig. 38, the forces are relatively constant. Once the cushion engages, the forces change more significantly (Fig. 38).

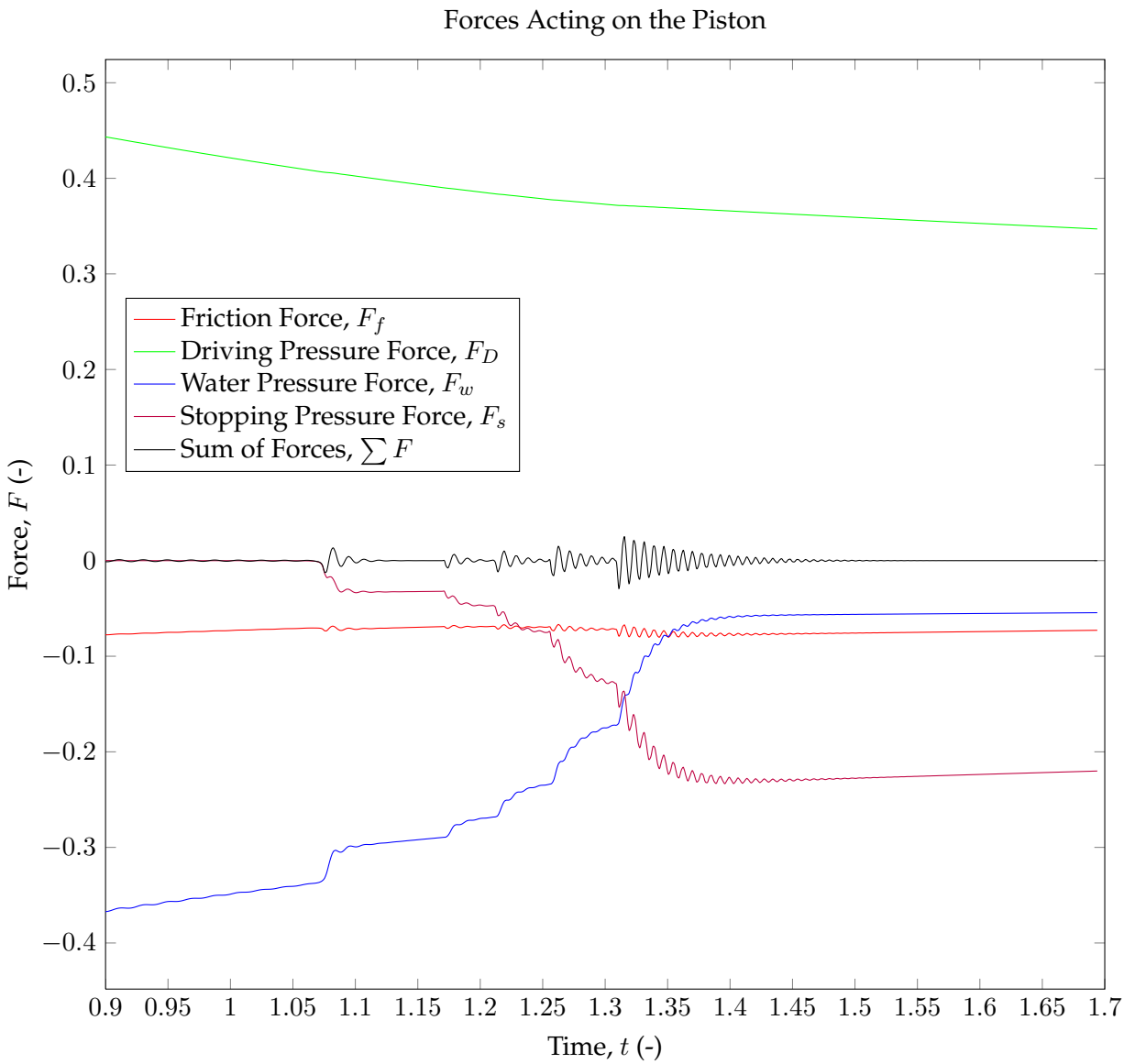

Figure 38: Dimensionless Forces Acting on the Piston after Cushion Engagement

The effect of the cushion on the piston's motion is present at $t \approx 1.1$, slowing the piston to a safer velocity. This change in motion is caused by the stopping pressure, shown in Fig. 39. The stopping pressure is the difference between the cushion pressure and the high pressure chamber water pressure. Each step in the stopping pressure is the result of a set of piccolo cushion orifices closing. These events are the cause of the last 5 spikes on the plot of stopping pressure rate vs. time (Fig. 39). The first spike on this plot is from the cushion initially "engaging." At this point, the gap before the cushion is not closed enough to have a large effect on the stopping pressure. This is the moment at which the cushion is first taken into account and is described as "cushion approach" in Section 4.4. By beginning this calculation before the cushion closes, the model does not need to cope with a large change in pressure when the cushion finally closes. The size of this

spike depends on the initial stopping pressure value that is used to soften the change. If the initial pressure is too low or too high, the spike could be orders of magnitude larger than the responses from the closing orifices in the positive or negative direction, respectively.

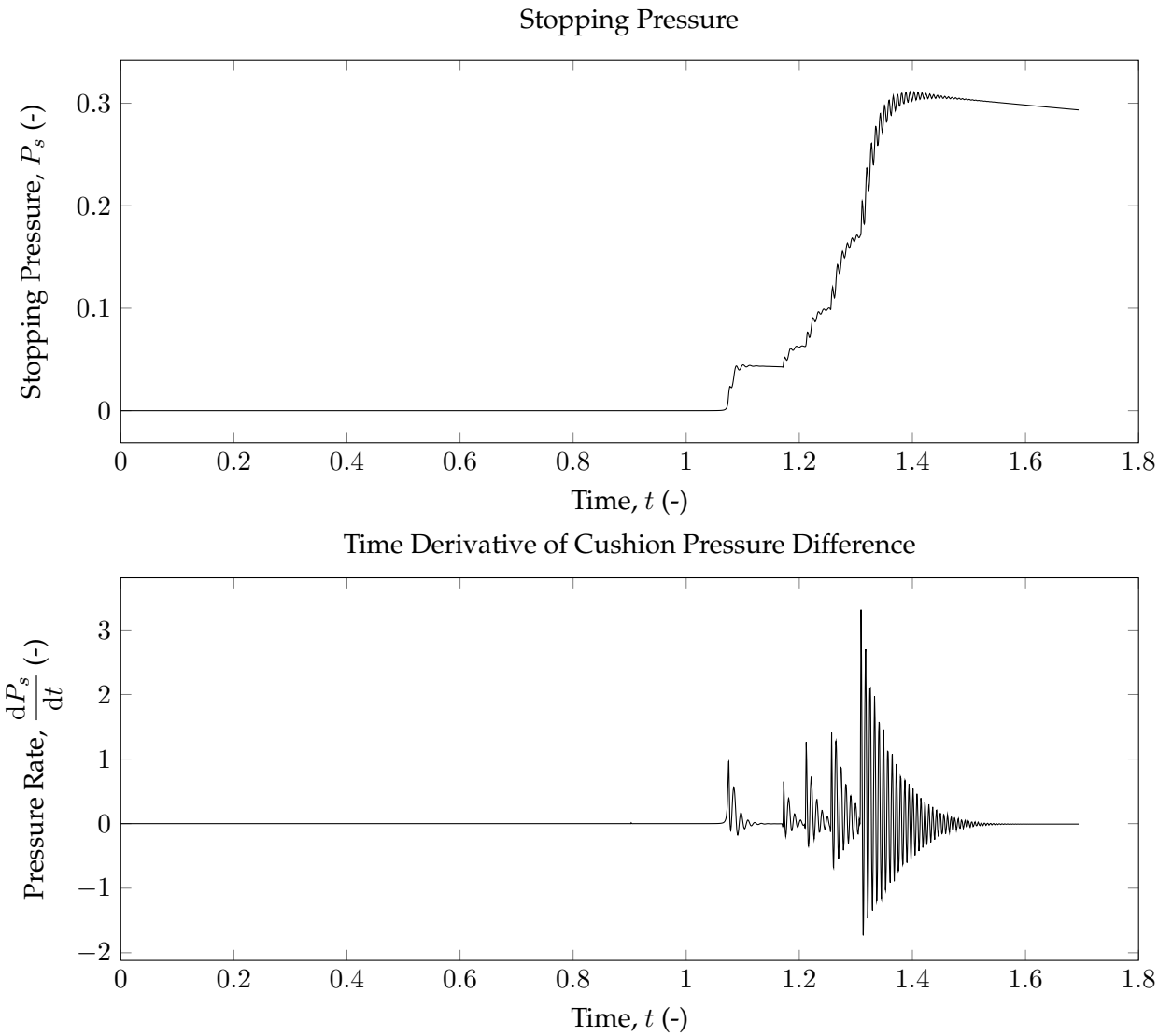

Figure 39: Dimensionless Stopping Pressure

Figures 40 and 41 show how the driving pressure varies with time. The compressed gas pressure decreases very quickly as the piston accelerates initially. The pressure remains constant when the piston stops and then continues to decay once the piston velocity is relatively constant.

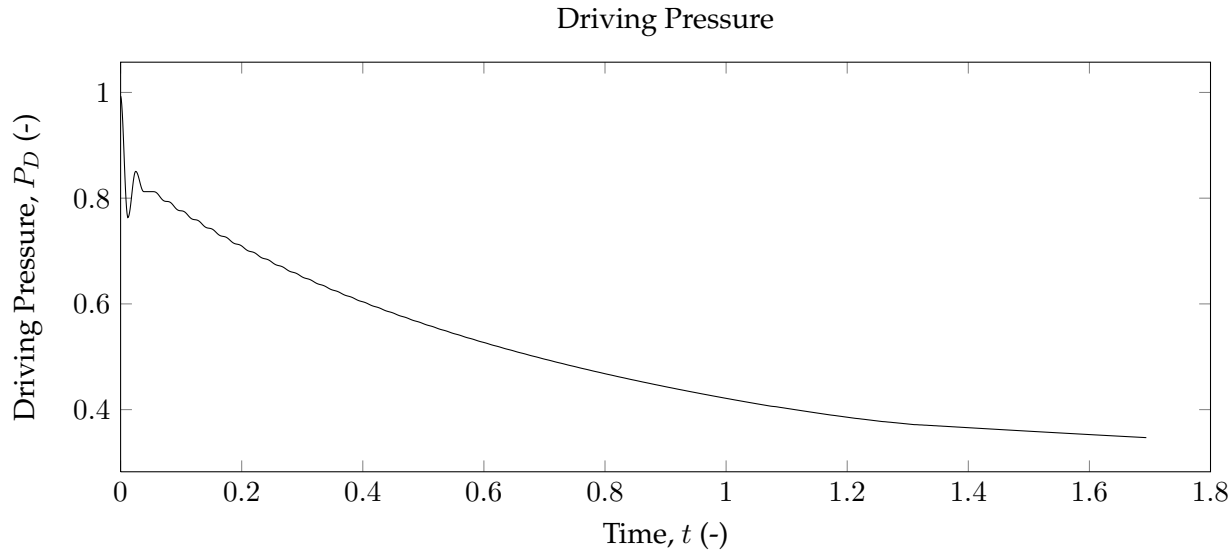

Figure 40: Dimensionless Driving Air Pressure

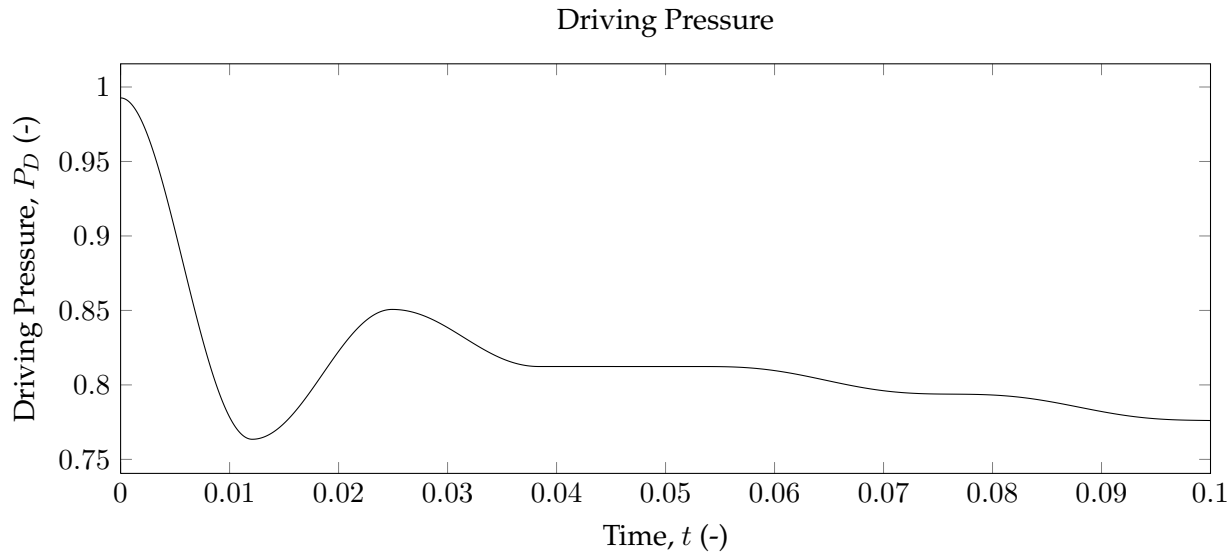

Figure 41: Dimensionless Driving Air Pressure - Detail

11 Results - CTH Hydrocode

The DAI water jet output velocity generated using the parameters listed in Table 4 and plotted in Fig. 29 was used for the CTH simulations presented in Sections 11.1 and 11.2. CTH input files for each of these simulations are presented in Appendix E. Contact the authors for the complete files. Additionally, a separate document detailing the usage and maintenance of the workstation will be drafted and submitted over the next few months.

11.1 Axisymmetric Simulation

The initial axisymmetric simulation used the built-in CTH material model for `SAC5` road-grade concrete [20]. This model treats the concrete as a homogeneous mixture, having properties calculated using a weighted average of typical cement-aggregate mixtures. The axisymmetric simulations would have required less time to compute than a three-dimensional simulation, however, several problems were uncovered.

First, the axisymmetric simulation yielded erosion rates far above those predicted by Burns [9]. Burns predicted hole depths h from between 20 and 30 times the nozzle diameter D_n for a single pulse. Consider the dimensionless hole depth (h/D_n) plotted as a function of time in Fig. 42. The axisymmetric simulation surpasses 40 dimensionless depths and erodes through the entire 15 cm thickness before the jet velocity has reached its peak.

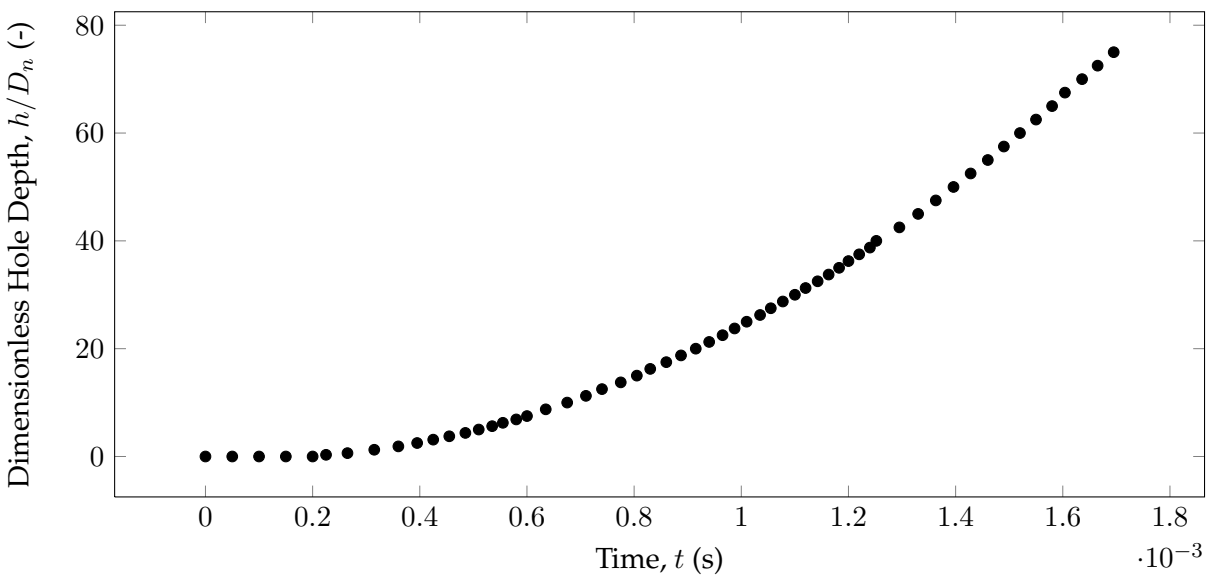

Figure 42: Cavity Depth vs. Time - Axisymmetric Geometry, Homogeneous Concrete

Since these results disagreed with Burns' predictions by nearly an order of magnitude, it became clear that the homogenized concrete model was unsuitable for modeling the erosion caused by the impinging water jet. A more detailed model incorporating a random distribution of aggregate matrix material within a cement binder was required. This could not be created in an axisymmetric geometry because the aggregates would become revolved around the entire domain and act as a continuous phase, which is not the case for concrete.

Another issue with the axisymmetric simulations was that the eroded cavities had little to no evidence of tapered sides. Figure 43 shows that the eroded cavity had little inward taper towards the top. This inward taper is necessary to generate the pressure forces in a direction which loads the concrete in tension.

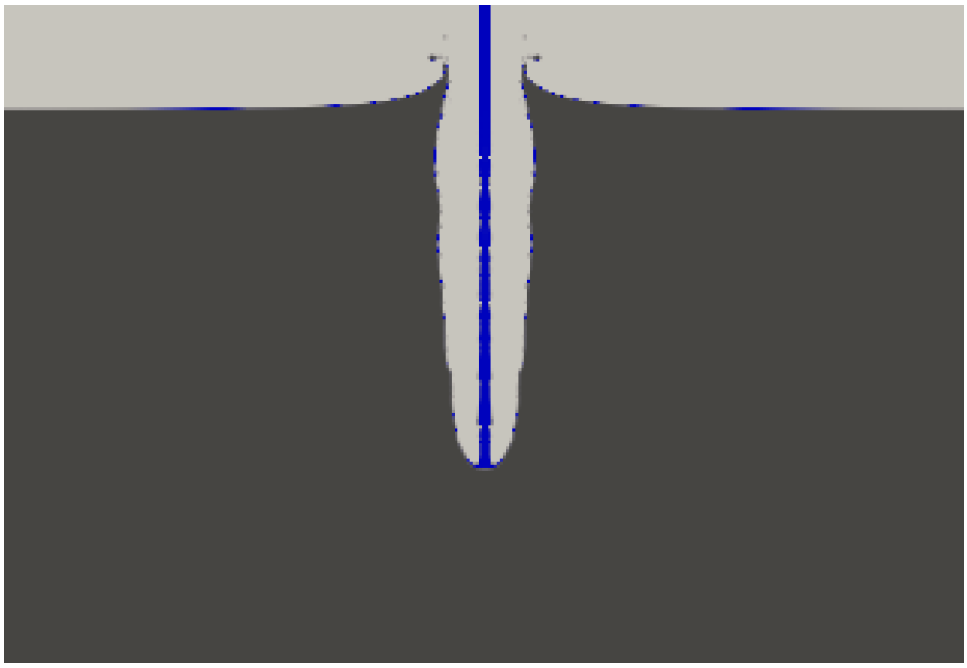

Figure 43: Eroded Cavity Shape - Axisymmetric Geometry, Homogeneous Concrete Model

Even though the axisymmetric simulation did not produce accurate erosion results, it was still useful to perform some basic verification of the solution. The stagnation pressure in the water jet upon impact was compared to the theoretical stagnation pressure on a rigid plate and numerical predictions by Pritchett [10] and agreed to within 7% in both cases.

Additionally, the water jet erosion at dimensionless time $t = 1.1$ from Pritchett's simulation was compared to that generated by the axisymmetric CTH simulation in Fig. 44. This qualitative comparison simply gives confidence that there are not major issues with the methods CTH is using to model the erosion of the impact surface.

Another verification tool was the pressure field in the concrete material, which was compared to the work of Daniel [8], who used a high-speed camera to capture the pressure field in photoelastic specimens upon impact of a water jet. Figure 45 shows the comparison of the pressure waves as computed by CTH alongside the pressure fields recorded experimentally by Daniel. Note that the experiments conducted by Daniel [8] included jet velocities up to three times higher than generated by the DAI model specifications of Table 4. In addition, the materials used by Daniel were Columbia Resin (CR-39), Plexiglas, Homalite-100, and glass [8], all of which behave quite differently from the SAC5 concrete used in the CTH model. For this reason a quantitative comparison is not attempted, but qualitative comparison of the experimental results to the CTH results shows that in both cases, the pressure front initially forms tangent to the impact surface and gradually evolves to a semi-circular front in the target material as the transient effects of the jet impact decay and quasi-steady conditions are achieved.

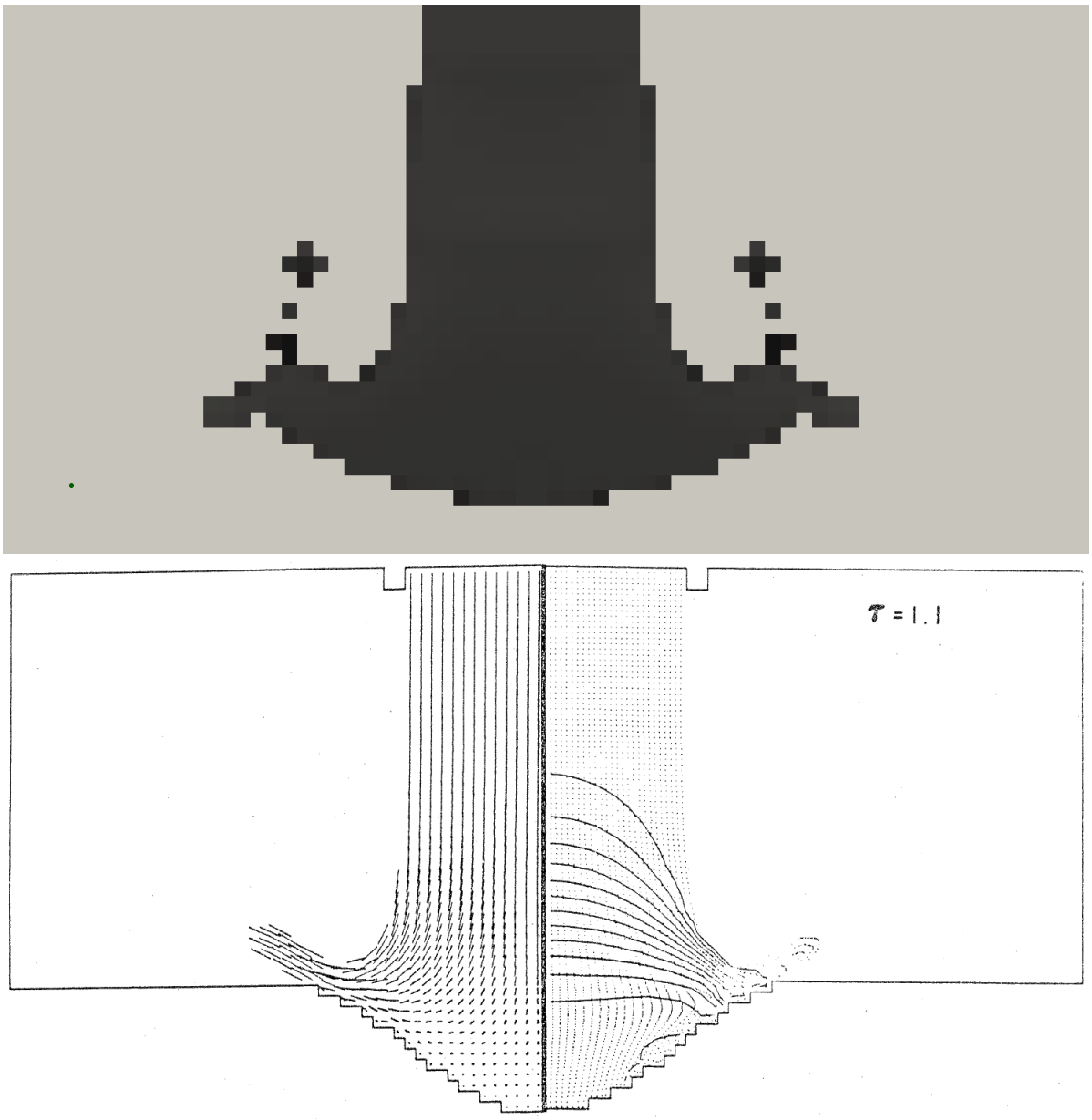

Figure 44: Comparison of CTH Jet/Impact Surface Interface Shape (top) with Pritchett Simulations (bottom) upon Impact ($t = 1.1$) [10]

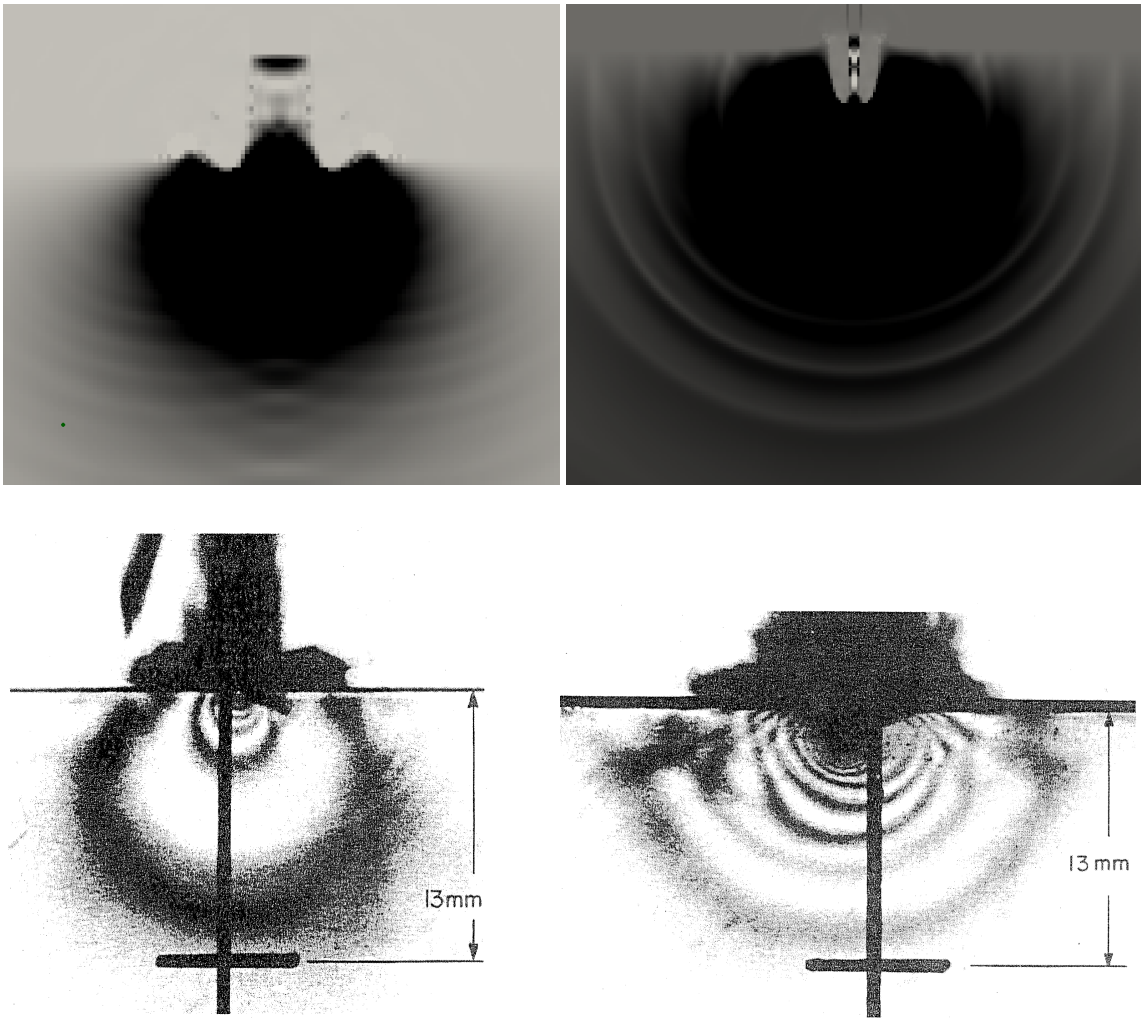

Figure 45: Material Pressure Field, Immediately After Impact (left) and After Onset of Erosion (right). CTH Results (top) and Photoelastic Experimental Results (bottom) [8].

11.2 Three-Dimensional Simulation

As discussed in Section 11.1, the axisymmetric simulations with homogenized concrete failed to produce the inward taper necessary to generate pressure forces placing the concrete into tension. First, to eliminate any effects of geometry selection, the homogenized concrete was used in a three-dimensional simulation under the same conditions used in the axisymmetric case. The results for hole depth and hole diameter agreed with the axisymmetric results to within 10%.

A random distribution of aggregate was then added to the computational domain using a MATLAB script which is available from the authors. The random arrangement of harder particles is a better representation of physical concrete, and provides some variability to the material so the impinging water jet can be deflected to produce a wider range of possible hole shapes. Initial results of this attempt are shown in Fig. 46. Three similar simulations (with a larger thickness of concrete) are running currently.

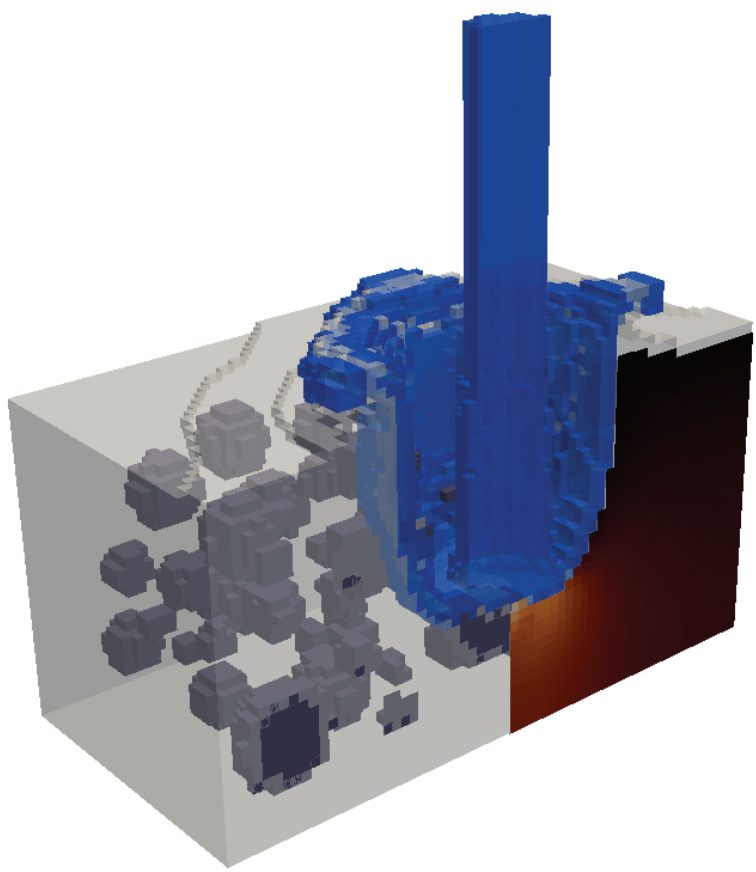

Figure 46: Three-Dimensional Simulation with Random Aggregate Distribution

The three-dimensional simulation results, such as those in Fig. 46, show that the aggregate does add significant variability to the jet path. The cavity is irregularly shaped after about 1 cm of penetration, and will get more irregular as the flow continues. Once the currently-running simulations produce a suitably-shaped cavity, the pressure forces on the walls should be calculated. These forces can then be compared to Ryhming's experimental data [2] to predict failure. The three simulations are expected to take about 24 days of computing time each.

12 Conclusion and Recommendations

The DAI model is complete and ready for validation whenever a physical DAI unit can be obtained and tested. The key variable to scrutinize is the jet velocity since this is used for the CTH simulations of concrete erosion and fraction. Ideally, a wide range of parameters should be tested eventually, in order to show the scalability of the model and the quality of the non-dimensionalization.

The CTH simulations require more effort and time than was available in the team's delayed schedule. The verification work discussed in Section 11.1 has proven that the CTH Hydrodynamics code is an appropriate tool for continued simulations. The initial axisymmetric results showed that modeling of each individual aggregate is required to produce flow patterns generating the bottle-shaped cavity. Several of these simulations with random aggregate distributions are in progress and are expected to finish by mid-June 2012.

Once a bottle geometry has been produced by the impinging water jet in a simulation, mesh independence studies and boundary independence studies should be conducted to isolate the solution from outside influences, such as pressure wave interactions at boundaries or loss of accurate interface tracking in large mesh cells. Once these studies are complete, several different random distributions of aggregate should be simulated to study the effect of the concrete itself on the bottle geometry. This information is crucial in any physical experiment if the results are to be compared to the CTH simulations.

One final issue to resolve in CTH is the output of stress deviators. These should be output in addition to the pressure, so the total stress state of the material can be calculated. The team has not yet successfully read these values from the output or history files. David Crawford at Sandia National Laboratories has been looking into this, but he has not responded yet. The stress deviators are critical if the pressure forces on the bottle walls are to be computed.

Another model parameter likely needing further investigation is the material selection for the cement binder portion of the concrete as well as the aggregate matrix portion. Presently, SAC5 concrete and steel are used, respectively. The CTH material library should be consulted to select more appropriate materials. Note that for the concrete models and several other SESAME tabular materials, the default properties cannot be edited from the CTH input file itself.

Once the model is finalized, it must be validated to prove its value. Here again, a wide range of DAI parameters should be tested and compared if at all possible. If the model is validated at only one operating point, its results are unknown elsewhere. A strategic set of tests at various parameter values ensures a reasonable level of confidence in the model over a given operating range.

Significant simulation work is required to obtain usable results from the CTH model. These simulations could take months to complete, given the requirements of three dimensionality imposed by the random aggregate distribution. The stress deviators must be extracted from the CTH output before the surface pressure forces can be predicted. Material model selection should be evaluated prior to a validation attempt. The basic framework for the simulations has been laid, but the amount of time required for each run prevented more simulations from being conducted during Spring Quarter.

References

[1] Labus, T., 1991. "Pulsed Fluid Jet Technology". In Proc. 1st Asian Conf. on Recent Advances in Jetting Technology, pp. 136–143.

[2] Ryhming, I., Cooper, G. A., and Berlie, J., 1980. "A Novel Concept for a Rock-Breaking Machine: I. Theoretical Consideration and Model Experiments". In Proc. R. Soc. Lond., Vol. 373 of *Series A, Containing papers of a mathematical and physical character*, Harrison, pp. 331–351.

[3] Zukas, J. A., 2004. *Introduction to Hydrocodes*, Vol. 49 of *Studies in Applied Mechanics*. Elsevier.

[4] Schwer, L. E., Salamon, N. J., and Liu, W. K., eds., 1989. Computational Techniques for Contact, Impact, Penetration and Perforation of Solids, Vol. 103 of *The Winter Annual Meeting of the American Society of Mechanical Engineers*, The Applied Mechanics Division, ASME, The American Society of Mechanical Engineers.

[5] Garity, M. M., 1995. Simulation of a Pulsed-Jet Water Intensifier.

[6] Bergesen, Andrew, et. al., 2007. Pulsed Jet Water Intensifier: Design Implementation Report.

[7] Bridgman, P. W., 1912. "Water, in the Liquid and Five Solid Forms, under Pressure". In The Proceedings of the American Academy of Arts and Sciences, Vol. 47, No. 13, pp. 441–558.

[8] Daniel, I. M., Rowlands, R. E., and Labus, T. J., 1974. "Photoelastic Study of Water Jet Impact". In Proc. Second Int. Sym. On Jet Cutting Technology, BHRA Fluid Engineering, pp. A1–1–A1–18. Paper No. A1.

[9] Burns, D. J., Vallvé, F. X., Mohaupt, U. H., and Kalfbleisch, J. G., 1980. "Relationship Between Jet Penetration and Design Parameters of a Pulsed Water Jet Machine". In Proc. Fifth Int. Sym. On Jet Cutting Technology, BHRA Fluid Engineering, pp. 215–228. Paper No. D2.

[10] Pritchett, J., and Riney, T., 1974. "Analysis of Dynamic Stresses Imposed on Rocks by Water Jet Impact". In Proc. Second Int. Sym. On Jet Cutting Technology, BHRA Fluid Engineering, pp. B2–15–B2–36. Paper No. B2.

[11] Hallquist, J. O., 1993. LS-DYNA3D Theoretical Manual. LSTC Report 1018 Rev. 2.

[12] Zukas, J. A., and Scheffler, D. R., 2000. Practical Aspects of Numerical Simulations of Dynamic Events: Effects of Meshing. ARL-TR 2303, Army Research Laboratory, Aberdeen Proving Ground, MD.

[13] Gessler, P. D., Schaeffer, M. D., and Zelhofer, A., 2011. Modeling of Pulsed Jet Impingement on Brittle Materials: Proposal Report. ME 490-006, MSOE, Milwaukee, WI.

[14] Merritt, H. E., 1967. *Hydraulic Control Systems*. Wiley.

[15] Silling, S. A., 2001. CTH Reference Manual: BFK Model for Concrete. Rev. 3, Sandia NL.

[16] Momber, A. W., 2004. "Aggregate liberation for concrete by flow cavitation". *International Journal of Mineral Processing,* **74**, pp. 177–187.

[17] Lauterborn, W., and Bolle, H., 1975. "Experimental Investigations of Cavitation-Bubble Collapse in the Neighbourhood of a Solid Boundary". *Journal of Fluid Mechanics,* **72**, pp. 391–399.

[18] Bourne, N. K., and Field, J. E., 1992. "Shock-induced Collapse of Single Cavities in Liquids". *Journal of Fluid Mechanics,* **244**, pp. 225–240.

[19] Dear, J. P., and Field, J. E., 1988. "A Study of the Collapse of Arrays of Cavities". *Journal of Fluid Mechanics,* **190**, pp. 409–425.

[20] Crawford, D., Bell, R., Brundage, A., E.S. Hertel, J., Schmitt, R., Schumacher, S., and Simmons, J., 2009. CTH User's Manual and Input Instructions. Version 9.0, Sandia National Laboratories.

[21] Union Carbide Chemicals & Plastics Technology Corporation, 2000. Material Safety Data Sheet: POLYOX (TM) WSR 301 (1798).

[22] SPX Fluid Power, 2004. Material Safety Data Sheet: Biodegradable Hydraulic Fluid.

Appendix A Team Member Résumés

Paul Donald Gessler

Contact Information

318 Margaret Loock Hall
MSOE P.O. Box 353
Milwaukee, WI 53201-0353

M: 414-241-1627
paul.gessler@marquette.edu
linkedin.com/in/pdgessler

Research Interests

Adaptive methods, computational fluid dynamics, distributed/parallel computing, multidisciplinary system modeling, numerical analysis, structural analysis, thermal/fluid systems, transport phenomena

Education

Marquette University, Milwaukee, Wisconsin

Master of Science, Mechanical Engineering **Aug. 2012 – May 2014 (Expected)**

- Specialization: Energy Systems
- Thesis: A One-Dimensional Model of a Centrifugal Compressor Gas Test Block System
- Teaching Assistant for Fluids and Thermodynamics Courses

Milwaukee School of Engineering, Milwaukee, Wisconsin

Bachelor of Science, Mechanical Engineering **Sept. 2008 – May 2012**

- Minor: Mathematics
- Senior Project: Hydrodynamic Modeling of Pulsed Jet Impingement on Brittle Materials
- Cumulative GPA: 3.59, Major GPA: 3.68

Software Proficiencies

Autodesk Products, SolidWorks, Matlab/Simulink, Real-Time Workshop, Visual Studio, C/C++, Ansys/Fluent, COMSOL Multiphysics, Star-CCM+, Adobe Creative Suite, Microsoft Office Suite, LaTeX, Linux (ArchLinux Distribution), Mac OS X, Windows

Honors and Awards

Outstanding Student Chapter Award, SAE International, Detroit, MI	2011, 2012
First Place, Design Report Competition, SAE SuperMileage, Marshall, MI	2011
Dean's List (All Quarters), MSOE, Milwaukee, WI	2008 – 2012

Professional Experience

Johnson Controls, Inc., Milwaukee, WI

Graduate Intern, Control Applications and Advanced Algorithms **March 2010 – Present**

- Design elements of chiller control applications, including safety events and diagnostics
- Extend chiller models to include a wide variety of compressors, vessels, and variable-speed drives
- Expand and improve automated test capabilities (simulation and emulation)

Research Experience

MSOE Rapid Prototyping Research, Milwaukee, WI

Undergraduate Research Assistant **Dec. 2009 – Jan. 2011**

- Performed pattern preparation and casting of alloy structures
- Designed and modeled mold flow passages to improve liquid metal flow and solidification
- Contributed to reports and presentations for two conformally-cooled nozzle research projects

Leadership Experience

MSOE Society of Automotive Engineers, Milwaukee, WI

Chairman **May 2011 – May 2012**

- Coordinated with professionals in nearby SAE Chapters to organize events
- Oversaw the general operation of the MSOE Student Chapter
- Other Previous Positions: Program Coordinator and Webmaster (2010-2011)

Technical Lead, SuperMileage Vehicle Steering Team **May 2010 – June 2011**

- Designed, analyzed, manufactured, and tested suspension frame
- Responsible for steering/brake system performance and component integration
- Co-authored and edited the 2011 Design Report (awarded First Place, Design Competition)

MSOE Residence Life, Milwaukee, WI

Resident Assistant **May 2010 – May 2012**

- Responsible for 32 residents, providing academic, personal, and professional advice
- Planned events for residents throughout the year, such as resume workshops and indoor climbing
- Enforced MSOE Residence Life policies, resolving conflicts and violations as needed

Activities and Interests

Varsity Lightweight Crew 2008-2010, Cyclocross and Mountain Bike Racing, Trumpet Performance, Running, Backpacking, Canoeing, Photography, Computer System Administration, Web Design

Marshall Schaeffer

Regents 303C PO BOX 353
Milwaukee, WI 53201
815-529-9664
schaefferm@msoe.edu

Education:

Milwaukee School of Engineering (MSOE), Milwaukee, WI
Major: BS, Mechanical Engineering Minor: Mathematics
Cumulative GPA: 3.92 Major Specific GPA: 3.95
Graduation: May 2012 BS completion in 3 years
Specialized Coursework: Advanced Finite Element Analysis (FEA), Computational Fluid Dynamics (CFD), Vibration Modeling, Advanced Differential Equations, Laplace Transforms, Linear Algebra
Capstone Project: Novel transient numerical modeling of a high velocity water jet impinging on a brittle material to optimize excavated mass per unit energy input. Included in the analysis was modeling the pulse jet intensifier.

Work Experience:

June 2011 – Present **Manufacturing Engineering Intern**, P&H Mining Equipment, Milwaukee, WI
New product development: designing factory for new product line
Large machining department: implemented overall equipment effectiveness (OEE) programs for three gantry mills and two horizontal boring bars, documented and improved part setups

June 2010 – Aug 2010 **Machinist**, Milwaukee School of Engineering, Milwaukee, WI
Rebuilt and repaired shop and laboratory machinery, manufactured parts as needed

June 2009 – Aug 2009 **CNC Mill Applications Programmer**, Iverson & Company, Des Plaines, IL
Programmed, set up, troubleshot, and ran both CNC mills and lathes

June 2009 – Aug 2009 **Quality Control Intern**, Numerical Precision Inc., Wheeling, IL
Inspected and documented aerospace parts

Involvement:

May 2010 – Present **Society of Automotive Engineers (SAE), MSOE Chapter**: Current vice chairman, secretary for 2010-2011 academic year; voted best collegiate chapter in the Milwaukee area by SAE Milwaukee in 2010; won SAE/Honeywell Outstanding Collegiate Branch Award in 2011

Nov 2009 – June 2011 **SAE Super Mileage Vehicle**: Led mechanical design and manufacture of steering components and framework, utilized finite element analysis to design for lightweight strength on complex parts; team placed first in technical design report at international competition in 2011

Honors and Awards: **Deans List with High Honors**: All quarters

Academic Scholarship: Milwaukee School of Engineering, 2009 – present

Skills: **Computer Skills**: Matlab, Simulink, SolidWorks, ANSYS, Solidcast, Microsoft Office

Manufacturing Skills: CNC mill programming (G-code), CNC lathe programming (G-code), manual machining

Interests: Designing and building projects, downhill skiing, hiking, traditional archery

Alex Zelhofer

Permanent Address:
3980 Prairie Ct
Oshkosh, WI 54901

Contact Information:
Cell: 920-379-4797
Email: zelhofera@msoe.edu

Academic Experience: Bachelors of Science: Mechanical Engineering (Anticipated: May 2012)
Milwaukee School of Engineering (MSOE), Milwaukee, WI
Cumulative GPA: 3.89/4.0
Minor: Mathematics
Concentrations: Modeling Fluid, Thermal, and Structural Systems
Capstone Project: Modeling of Jet Impingement on Brittle Material

Work Experience: MSOE Rapid Prototyping Research (Sept. 2011 - Current ; June 2009 - August 2010)
Title: Undergraduate Research Assistant
Utilize CFD and FEA software to model fluid and mechanical system dynamics
Conduct research into development of aerospace materials
Design and analysis of prototype part manufacturing for private industry

NASA Dryden Flight Research Center (DFRC) (June 2011 - August 2011)
Title: Composite Structures Intern
Design and fabrication of composite parts
Support development of composite standards at NASA DFRC
Develop and conduct composite workshop educating NASA employees about composites

Skills: Engineering Software
MATLAB/Simulink, ANSYS, MSC Patran, ProEngineer, SolidWorks,
StarCCM+, Autodesk Inventor, SolidCast, FlowCast, Magics

Applicable Courses: Courses Completed or In Progress
Finite Element Methods
Modeling and Numerical Analysis
Heat Transfer
Thermodynamic Applications
Thermodynamics I and II
Partial Differential Equations
Linear Algebra

Campus Leadership: MSOE SAE SuperMileage Vehicle Team
Team Student Mentor (June 2011 - Present)
Chairman (July 2010 - June 2011)
Project Co-Manager (September 2009 - July 2010)
Donations Coordinator (September 2009 - July 2010)
Treasurer (September 2008 - July 2010)

MSOE Society of Automotive Engineers
Senior Design Liaison (June 2011 - Present)
Chairman (June 2010 - June 2011)
Secretary (April 2009 - June 2010)

Circle K
Treasurer (February 2009 - June 2010)

Honors and Awards: Awards
SAE Tier 1 Outstanding Collegiate Branch Award (2011)
SAE Outstanding Collegiate Chapter in Milwaukee Section (2010–2011)
Dean's List (2008–Present)

Scholarships and Fellowships
NASA Aeronautics Fellowship Recipient (2010)
American Society of Mechanical Engineering Foundation Gratitude Scholarship (2009–2010)
Project Lead the Way Scholarship Recipient (2008–2012)

Appendix B DAI Model and Scripts

Figures 47 and 48 present the MATLAB/Simulink block diagrams used for the DAI model simulations.

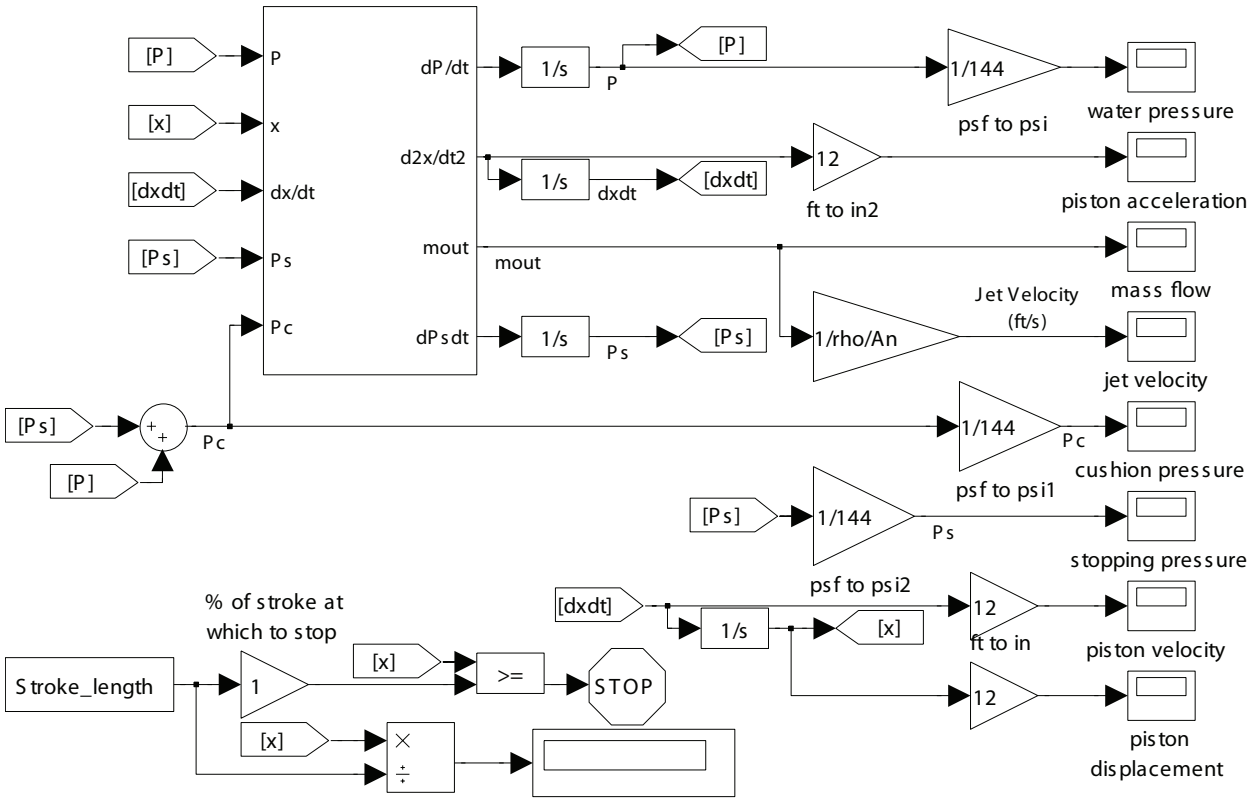

Figure 47: DAI Model - MATLAB/Simulink Block Diagram Top Level

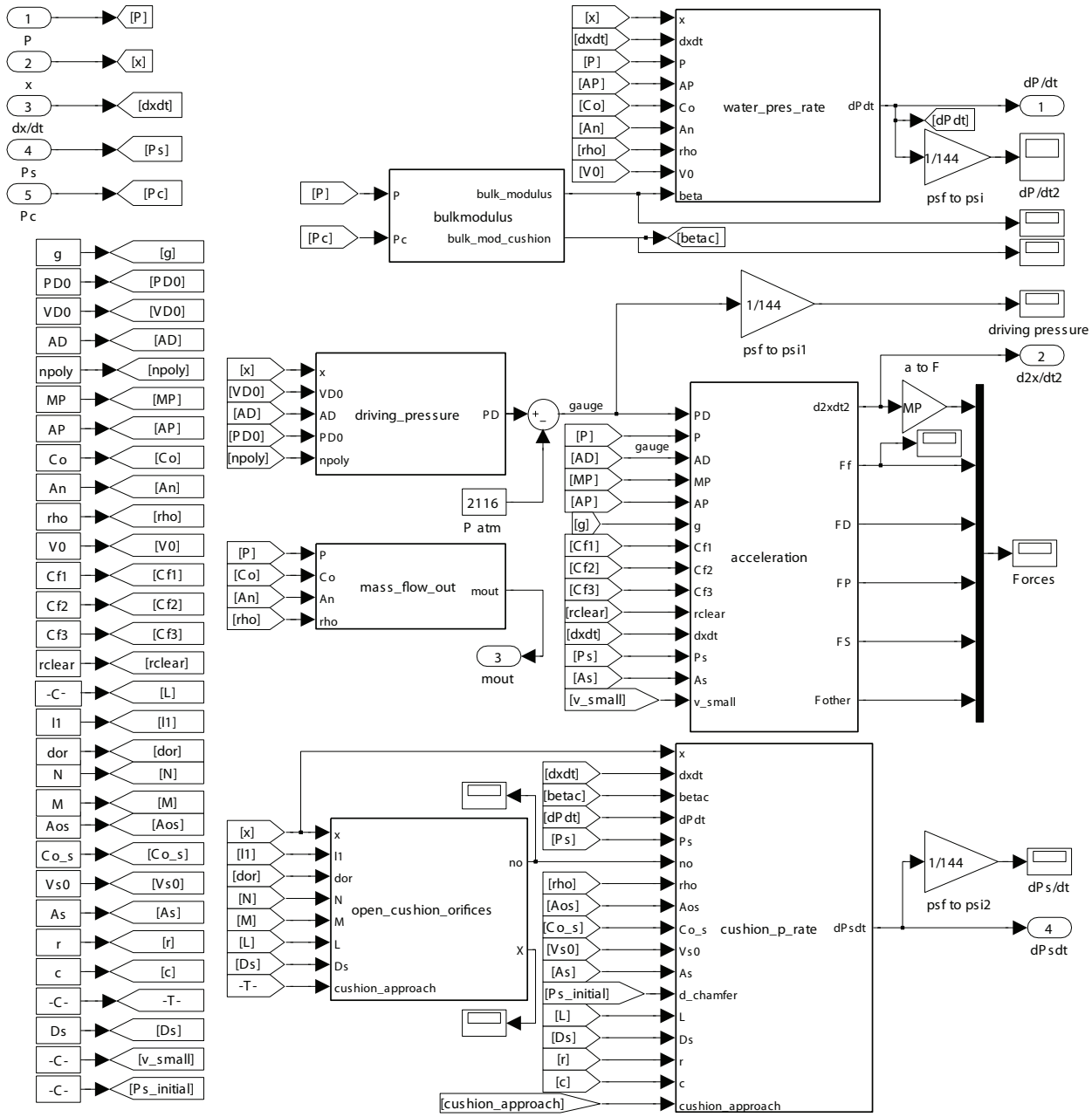

Figure 48: DAI Model - MATLAB/Simulink Block Diagram Subsystem

The following MATLAB m-script was used to define the parameters and run the simulation of the block diagrams in Figs. 47 to 48.

```
% Defines constants and runs differential area intensifier (DAI) model v5.0
% Uses Bridgman bulk modulus formulation
%
% Marshall Schaeffer  01-13-12

clear;

%%%%%%%%%%%%%%%%%%
% INPUTS SECTION %
%%%%%%%%%%%%%%%%%%

%% Simulation Parameters
model_number   = 5;
version_number = 0;

maxtstep       = 1e-6;
mintstep       = 2e-12;
initialtstep   = 1e-8;
relative_tol   = 5e-10;

number_of_runs = 5;
repeating      = 0;

if repeating ~= 1
    number_of_runs = 1;
end

%% Initial Conditions
PD0i = 2514.7;        % (psia) initial driving gas pressure
VD0i = 0.316000*12^3; % (in^3) initial driving gas volume

%% DAI Design Parameters
Driving_piston_dia = 10;      % (in)
Water_piston_dia   = 2;       % (in)
Nozzle_dia         = 0.07874; % (in) = 2mm
Stroke_lengthi     = 6;       % (in)
MPi                = 75;      % (lbm) mass of the piston

%% Water Properties
rho  = 1.937;      % (slugs/ft^3) water density at atm. pressure
beta = 3.12e5*144; % (psf) bulk modulus of water

%% Other Constants
npoly = 1.4;    % (-) polytropic exponent
Co    = 0.62;   % (-) orifice coefficient
g     = 32.174; % (ft/s^2) acceleration due to gravity

%% Friction Model Parameters
rboi           = 5.75/2;  % (in) high pressure outer radius
rsii           = 1.625/2; % (in) seal inner radius
rcleari        = 0.0005;  % (in) radial clearance of seal
```

```
sealthicknessi = 0.6;      % (in) thickness
coef_f         = 0.25;     % (-) high pressure seal friction coefficient
Esi            = 18e6;     % (psi) seal elastic modulus
Ebi            = 29e6;     % (psi) barrel elastic modulus
seal_v         = 0.295;    % (-) seal Poisson's ratio
barrel_v       = 0.3;      % (-) barrel Poisson's ratio

%% Cushion Model Parameters
Ri = Water_piston_dia/2;%inches, barrel innner radius
ri   = 0.5;      % (in) cushion small radius
Dsi  = 1;        % (in) stopping distance
l1i  = 0.25;     % (in) distance to first orifice ring
dori = 0.1;      % (in) distance between orifice rings
N    = 4;        % (-) number of orifice rings >>>must check s array creation in ...
                 %         "no" eml, N ~> than the array<<<
M    = 4;        % (-) orifices per ring
ci   = 0.0005;   % (in) radial clearance between piccolo and cushion small radius
mu   = 2.34e-5;  % (lb-s/ft^2) dynamic viscosity
Co_s = 0.62;     % (-) cushion orifice coefficient
cushion_orifice_diameteri = 0.025;           % (in)
Aos = pi/4*(cushion_orifice_diameteri/12)^2; % (ft^2) cushion orifice area
d_chamfer = 0.001/12;                        % (ft) chamfer on cushion engagement edge

%% Velocity and Flow Tolerances
m_flow_tolerance = 1e-4;
v_small = 1.065e-4*12;   % (ft/s) piston velocity small enough to be considered stopped

%% Unit Conversions
PD0           = PD0i*144;          % (psfa)
VD0           = VD0i/12^3;         % (ft^3) initial driving gas volume
MP            = MPi/32.174;        % (slugs) mass of the piston
Stroke_length = Stroke_lengthi/12; % (ft)

AD = pi/4*(Driving_piston_dia/12)^2; % (ft^2) driven CS area of the piston
AP = pi/4*(Water_piston_dia/12)^2;   % (ft^2) CS area, high press. side
An = pi/4*(Nozzle_dia/12)^2;         % (ft^2) nozzle exit area
V0 = 4/3*Stroke_length*AP; % (ft^3) initial water vol., assume 4/3 of stroke for now

rbo           = rboi/12;               % (ft) high pressure outer radius
rsi           = rsii/12;               % (ft) seal inner radius
rclear        = rcleari/12;            % (ft) radial clearance of seal
sealthickness = sealthicknessi/12;     % (ft) thickness
rbi           = Water_piston_dia/12/2; % (ft) barrel inner radius
rso           = rbi - rclear;          % (ft) seal outer radius
Es            = Esi*144;               % (psf) seal elastic modulus
Eb            = Ebi*144;               % (psf) barrel elastic modulus

%% Friction Model Constants
Cf1 = 2*rso*rsi^2/(Es*(rso^2 - rsi^2));
Cf2 = ((1 - seal_v)*rso^3 + (1 + seal_v)*rso*rsi^2)/(Es*(rso^2 - rsi^2)) + ...
    rsi*((1 - barrel_v)*rbi^2 + (1 + barrel_v)*rso^2)/(Eb*(rbo^2 - rbi^2));
Cf3 = coef_f*2*pi*rso*sealthickness;

%% More Unit Conversions
```

```
R   = Ri/12;   % (ft) barrel innner radius
r   = ri/12;   % (ft) cushion small radius
Ds  = Dsi/12;  % (ft) stoppong distance
l1  = l1i/12;  % (ft) distance to first orifice ring
dor = dori/12; % (ft) distance between orifice rings
c   = ci/12;   % (ft) radial clearance between piccolo and cushion small radius
cushion_approach_factor = 1000;
cushion_approach = cushion_approach_factor*c; % (ft) distance to cushion when ...
                                              %      cushion calcs begin
Ps_initial  = 1*144;        % (psf) used to soften dPsdt when cushion engages
As          = pi*(R^2-r^2); % (ft^2) area to which stopping force is applied
Vs0         = As*Ds*1.002;  % (ft^3) volume when cushion closes initially, ...
                            % the extra is so that dPsdt !-> inf on the last time step

%% Values for Non-Dimensionalization
PI      = PD0*AD/AP;                % (psfa) intensified pressure
mI      = rho*Co*An*sqrt(2*PI/rho); % (slugs/s) intensified flowrate
vI      = mI/rho/An;                % (ft/s) intensified velocity
dxdtmax = vI*An/AP;                 % (ft/s) piston velocity to sustain vI
a0      = PD0*AD/MP;                % (ft/s^2) initial acceleration of the piston
ND      = [PI;mI;vI;dxdtmax;a0];

%%%%%%%%%%%%%%%%%%%%%%%%
% COMPUTATIONS SECTION %
%%%%%%%%%%%%%%%%%%%%%%%%

for runs=1:number_of_runs

    %% Run simulink diagram
    %open('Model5_v0_block_digram');
    %disp('Ready to start simulation?');

    %pause
    disp('Running simulation...');
    tic;
    sim('Model5_v0_block_digram'); %Bridgman water model
    Sim1time=toc;

    %%%%%%%%%%%%%%%%%%%%%%%%%%%%
    % POST-PROCESSING SECTION %
    %%%%%%%%%%%%%%%%%%%%%%%%%%%%

    %%%%%%%%%%%%%%%%%%%%%%%%%%%%%%%%%%%%%%%%%%%%
    %   PLOT SECTION OMITTED TO SAVE SPACE   %
    % PLEASE CONTACT AUTHORS FOR FULL SCRIPT %
    %%%%%%%%%%%%%%%%%%%%%%%%%%%%%%%%%%%%%%%%%%%%

    disp('Simulation time:')
    disp(Sim1time)

    %%%%%%%%%%%%%%%%%%%%%%%%%%%%
    % RESULTS ARCHIVE SECTION %
    %%%%%%%%%%%%%%%%%%%%%%%%%%%%
```

```
%% Save inputs and outputs
disp('Save sim?')
simnumint=input('Enter sim number (1 to 99999):  '); % TODO: check for duplicates
time=datestr(now,'yyyy-mm-dd-HHMMSS');                % Unique Time Stamp

% Define Number Strings
for i=1:8
    switch i
        case 1
            variable=simnumint;
        case 2
            variable=Nozzle_dia*1e4;
        case 3
            variable=PD0i*10;
        case 4
            variable=VD0i;
        case 5
            variable=Driving_piston_dia*1e3;
        case 6
            variable=Water_piston_dia*1e3;
        case 7
            variable=Stroke_lengthi*1e3;
        case 8
            variable=MPi*1e2;
    end

    % Keep Leading Zeros in the String
    tenthousands = floor(variable/10000);
    tenthoustr = int2str(tenthousands);
    variable = variable-tenthousands*10000;
    thousands = floor(variable/1000);
    thoustr = int2str(thousands);
    variable = variable-thousands*1000;
    hundreds = floor(variable/100);
    hundstr = int2str(hundreds);
    variable = variable-hundreds*100;
    tens = floor(variable/10);
    tenstr = int2str(tens);
    variable = variable-tens*10;
    ones = floor(variable);
    onestr = int2str(ones);

    switch i
        case 1
            simnum=strcat(tenthoustr,thoustr,hundstr,tenstr,onestr);
        case 2
            dn=strcat('dn',tenthoustr,thoustr,hundstr,tenstr,onestr,'_');
        case 3
            PDo=strcat('PDo',tenthoustr,thoustr,hundstr,tenstr,onestr,'_');
        case 4
            VDo=strcat('VDo',tenthoustr,thoustr,hundstr,tenstr,onestr,'_');
        case 5
            dD=strcat('dD',tenthoustr,thoustr,hundstr,tenstr,onestr,'_');
        case 6
```

```
                dP=strcat('dP',tenthoustr,thoustr,hundstr,tenstr,onestr,'_');
            case 7
                L=strcat('L',tenthoustr,thoustr,hundstr,tenstr,onestr,'_');
            case 8
                MP=strcat('MP',tenthoustr,thoustr,hundstr,tenstr,onestr,'_');
        end
    end

    % Record Model Number and Version
    mdlstr = int2str(model_number);
    verstr = int2str(version_number);

    % Store Filenames
    fnameI=strcat(simnum,'_M',mdlstr,'v',verstr,'_I_',time,'.csv');
    fnameO=strcat(simnum,'_M',mdlstr,'v',verstr,'_O.csv');
    fnameCTH = strcat(simnum,'_M',mdlstr,'v',verstr,'_',dn,PDo,VDo,...
            dD,dP,L,MP,time,'.csv');

    % Build Output Matrices
    disp('Constructing archive matrices...')
    input_matrix = [ simnumint 0 Sim1time PD0i VD0i Driving_piston_dia ...
            Water_piston_dia Nozzle_dia Stroke_lengthi MPi rho beta 0 0 npoly ...
                Co g 0 0 rboi rsii rcleari sealthicknessi coef_f Esi Ebi seal_v ...
        barrel_v 0 ri Dsi l1i dori N M ci mu Co_s cushion_orifice_diameteri ...
                0 0 0 d_chamfer m_flow_tolerance v_small 0 0 0 PI mI vI dxdtmax a0 ];

    output_matrix(:,1)  = tout;
    output_matrix(:,2)  = P(:,2);
    output_matrix(:,3)  = dPdt(:,2);
    output_matrix(:,4)  = x(:,2);
    output_matrix(:,5)  = dxdt(:,2);
    output_matrix(:,6)  = d2xdt2(:,2);
    output_matrix(:,7)  = mout(:,2);
    output_matrix(:,8)  = Vjet(:,2);
    output_matrix(:,9)  = PD(:,2);
    output_matrix(:,10) = Ps(:,2);
    output_matrix(:,11) = dPsdt(:,2);

    CTH_matrix(:,1) = tout;
    CTH_matrix(:,2) = Vjet(:,2);

    % Write Output Matrices
    disp('Saving archive matrices...')
    first_cd = cd;
    cd 'D:\MyDocs\ME 490\Simulation_Archives'
    csvwrite(fnameI,input_matrix);
    csvwrite(fnameO,output_matrix);
    csvwrite(fnameCTH,CTH_matrix);
    disp('Archive complete!')
    cd(first_cd)

end
```

Appendix C Embedded MATLAB Functions

The embedded MATLAB functions used within the DAI model are presented in this section.

```
function [d2xdt2,Ff,FD,FP,FS,Fother] = acceleration(PD,P,AD,MP,AP,g,Cf1,Cf2,Cf3,...
    rclear,dxdt,Ps,As,v_small)

% the frictional force should never help motion

if Cf1*P - rclear > 0   % makes sure gap is closed before friction is applied
    Ff = -Cf3*(Cf1*P - rclear)/Cf2;
    if dxdt < 0
        Ff = -Ff;
    end
else
    Ff = 0;
end

FD = PD*AD;
FG = g*MP;
FP = -P*AP;
FS = -Ps*As;
Fother = FD + FP + FS + FG;

%if the piston has essentially stopped
if abs(dxdt) < v_small
    if Ff*Fother < 0 && abs(Ff) > abs(Fother)
        Ff = -Fother;
    end
end

d2xdt2 = (Fother+Ff)/MP;

function dPsdt = cushion_p_rate(x,dxdt,betac,dPdt,Ps,no,rho,Aos,Co_s,Vs0,As,...
    d_chamfer,L,Ds,r,c,cushion_approach)

%Piccolo cushion pressure/flow model
coder.extrinsic('disp')

X = x - L + Ds;
if X >= -cushion_approach
    if X < 0
        c = sqrt(c^2 + X^2);
    end

    if Ps >= 0
        Q_gap     = -Co_s*2*pi*r*c*sqrt(2*Ps/rho);
        Q_orifice = -Co_s*Aos*sqrt(2*Ps/rho)*no;
    else
        Q_gap     = Co_s*2*pi*r*c*sqrt(2*-Ps/rho);%-pi*r*c^3/(6*mu*X)*Ps;
        Q_orifice = Co_s*Aos*sqrt(2*-Ps/rho)*no;
    end
        Q_CV_resize = As*dxdt;
        dPsdt       = betac/(Vs0 - As*X)*(Q_CV_resize + Q_gap+Q_orifice) - dPdt;
```

```
else
    dPsdt = 0;
end

function PD = driving_pressure(x,VD0,AD,PD0,npoly)

PD = PD0*(VD0/(VD0+AD*x))^npoly;

function mout = Mass_flow_out(P,Co,An,rho)

mout = Co*An*sqrt(2*P*rho);

function [no,X] = open_cushion_orifices(x,l1,dor,N,M,L,Ds,cushion_approach)
% calculates the number of open orifices in the piccolo cushion

X = x - L + Ds;
if X >= -cushion_approach
    if X < 0
        no = M*N;
    else
        s = zeros(1,4);
        covered_o = 0;
        for i = 1:N
            s(i) = l1 + dor*(i-1); % generate s sequence
            if X> = s(i)           % unit step function, total up the covered orifices
                covered_o = covered_o + 1;
            end
        end
        no = M*(N - covered_o);
    end
else
    no = 0;
end

function dPdt = water_pres_rate(x,dxdt,P,AP,Co,An,rho,V0,beta)

dPdt = (AP*dxdt - Co*An*sqrt(2*P/rho))/(V0 - AP*x)*beta;
```

Appendix D Compressibility Model MATLAB Functions

The MATLAB function for Bridgman compressibility of water is listed in this section.

```
function beta = bridgman_bulk(P)
% Gives bulk modulus from bridgman data using CDD differentiation
% INEFFICIENT
% Gives bulk modulus as a function of pressure at a constant
% temperature using Bridgman data, good for 0 to 7 kbar
% Output is in kbar, P is kbar
% Marshall Schaeffer  10-28-11

pres = [    0  500 1000 1500 2000 2500 3000 3500 4000 4500 5000 ...
         5500 6000 6500 7000 7500 8000 8500 9000 9500 10000];       % (kgm/cm^2)

pres = pres * 0.98/1000; % (kbar)

% Volume at 20 degC (compared to 0 kgm/cm^2 at 0 deg C)
V = [ 1.0016 0.9812 0.9638 0.9467 0.9332 0.9203 0.9081 0.8984 ...
      0.8878 0.8785 0.8696 0.8616 0.8545 0.8475 0.8412 0.8346 ...
      0.8284 0.8218 0.8157 0.8099 0.8046 ];

dvdp  = zeros(21);
dpdv  = zeros(21);
betaa = zeros(21);

v = V/0.9999;  % (cm^3/g) engineering toolbox.com
i = length(v); % gives water density at 0 deg C

% Forward Difference for First Point
dvdp(1) = (v(2) - v(1))/(pres(2) - pres(1));
dpdv(1) = 1/dvdp(1);

% Central Difference for Intermediates
for k = 2:i-1
    dvdp(k) = (v(k+1) - v(k-1))/(pres(k+1) - pres(k-1));
    dpdv(k) = 1/dvdp(k);
end

% Backward Difference for Last Point
dvdp(i) = (v(i) - v(i-1))/(pres(i) - pres(i-1));
dpdv(i) = 1/dvdp(i);

for j=1:i
    betaa(j) = -dpdv(j)*v(j);
end

for i = 1:length(pres)
    if P < pres(i+1) && P >= pres(i);
        beta = betaa(i) + ((betaa(i+1) - betaa(i))/(pres(i+1) -...
            pres(i)))*(P-pres(i)); % (kbar)
        break
    end
end
```

Appendix E Sample CTH Input Files

Two sample CTH input files are listed in this appendix. Note that the complete aggregate distributions and velocity tables have been truncated to save space. The original files are available from the authors. A more complete description of the operation, maintenance, and usage of the workstation will be developed and delivered over the coming summer months.

The first is an axisymmetric simulation with homogenized concrete.

```
*eor* cthin
test with 4 mm standoff, 2mm diameter jet, and air
*
******************************
* Paul Gessler, Alex Zelhofer *
* Adapted from 'drip5'  *
*         2012-04-03          *
******************************
*
******************************
* SIMULATION CONTROL SECTION *
******************************
control
  mmp                  * Enables per-material Temp. and Press.
                       *    in mixed-material cells (Eulerian)
  tstop = 0.05         * Simulation Stop Time (s)
endcontrol
*
*********
*RESTART*
*********
*********************************
* HISTORY FILE CREATION SECTION *
*********************************
spy
  Save("VOLM","VX","VY","P","T","DENS");
  SaveTime(0.0,5e-6);
endspy
*
************************
* MESH CREATION SECTION *
************************
*
mesh
  block 1 geometry 2dc type eulerian * 2D Cylindrical (symmetric), Eulerian Mesh
    x0=0.                            * Initial x-value (cm)
      x1  dxf=0.0625 dxl=0.0625 w=10    * Grid size grows from 0.01 - 0.5 cm
                                        *    from x0 to x1 = 10 cm
    endx
    y0=-15.2                            * Initial y-value (cm)
      y1  dyf=0.0625 dyl=0.0625 w=17.2  * Constant y-grid size of 0.05 cm
    endy
  endb
endmesh
*
```

```
******************************
* INTERFACE TRACKING SECTION *
******************************
convct
  interface=smyra
endc
*
****************************
* EQUATION OF STATE SECTION *
****************************
eos
  mat1 ses air
  mat2 ses water
  mat3 conc SAC5
endeos
*
******************************
* MATERIAL INSERTION SECTION *
******************************
diatoms
*************************
***Larger chunk of air***
*************************
  package 'air'
    material 1
    pressure=1013250
    temperature=2.568e-2
    insert box
      p1 0.1 -0.2
      p2 10.0 2.0
    endinsert
  endpackage
*
*************************
***Air right under jet***
*************************
  package 'air'
    material 1
    pressure=1013250
    temperature=2.568e-2
    insert box
      p1 0.0 -0.2
      p2 0.1 0.2
    endinsert
  endpackage
*
************************
***Start of water jet***
************************
  package 'water'
    material 2
    pressure=1013250
    temperature=2.568e-2
    YV=-500
```

```
    insert box
      p1 0. 0.2
      p2 0.1 2.0
    endinsert
  endpackage
*
***************
***Water jet***
***************
  replace_package 'water'
    material 2
    pressure=1013250
    temperature=2.568e-2
    MVelocity=<0,t1>
    insert box
      p1 0. 0.2
      p2 0.1 2.0
    endinsert
    ON=1e-9
    OFF=100
  endreplace
*
************************************
***Water damper in front of nozzle***
************************************
replace_package 'water'
    material 2
    pressure=1013250
    temperature=2.568e-2
    MVelocity=<0,0>
    insert box
      p1 0.0 0.15
      p2 0.1 0.2
    endinsert
  endreplace
*
*******************************************
***Remove all rigid material from domain***
*******************************************
remove_package
   material rigid
endremove_package
*
*************************
***Side wall of nozzle***
*************************
   replace_package
      rigid
      insert box
         p1 0.1 0.2
         p2 0.2 2.0
      endinsert
   endreplace
*
```

```
****************************
***Semi-infinite concrete***
****************************
  package 'concrete'
    material 3
    pressure=1013250
    insert box
      p1 0 -15.2
      p2 10.0 -0.2
    endinsert
  endpackage
enddiatoms
*
*
*********************
* FILE EDIT SECTION *
*********************
edit
  shortc
    cy  0     dc 1000
  ends
  longt
   tim 1.e-6 dt 1.0
  endl
  restt
    tim 0     dt 5e-4
  endr
ende
*
*******************************
* BOUNDARY CONDITIONS SECTION *
*******************************
boundary
  bhy
      bxb=0 bxt=1 byb=1 byt=1
  endh
endb
*
****************************
* FRACTURE STRENGTH SECTION *
****************************
*fracts
*  pfrac1 -1.0   *water
*  pfvoid -1.0e20
*endf
*

****************************
* TIME STEP CONTROL SECTION *
****************************
mindt
  time 0 dtmin 1e-50 dtmax 1e-6
endm
```

```
***********************************
* VELOCITY INPUT CREATION SECTION *
***********************************
deftable=1
0 -1125.88434646
0.0001 -3549.64090022
0.0002 -6841.16985348
0.0003 -10195.7085154
* < complete velocity input omitted >
0.197 -29659.2872438
0.1975 -29622.6217137
0.198 -29595.0986871
0.1985 -29580.6371105
enddeftable
*
*******END OF INPUT DECK******
```

The second is a 3D simulation with homogenized concrete binder and randomly distributed aggregate spheres.

```
*eor* cthin
3d simulation with aggregate sphere
*
*******************************
* Paul Gessler, Alex Zelhofer *
* Adapted from 'drip6'  *
*         2012-05-05          *
*******************************
*
******************************
* SIMULATION CONTROL SECTION *
******************************
control
  mmp                  * Enables per-material Temp. and Press.
                       *    in mixed-material cells (Eulerian)
  tstop = 0.05         * Simulation Stop Time (s)
  rigid
endcontrol
*
*********************************
* HISTORY FILE CREATION SECTION *
*********************************
spy
  Save("VOLM","VX","VY","P","T","DENS");
  SaveTime(0.0,5e-6);
endspy
*
************************
* MESH CREATION SECTION *
************************
*
mesh
  block 1 geometry 3dr type eulerian
    x0=-5.
      x1  dxf=0.0625 dxl=0.0625 w=10
    endx
    y0=-5
      y1  dyf=0.0625 dyl=0.0625 w=10
    endy
    z0=-8
      z1 dzf=0.0625 dzl=0.0625 w=10
    endz
    xact -5 5
    yact -5 5
    zact -8 2
  endb
endmesh

*****************************
* INTERFACE TRACKING SECTION *
*****************************
```

```
convct
  interface=smyra
endc
*
****************************
* EQUATION OF STATE SECTION *
****************************
eos
  mat1 ses air
  mat2 ses water
  mat3 conc SAC5
, mat4 ses steel_V300
endeos
*
******************************
* MATERIAL INSERTION SECTION *
******************************
diatoms
*
***************************
***Semi-infinite concrete***
***************************
  package 'concrete'
    material 3
    pressure=1013250
    insert box
      p1 -5 -5 -8
      p2 5 5 -.2
    endinsert
  endpackage
*
********************
*Aggregate Sphere 1*
********************
replace_package steel_v300
material 4
pressure=1013250
temperature=2.568e-2
insert sphere
center 3.295 -2.162 -6.396
radius 0.134
endinsert
endpackage
*
* < random distribution of aggregate omitted >
*
********************
*Aggregate Sphere 8*
********************
replace_package steel_v300
material 4
pressure=1013250
temperature=2.568e-2
insert sphere
```

```
center -2.243 3.633 -2.468
radius 0.353
endinsert
endpackage
*
*************************
***Air***
*************************
  package 'air'
    material 1
    pressure=1013250
    temperature=2.568e-2
    insert box
      p1 -5.0 -5.0 -0.2
      p2  5.0  5.0  2.0
    endinsert
  endpackage
*
*************************
***Side wall of nozzle***
*************************
replace_package
      rigid
      insert cylinder
         ce1 0 0 0.2
         ce2 0 0 2.0
         radius 0.3
      endinsert
endreplace_package
*
***************
***Water jet***
***************
  replace_package 'water'
    material 2
    pressure=1013250
    temperature=2.568e-2
    MVelocity=<0,0,t1>
    insert cylinder
      ce1 0.0 0.0 0.2
      ce2 0.0 0.0 2.0
      radius 0.2
    endinsert
    ON=0
    OFF=100
  endreplace
*
************************************
***Water damper in front of nozzle***
************************************
replace_package 'water'
    material 2
    pressure=1013250
    temperature=2.568e-2
```

```
    MVelocity=<0,0,0>
    insert cylinder
       ce1 0 0 0.15
       ce2 0 0 0.2
       radius 0.2
    endinsert
  endreplace
enddiatoms
*********************
* FILE EDIT SECTION *
*********************
edit
  shortc
    cy  0     dc 1000
  ends
  longt
   tim 1.e-6 dt 1.0
  endl
  restt
    tim 0     dt 5e-4
  endr
ende
*
*******************************
* BOUNDARY CONDITIONS SECTION *
*******************************
boundary
  bhy
      bxb=1 bxt=1 byb=1 byt=1 bzb=1 bzt=1
  endh
endb
*
****************************
* TIME STEP CONTROL SECTION *
****************************
mindt
  time 0 dtmin 1e-20 dtmax 1e-6
endm
***********************************
* VELOCITY INPUT CREATION SECTION *
***********************************
deftable=1
0 -1125.88434646
0.0001 -3549.64090022
0.0002 -6841.16985348
0.0003 -10195.7085154
* < complete velocity input omitted >
0.197 -29659.2872438
0.1975 -29622.6217137
0.198 -29595.0986871
0.1985 -29580.6371105
enddeftable
*
*******END OF INPUT DECK******
```

Appendix F POLYOX MSDS

This appendix contains the material safety data sheet obtained from Union Carbide Corporation for the long-chain polymer used in the differential area intensifier (DAI) to promote jet stability. [21]

UNION CARBIDE CORPORATION
A Subsidiary of The Dow Chemical Company

MATERIAL SAFETY DATA SHEET

Product Name: POLYOX(TM) WSR 301 **Effective Date:** 06/26/2000
MSDS#: 1798 **Page** 1 of 15

Union Carbide urges each customer or recipient of this MSDS to study it carefully to become aware of and understand the hazards associated with the product. The reader should consider consulting reference works or individuals who are experts in ventilation, toxicology, and fire prevention, as necessary or appropriate to use and understand the data contained in this MSDS.

To promote safe handling, each customer or recipient should: 1) Notify its employees, agents, contractors and others whom it knows or believes will use this material of the information in this MSDS and any other information regarding hazards or safety; 2) Furnish this same information to each of its customers for the product; and 3) Request its customers to notify their employees, customers, and other users of the product of this information.

1. CHEMICAL PRODUCT AND COMPANY IDENTIFICATION

1.1 IDENTIFICATION

Product Name	POLYOX(TM) WSR 301
Chemical Name	Poly(ethylene oxide)
Chemical Family	Polyethers
Formula	(CH2CH2O)x
Synonym	Poly(oxyethylene)

1.2 COMPANY IDENTIFICATION

Union Carbide Corporation
A Subsidiary of The Dow Chemical Company
39 Old Ridgebury Road
Danbury, CT 06817-0001

1.3 EMERGENCY TELEPHONE NUMBER

24 hours a day: CHEMTREC 1-800-424-9300.
Number for non-emergency questions concerning MSDS (732) 563-5522
Additional information on this product may be obtained by calling the Union Carbide Corporation Customer Service Center at 1-800-568-4000.

Copyright© 2000, Union Carbide Chemicals & Plastics Technology Corporation.
POLYOX is a trademark of Union Carbide.

MATERIAL SAFETY DATA SHEET

2. COMPOSITION INFORMATION

Component	CAS #	Amount (%W/W)
Poly(ethylene oxide)	25322-68-3	>= 95 %
Fumed silica (generic)	112945-52-5	<= 3%
Calcium as mixed salts	Not available	<= 1%
BHT	128-37-0	<= 0.1%
Ammonia	7664-41-7	<= 0.02%
Monoethylamine	75-04-7	<= 0.02%
Ethylene oxide	75-21-8	<= 0.004%

3. HAZARDS IDENTIFICATION

3.1 EMERGENCY OVERVIEW

Appearance White to off-white

Physical State Powder

Odor Mild ammoniacal

Hazards of product WARNING! CAUSES EYE IRRITATION.
STATIC IGNITION HAZARD CAN RESULT FROM HANDLING AND USE.
DUST DISPERSED IN AIR MAY BE IGNITED AND BURN RAPIDLY.
PLASTIC CONTAINER, IF PRESENT, MAY CAUSE STATIC IGNITION HAZARD.
SLIPPERY WHEN WET.

3.2 POTENTIAL HEALTH EFFECTS

Effects of Single Acute Overexposure

Inhalation Dust may cause irritation of the respiratory tract, experienced as nasal discomfort and discharge.

Eye Contact Dust may cause discomfort in the eye with slight excess redness and possibly swelling of the conjunctiva.

Skin Contact No evidence of harmful effects from available information.

Skin Absorption No evidence of adverse health effects from available information.

Swallowing Slightly toxic. May cause abdominal discomfort, nausea, vomiting and diarrhea.

Chronic, Prolonged or Repeated Overexposure

Effects of Repeated Overexposure This product may contribute to nuisance dusts and possibly to respirable dusts. Avoid breathing dusts.

Other Effects of Overexposure None currently known.

Medical Conditions Aggravated by Exposure

A knowledge of the available toxicology information and of the physical and chemical properties of the material suggests that overexposure is unlikely to aggravate existing medical conditions.

3.3 POTENTIAL ENVIRONMENTAL EFFECTS

See Section 12 for Ecological Information.

4. FIRST AID PROCEDURES

4.1 INHALATION

No emergency care anticipated.

4.2 EYE CONTACT

Immediately flush eyes with water and continue washing for several minutes. Remove contact lenses, if worn. Obtain medical attention

4.3 SKIN CONTACT

Wash skin with soap and water.

4.4 SWALLOWING

MATERIAL SAFETY DATA SHEET

If a large quantity (several ounces) has been swallowed, and if patient is fully conscious, give two glasses of water. Induce vomiting. This should be done only by medical or experienced first-aid personnel. Obtain medical attention.

4.5 NOTES TO PHYSICIAN

There is no specific antidote. Treatment of overexposure should be directed at the control of symptoms and the clinical condition of the patient.

5. FIRE FIGHTING MEASURES

5.1 FLAMMABLE PROPERTIES

Flash Point - Closed Cup: *Not currently available.*

Flash Point - Open Cup: *Not currently available.*

Autoignition Temperature: **280 - 330 °C** **536 - 626 °F**

Flammable Limits In Air:

Lower	*Not determined.*
Upper	*Not determined.*

5.2 EXTINGUISHING MEDIA

Extinguish fires with water spray or apply alcohol-type or all-purpose-type foam by manufacturer's recommended techniques for large fires. Use carbon dioxide or dry chemical media for small fires.

5.3 EXTINGUISHING MEDIA TO AVOID

No information currently available.

5.4 SPECIAL FIRE FIGHTING PROCEDURES

Do not direct a solid stream of water or foam into burning molten material; this may cause spattering and spread the fire. Fire fighters and others involved in a fire situation should be aware that this material in contact with water can create an extremely slippery walking surface.

5.5 SPECIAL PROTECTIVE EQUIPMENT FOR FIREFIGHTERS

Use self-contained breathing apparatus and protective clothing.

5.6 UNUSUAL FIRE AND EXPLOSION HAZARDS

Avoid dispersion of dust in air to reduce potential for dust ignition/explosions. Dust is easily ignited; avoid ignition sources. Handle and convey in inert nitrogen-blanketed atmospheres.

Refer to National Fire Protection Association Document NFPA 69 for descriptions of explosion prevention systems.
Static ignition hazard can result from handling and use. Electrically bond and ground all containers, personnel and equipment before transfer or use of material. Special precautions may be necessary to dissipate static electricity for non-conductive containers. Use proper bonding and grounding during product transfer as described in National Fire Protection Association Document NFPA 77.

For POLYOX WSR products in flexible intermediate bulk containers, a static ignition hazard can result from handling and use. Non-conductive containers cannot be grounded. For transfers between flexible intermediate bulk containers and another non-conductive container, special precautions may be necessary to dissipate static electricity. For conductive components (containers, personnel, equipment) use proper bonding and grounding during product transfer as described in National Fire Protection Association Document NFPA 77. Refer to National Fire Protection Association Document NFPA 69 for descriptions of explosion prevention systems.
See Section 8.3 - Engineering Controls

5.7 HAZARDOUS COMBUSTION PRODUCTS

Burning can produce the following products: Carbon monoxide and/or carbon dioxide. Carbon monoxide is highly toxic if inhaled. Carbon dioxide in sufficient concentrations can act as an asphyxiant.

6. ACCIDENTAL RELEASE MEASURES

Steps to be Taken if Material is Released or Spilled:
Remove spills promptly. Floors can be slippery where this product has been spilled, especially when wet. Vacuum up solids or liquid spills as thoroughly as possible. Apply a 10% soda ash (sodium carbonate) solution to the surface and collect. Note that a 10% soda ash solution is caustic. If soda ash is not available, laundry bleach may be used; if used, allow to stand one hour and flush thoroughly with water. Collect liquid for disposal and rinse the surface thoroughly with water. Repeat if necessary.

Personal Precautions: Wear suitable protective equipment. Floor may be slippery. Use care to avoid falling. See Section 8.2 - Personal Protection.

7. HANDLING AND STORAGE

7.1 HANDLING

General Handling

MATERIAL SAFETY DATA SHEET

Avoid contact with eyes.
Electrically bond and ground all containers, personnel and equipment before transfer or use of material.
Avoid heat, sparks and flame under dust conditions.
Do not handle or empty in presence of flammable vapor.
Keep container closed.
Use with adequate ventilation.
Clean up spills.
Wash thoroughly after handling.

FOR INDUSTRY USE ONLY.

Ventilation
Special, local ventilation is recommended in areas where containers are opened and their contents are discharged or in any other areas where dusting conditions may develop.

7.2 STORAGE

Store in accordance with good industrial practices. Storage information may be obtained from product-specific Union Carbide Storage and Handling Guides, or by calling a Union Carbide Customer Service Representative.

8. EXPOSURE CONTROLS AND PERSONAL PROTECTION

8.1 EXPOSURE LIMITS

Component	Exposure Limits	Skin	Form
Nuisance Dust	10 mg/m3 TWA8 ACGIH		Inhalable Particulate Particulate matter containing no asbestos and crystalline silica <1%
Nuisance Dust	3 mg/m3 TWA8 ACGIH		Respirable particulate Particulate matter containing no asbestos and crystalline silica <1%
Nuisance Dust	5 mg/m3 TWA8 OSHA 15 mg/m3 TWA8 OSHA		Respirable fraction Total dust
Fumed silica (generic)	2 mg/m3 TWA8 ACGIH		Respirable particulate
BHT	10 mg/m3 TWA8 ACGIH		
BHT	10 mg/m3 TWA8 OSHA-Vacated		
Ammonia	17 mg/m3 TWA8 ACGIH 25 ppm TWA8 ACGIH		

MATERIAL SAFETY DATA SHEET

	24 mg/m3 STEL ACGIH	
	35 ppm STEL ACGIH	
Ammonia	27 mg/m3 STEL OSHA-Vacated	
	35 ppm STEL OSHA-Vacated	
	50 ppm TWA8 OSHA	
	35 mg/m3 TWA8 OSHA	
Monoethylamine	5 ppm TWA8 ACGIH	Yes
	9.2 mg/m3 TWA8 ACGIH	Yes
	15 ppm STEL ACGIH	Yes
	27.6 mg/m3 STEL ACGIH	Yes
	10 ppm TWA8 OSHA	
	18 mg/m3 TWA8 OSHA	
Ethylene oxide	1 ppm TWA8 ACGIH	
	1.8 mg/m3 TWA8 ACGIH	
	1 ppm TWA8 UCC	
	1 ppm TWA8 OSHA	
	5 ppm Excursion Limit OSHA	

In the Exposure Limits Chart above, if there is no specific qualifier (i.e., Aerosol) listed in the Form Column for a particular limit, the listed limit includes all airborne forms of the substance that can be inhaled.

A "Yes" in the Skin Column indicates a potential significant contribution to overall exposure by the cutaneous (skin) route, including mucous membranes and the eyes, either by contact with vapors or by direct skin contact with the substance. A "Blank" in the Skin Column indicates that exposure by the cutaneous (skin) route is not a potential significant contributor to overall exposure.

8.2 PERSONAL PROTECTION

Respiratory Protection: Dust respirator, if dusting conditions exist.

Ventilation: Special, local ventilation is recommended in areas where containers are opened and their contents are discharged or in any other areas where dusting conditions may develop.

Eye Protection: Monogoggles

Protective Gloves: Neoprene
Butyl
PVC-coated

MATERIAL SAFETY DATA SHEET

Other Protective Equipment: Eye Bath, Safety Shower

8.3 ENGINEERING CONTROLS

Dust explosion hazard: See Section 5.6 - Unusual Fire and Explosion Hazards - regarding dust explosion hazard.
FIBC: For Flexible Intermediate Bulk Containers - before transferring material, ground workers and conductive equipment to dissipate static electricity.

9. PHYSICAL AND CHEMICAL PROPERTIES

Physical State: Powder

Appearance: White to off-white

pH: *Not currently available.*

Solubility in Water (by weight): *Not determined.*

Odor: Mild ammoniacal

Percent Volatiles: **< 1.0 Wt%**

Molecular Weight: **100000 - 8000000 g/mol**

Boiling Point (760 mmHg): *Not determined.*

Freezing Point: *Not determined.*

Specific Gravity (H2O = 1): *Not applicable.*

Vapor Pressure at 20°C: *Not applicable.*

Vapor Density (air = 1): *Not applicable.*

Melting Point: **62 - 67 °C 143 - 153 °F** , Crystalline melting point

Bulk Density: **500 kg/m3 31 lb/ft3**

MATERIAL SAFETY DATA SHEET

10. STABILITY AND REACTIVITY

10.1 STABILITY/INSTABILITY Stable

10.2 HAZARDOUS POLYMERIZATION Will Not Occur.

10.3 INHIBITORS/STABILIZERS Not applicable.

11. TOXICOLOGICAL INFORMATION

The following information is based on analogy with a similar material.

ACUTE TOXICITY

Peroral

Rat; female; LD50 = > 4.0 g/kg

Percutaneous

Rat; female; LD50 = > 2.0 g/kg; 4 h occluded contact.

IRRITATION

Skin: Rabbit; 4 h occluded contact; 0.5 g; moistened with water
Results: no irritation

Eye: Rabbit; 0.5 ml; 5% in water
Results: no irritation

REPEATED EXPOSURE

Fourteen days of inclusion of POLYOX Water Soluble Resin in the diet of rats at 50000 ppm resulted in only the presence of loose feces. No effects were seen at 20000 ppm.

CHRONIC TOXICITY AND CARCINOGENICITY

Inclusion of POLYOX Water Soluble Resin in the diet of rats for 2 years at 20000 ppm (1000-1300 mg/kg/day) did not result in treatment-related effects or evidence of oncogenicity.

PHARMACOKINETICS AND METABOLISM

In Vitro
Pharmacokinetic and material balance studies conducted with a radiocarbon labeled water soluble POLYOX Resin showed nearly total quantitative recovery of the material in feces, with insignificant amounts in blood and tissues, indicating the material is not absorbed from the gastrointestinal tract.

In Vivo
Pharmacokinetic and material balance studies conducted with a radiocarbon labeled water soluble POLYOX Resin showed nearly total quantitative recovery of the material in feces, with insignificant amounts in blood and tissues, indicating the material is not absorbed from the gastrointestinal tract.

SIGNIFICANT DATA WITH POSSIBLE RELEVANCE TO HUMANS
Pharmacokinetic and material balance studies conducted with a radiocarbon labeled water soluble POLYOX resin showed nearly total quantitative recovery of the material in feces, with insignificant amounts in blood and tissues, indicating the material is not absorbed from the gastrointestinal tract.

12. ECOLOGICAL INFORMATION

12.1 ENVIRONMENTAL FATE

Information may be available, call Union Carbide.

12.2 ECOTOXICITY

The following information is based on analogy with a similar material.

Toxicity to Aquatic Invertebrates
Daphnia; 48 h; LC50
Result value: 7550 mg/l

Toxicity to Fish
Fathead Minnow; 96 h; LC50
Result value: > 10000 mg/l

12.3 FURTHER INFORMATION

None.

13. DISPOSAL CONSIDERATIONS

13.1 WASTE DISPOSAL METHOD

Bury in a landfill where permitted under appropriate Federal, State, and local regulations. Potential for dust explosion exists if an attempt is made to incinerate organic powders. If incineration is desired, dissolve in a suitable solvent and burn as a solution. Dispose in accordance with all applicable Federal, State, and local environmental regulations. Do not reuse drums. Disassembled components of the empty container/drums can be recycled. Empty containers/drums should be recycled or disposed of through an approved waste management facility.

13.2 DISPOSAL CONSIDERATIONS

See Section 13.1

Disposal methods identified are for the product as sold. For proper disposal of used material, an assessment must be completed to determine the proper and permissible waste management options permissible under applicable rules, regulations and/or laws governing your location.

14. TRANSPORT INFORMATION

14.1 U.S. D.O.T.

NON-BULK
Proper Shipping Name : NOT REGULATED

BULK
Proper Shipping Name : NOT REGULATED

MATERIAL SAFETY DATA SHEET

This information is not intended to convey all specific regulatory or operational requirements/information relating to this product. Additional transportation system information can be obtained through an authorized sales or customer service representative. It is the responsibility of the transporting organization to follow all applicable laws, regulations and rules relating to the transportation of the material.

15. REGULATORY INFORMATION

15.1 FEDERAL/NATIONAL

COMPREHENSIVE ENVIRONMENTAL RESPONSE, COMPENSATION, AND LIABILITY ACT OF 1980 SECTION 103 (CERCLA)

The following components of this product are specifically listed as hazardous substances in 40 CFR 302.4 (unlisted hazardous substances are not identified) and are present at levels which could require reporting:

Component	CAS #	Amount
Ammonia	7664-41-7	<= 0.0200%
Monoethylamine	75-04-7	<= 0.0200%
Ethylene oxide	75-21-8	<= 0.0040%

SUPERFUND AMENDMENTS AND REAUTHORIZATION ACT OF 1986 TITLE III (EPCRA) SECTIONS 302 AND 304

The following components of this product are listed as extremely hazardous substances in 40 CFR Part 355 and are present at levels which could require reporting and emergency planning:

None.

SUPERFUND AMENDMENTS AND REAUTHORIZATION ACT OF 1986 TITLE III (EPCRA) SECTION 313

The following components of this product are listed as toxic chemicals in 40 CFR 372.65 and are present at levels which could require reporting and customer notification under Section 313 and 40 CFR Part 372:

- This product does not contain toxic chemicals at levels which require reporting under the statute.

MATERIAL SAFETY DATA SHEET

SUPERFUND AMENDMENTS AND REAUTHORIZATION ACT OF 1986 TITLE III (EPCRA) SECTIONS 311 AND 312

Delayed Hazard : No
Fire Hazard : No
Immediate Health Hazard : Yes
Reactive Hazard : No
Sudden Release of Pressure Hazard : No

TOXIC SUBSTANCES CONTROL ACT (TSCA)

All components of this product are on the TSCA Inventory or are exempt from TSCA Inventory requirements.

EUROPEAN INVENTORY OF EXISTING COMMERCIAL CHEMICAL SUBSTANCES (EINECS)

The component of this product is on the EINECS inventory.

CEPA - DOMESTIC SUBSTANCES LIST (DSL)

The components of this product are on the DSL or are exempt from reporting under the New Substances Notification Regulations.

15.2 STATE/LOCAL

PENNSYLVANIA (WORKER AND COMMUNITY RIGHT-TO-KNOW ACT)

This product is subject to the Worker and Community Right-to-Know Act. The following components of this product are at levels which could require identification in the MSDS: None.

MASSACHUSETTS (HAZARDOUS SUBSTANCES DISCLOSURE BY EMPLOYERS)

The following components of this product appear on the Massachusetts Substance List and are present at levels which could require identification in the MSDS:

Component	CAS #	Amount
Ammonia	7664-41-7	<= 0.0200%
Ethylene oxide	75-21-8	<= 0.0040%

MATERIAL SAFETY DATA SHEET

CALIFORNIA PROPOSITION 65 (SAFE DRINKING WATER AND TOXIC ENFORCEMENT ACT OF 1986)

This product contains the following chemical(s) known to the State of California to cause cancer and birth defects or other reproductive harm.

Component	CAS #	Amount
Ethylene oxide	75-21-8	<= 0.0040%

CALIFORNIA SOUTH COAST AIR QUALITY MANAGEMENT DISTRICT (SCAQMD) RULE 443.1:

VOC: Volatiles = Substances with a vapor pressure of > 0.5 mmHg @ 104 °C (219.2 °F)
0.0 g/l
0.00 g/l of material less water and less exempted solvents.

This section provides selected regulatory information on this product including its components. This is not intended to include all regulations. It is the responsibility of the user to know and comply with all applicable rules, regulations and laws relating to the product being used.

16. OTHER INFORMATION

16.1 AVAILABLE LITERATURE AND BROCHURES

Additional information on this product may be obtained by calling the Union Carbide Corporation Customer Service Center at 1-800-568-4000.

Ask for the brochure:
POLYOX WSR Storage and Handling (report).

16.2 SPECIFIC HAZARD RATING SYSTEM

HMIS ratings for this product are: H - 0 F - 1 R - 0

NFPA ratings for this product are: H - 0 F - 1 R - 0

MATERIAL SAFETY DATA SHEET

These ratings are part of specific hazard communications program(s) and should be disregarded where individuals are not trained in the use of these hazard rating systems. You should be familiar with the hazard communication applicable to your workplace.

16.3 RECOMMENDED USES AND RESTRICTIONS

FOR INDUSTRY USE ONLY

16.4 REVISION

Version: 3.
Revision: 06/26/2000
Most recent revision(s) are noted by the bold, double bars in left-hand margin throughout this document.

16.5 LEGEND

A	Asphyxiant
Bacterial/NA	Non Acclimated Bacteria
F	Fire
H	Health
HMIS	Hazardous Materials Information System
N/A	Not available
NFPA	National Fire Protection Association
O	Oxidizer
P	Peroxide Former
R	Reactivity
TS	Trade Secret
VOL/VOL	Volume/Volume
W	Water Reactive
W/W	Weight/Weight

The opinions expressed herein are those of qualified experts within Union Carbide. We believe that the information contained herein is current as of the date of this Material Safety Data Sheet. Since the use of this information and the conditions of the use of the product are not under the control of Union Carbide, it is the user's obligation to determine conditions of safe use of the product.

Appendix G Hydraulic Fluid MSDS

This appendix contains the material safety data sheet obtained from SPX Fluid Power for the biodegradable hydraulic fluid used in the differential area intensifier (DAI). [22]

Material Safety Data Sheet

Material Safety Data Sheet Page 1.
Biodegradable Hydraulic Fluid

Section1. Chemical Product and Company Identification. Product Name:
Biodegradable Hydraulic Fluid
Code / Part Number:9645, 9646
Manufacturer: SPX Fluid Power
5885 11th Street
Rockford, IL 61109, USA
Phone: 815-874-5556

CHEMTREC 24 Hr Emergency Number: 800-424-9300
Material Use: The product designed for use in a Hydraulic fluid applications.
Validated January, 2004

Section 2. Composition and Information on Ingredients.
Name: Rapeseed oil, ethylhexyl oleate and proprietary additives
CAS#: Mixture
% (V/V): 100
Exposure Limits:
TLV-TWA (8hr): not established
STLE: not established
Manufacturer Recommendation: Not applicable
Other Exposure Limits: Consult local, state, provincial or territorial authorities for acceptable exposure limits.

Section 3. Hazardous Identification.
Potential Health Effects: Not irritating to slight irritation to skin and eyes with no permanent damage. Relatively non-toxic via ingestion. This product has a low vapor pressure and is not expected to present an inhalation exposure at ambient conditions. At high temperatures or mechanical actions may produce vapors or mists, inhalation may cause irritation of the breathing passages. See section 11.

Section 4. First Aid Measures
Eye contact: Immediately flush eyes with running water for at least 15 minutes, keeping eyelids open. Seek medical attention.
Skin Contact: Remove contaminated clothing – launder before reuse. Wash contaminated skin with running water and non-abrasive soap. Get medical attention if irritation develops or if product is injected under pressure into or under the skin.
Inhalation: Remove to fresh air. Get medical attention if breathing difficulty persists. If victim is not breathing, perform artificial respiration.
Ingestion: DO NOT induce vomiting. Seek medical attention.

Section 5. Fire-fighting Measures
Flammability: May be combustive at high temperature.
Flash point: 193 deg C (380 deg F) (COC)
Flammable Limits: Not available
Auto-Ignition Temperature: Not available
Fire Hazard in Presence of Various Substances: Low fire hazard. This material must be heated before ignition will occur.
Explosion Hazards in Presence of Various Substances: Do not cut, weld, drill or pressurize empty container. Containers may explode in heat of fire.
Products of Combustion: various oxides of carbon, smoke and irritating vapors from incomplete combustion.
Fire Fighting Media Instructions: NAERG96, Guide 171, Substances (low to moderate hazard). If tank, rail car or tank is involved in fire, ISOLATE for 800 meters (0.5 mile) in all directions. Shut off fuel to fire if it is possible to do without hazard. If it is not possible, withdraw from area and let fire burn out under controlled conditions. Withdraw immediately in case of rising sound from venting safety device or any discoloration of tank due to fire. Cool containing vessels with water spray in order to prevent pressure build-up, auto ignition or explosion.
Small fire: use DRY chemicals, foam, water spray or CO2.
Large Fire: use water spray, fog or foam. For small outdoor fires, portable fire extinguishers may be used. For all indoor fires and significant outdoor fires self-contained breathing apparatus is required. Respiratory and eye protection are required for fire fighting personnel.

Section 6. Accidental Release Measures
Material Release or Spill: NAERG96, Guide 171, Substances (low to moderate hazard). ELIMINATE ALL IGNITION SOURCES. Avoid contact. Stop leak if without risk. Contain spill. Absorb with inert absorbents. Place used absorbent in closed metal containers for later disposal or burn absorbent in suitable combustion chamber. DO NOT FLUSH TO SEWERS, STREAMS OR OTHER BODIES WATER. Check with applicable jurisdiction for specific disposal requirements of spilled materials and empty containers. Notify the appropriate authorities immediately.

Section 7. Handling and Storage.
Handling: Avoid inhalation and skin contact especially when handling used oil. Keep away from sources of ignition. Do not reuse empty containers without commercial reconditioning. Practice good personal hygiene. Wash hands after handling oil and before eating. Launder work clothes frequently. Discard saturated leather goods.
Storage: Store in tightly closed containers in cool, dry, isolated, well-ventilated area, and away from incompatibles.

Section 8. Exposure Control / Personal Protection.
Engineering Controls: For normal application, special ventilation is not necessary. If user's operations generate vapors or mists, use ventilation to keep contaminants below exposure limits. Make-up air should always be supplied to balance air removed by exhaust. Have eyewash station and safety-shower close to workstation.
Personal Protection:
Eyes: Eye protection should be determined based on conditions of use. If product is used in application where splashing may occur, the use of safety goggles and/or a face shield should be considered.
Hands and Body: Wear appropriate chemically protective gloves and wear appropriate clothing to prevent skin contact.
Respiratory: NIOSH approved respirators should be used when airborne contamination is above exposure limits.
Feet: Wear appropriate footwear to prevent product form coming in contact with feet and skin.

Section 9. Physical and Chemical Properties.
Appearance, Physical State: Bright, Clear Liquid
Odor: not determined
Viscosity: 33 cSt @ 40 deg C
Flash Point: 193 deg.C (380 deg. F)
Vapor Pressure: Negligible at ambient temperature and pressure
Specific Gravity: 0.918 kg/L @20 deg. C (68 deg.F)
Water solubility: Insoluble in water
pH: Not applicable

Section 10. Stability and Reactivity
Stability: Stable under normal handling and storage condition
Hazardous Polymerization: Will not occur at normal working conditions.
Incompatible Substances / Conditions to Avoid: oxidizing agents and acids.
Decomposition Products: Combustion can yield carbon, oxides, aldehydes, ketones

Material Safety Data Sheet Page 2.
Biodegradable Hydraulic Fluid

Section 11. Toxicological information

Routes of entry: Skin and eye contact, inhalation, ingestion.
Acute Lethality: Based on toxicity of components.
Acute oral toxicity (LD50): >5000mg/kg rat.
Chronic or Other Toxic Effects.
Dermal Route: Prolonged or repeated contact may cause skin irritation characterized by dermatitis or oil acne.
Inhalation Route: Negligible breathing hazard at normal temperature. Elevated temperatures or mechanical action may form vapors, mists or fumes. Inhalation of oil mists or vapors from hot oil may cause irritation of the upper respiratory track.
Oral Route: Low toxicity.
Eye Irritation / Inflammation: Repeated or prolonged contact may cause irritation but not permanent damage.
Immunotoxicity: Not available.
Skin Sensitization: Not expected to be skin sensitizer.
Respiratory Tract Sensitization: Not expected to be respiratory tract sensitizers.
Carcinogenicity: This product is not known to contain any chemicals at reportable quantities that are listed as carcinogens by NTP, IARC, OSHA.
Other Considerations: No additional remark.

Section 12. Ecological Information

Aquatic Toxicity based on similar product:
EC50-96 hr 7.7 mg/L Selenastrum (cell dens.) mod. Toxic
LC50-96hr >1000mg /L rainbow trout- practically non-toxic
LC50-96hr >1000mg/L mysid shrimp- practically non-toxic
EC50-48hr >1000mg/L Daphnia magna- practically nontoxic
LC50-96hr >1000mg/L sheepshead minnow- pract. Nontoxic
Mobility:
Not determined.
Persistence and Biodegradability:
This product is estimated to have a moderate (>=30%) rate of biodegradation in a test for ready biodegradation.
Potential to bioaccumulation:
Not determined.
Remarks:
None

Section 13. Disposal Considerations

Waste Disposal: Spent/used/waste oil may meet the requirements of a hazardous waste. Consult your local or regional authorities. Preferred waste management priorities are: (1) recycle or reprocess, (2) incinerate with energy recovery, (3) disposal at licensed waste disposal facility. Ensure that disposal or reprocessing is in compliance with government requirements and local disposal regulations.

Section14. Transport Information

TDG Classification: Not controlled under TDG (Canada).
DOT Shipping Description: Not classified as hazardous.
Special Provisions for Transport: Not applicable.

Section 15. Regulatory Information

This product is acceptable for use under the provisions of WHMIS-CPR. All components of this formulation are listed on the CEPA-DSL (Domestic Substances List).

All components of this formulation are listed on the US EPA-TSCA Inventory.

This product has been classified in accordance with the hazard criteria of the Controlled Products Regulations (CPR) and the MSDS contains all of the information required By the CPR.

This product is not known to contain any chemicals at reportable quantities that are listed on the SARA 313 and 40 CFR 372.

This product is not controlled under the HCS.

HMIS (USA):	Health Hazard	0
	Fire Hazard	1
	Reactivity	0
	Personal Protection	B

NFPA (USA):	Health Hazard	0
	Fire Hazard	1
	Reactivity	0
	Specific Hazard	none

Rating: 0 Insignificant
Slight
Moderate
High
Extreme

Section 16. Other Informations

Prepared by SPX Fluid Power
5885 11th Street
Rockford, IL 61109, USA

Phone: 815-874-5556

Fax: 815-874-7886

Date of preparation: January, 2004

The information presented herein has been complied from source considered to be dependable and accurate to the best of SPX Fluid Power knowledge; however, SPX Fluid Power, makes no warranty whatsoever, expressed or implied, of Merchantability or Fitness **for the Particular Purpose**, regarding the accuracy of such data or the results to be obtained from the user thereof. SPX Fluid Power assumes no responsibility for the injury to recipient or to the third persons or for any damage to any property and recipient assumes all such risks.

Rev1

Product: Biodegradable Hydraulic Fluid
Part Number: 9645,9646